ELUCIDATION OF THE ROLES OF THE CARBONIC ANHYDRASE ENZYMES, CANA & CANB, IN THE PHYSIOLOGY OF *MYCOBACTERIUM SMEGMATIS*

A thesis submitted in the fulfilment of the requirements for the degree of

MASTER OF SCIENCE

Microbiology

of

RHODES UNIVERSITY

Makhanda / Grahamstown

by

GABRIELLA T. JACKSON

November 2023

Abstract

The bacterial pathogen *Mycobacterium tuberculosis* (*Mtb*) is the causative agent of tuberculosis (TB) and one of the leading infectious causes of death globally. The success of *Mtb* as a pathogen depends on its ability to detect and respond to a variety of physical and chemical stresses it encounters during infection of its human host. These environmental stresses include shifts in temperature, oxygen concentration, osmolarity and nutrient availability. *Mtb* is, in addition, exposed to changes in pH and CO_2 concentration in the intracellular and extracellular environments it inhabits, which the bacterium has to adapt to in order to ensure its growth, survival and/or persistence during infection. Carbonic anhydrases (CAs) are a widely distributed family of enzymes that catalyse the reversible hydration of carbon dioxide (CO_2) to bicarbonate (HCO_3^-) in the reaction: $CO_2 + H_2O \rightleftarrows HCO_3^- + H^+$. In microbes, CA activity is important for the activity of enzymes involved in carbon fixation as well as for maintaining pH homeostasis. *Mtb* is known to express three CAs, encoded by the Rv3588c, Rv1284 and Rv3273 genes (*canA*, *canB* and *canC,* respectively). The role(s) of these CA enzymes in the physiology of *Mtb* and other mycobacterial species, such as *Mycobacterium smegmatis* (*Msm*), has not been elucidated to date. To gain insights into the function of the CanA and CanB enzymes in mycobacterial species, we generated both *canA* and *canB* knockdown (KD) and knockout (KO) mutants in the fast-growing mycobacterial species, *Msm,* and analysed their growth phenotypes under several growth conditions where CA activity is known to be required. Notably, *Msm* lacks the CanC homologue, which makes it an ideal surrogate to focus on CanA and CanB. The *Msm canA* KD mutant was found to display a growth defect following anhydrotetracycline (ATc)-mediated gene silencing at atmospheric (low) CO_2 concentrations [~0.035% CO_2 (v/v)]. The growth defect could be rescued by incubating cells at physiological (high) CO_2 concentrations [~5% CO_2 (v/v)] or by supplementing the growth media with either HCO_3^- or the metabolic end-products of certain HCO_3^--dependent-carboxylase enzymes at low CO_2 concentrations. The ability of these compounds to rescue the growth of the *canA* KD mutants was, however, dependent on the extent of ATc-mediated gene silencing, suggesting that the *canA* gene is required for *Msm* growth at both low and high CO_2 concentrations. This was confirmed by our findings that *canA* could only be genetically inactivated when a second copy of the gene was provided on the chromosome *in trans*, regardless of the CO_2 concentration used. In contrast to our observations for *canA,* no differences in the growth phenotypes of the *Msm* wild type (WT) and *canB* KD or knockout (KO) mutant strains were observed following silencing or inactivation of the *canB* gene at either low or high CO_2 concentrations or different

pH values. These observations suggest that, in contrast to *canA*, the *canB* gene is dispensable for the growth of *Msm* under standard laboratory growth conditions. The *canB* KO mutant strain, nevertheless, displayed a slight decrease in its ability to form biofilms when compared to the WT strain, which could be restored by genetic complementation. CanB activity may, therefore, be required to promote bacterial growth and/or survival under biofilm conditions where CO_2 diffusion into cells is limited, a phenomenon that has recently been observed in other microbes. Further studies are required to confirm the role of CanB in biofilm formation and to determine how the different CA enzymes cooperate to promote the growth and survival of mycobacterial species in the various environments they are known to inhabit.

Keywords: *Mycobacterium tuberculosis*, *Mycobacterium smegmatis*, β-carbonic anhydrases, CRISPRi, homologous recombination, drug targets

Table of Contents

List of Abbreviations

AES	Allelic Exchange Substrate
AGE	Agarose Gel Electrophoresis
Amp	Ampicillin
Amp^R	Ampicillin Resistant
ATc	Anhydrotetracycline
BCG	Bacille Calmette Guerin
Ci	Inorganic Carbon
CRISPR	Clustered Regularly Interspaced Short Palindromic Repeats
CRISPRi	CRISPR interference
dcas9	Deactivated *cas9*
ddH_2O	Double distilled water
dH_2O	Distilled water
DMSO	Dimethyl sulphoxide
dNTPs	Dinucleotide Triphosphates
DS	Downstream
Ec	*Escherichia coli*
G+C	Guanine and Cytosine
HIV/AIDS	Human Immunodeficiency Virus/Acquired Immune Deficiency Syndrome
Hyg	Hygromycin
Hyg^R	Hygromycin Resistant
INH	Isoniazid
Kan	Kanamycin
Kan^R	Kanamycin Resistant
KD	Knockdown
KO	Knockout
LA	Lysogeny (Broth) Agar
LB	Lysogeny Broth

LTBI	Latent Tuberculosis Infection
MCS	Multiple Cloning Site
MDR	Multidrug-Resistant
Msm	*Mycobacterium smegmatis*
Mtb	*Mycobacterium tuberculosis*
MW	Molecular Weight
OD_{600}	Optical Density at 600 nm
ORF	Open Reading Frame
PAM	Protospacer Adjacent Motif
PBS	Phosphate Buffered Saline
qPCR	Quantitative Real-Time Polymerase Chain Reaction
RT	Reverse Transcriptase/Reverse Transcribed
RT-PCR	Reverse Transcription Polymerase Chain Reaction
sgRNA	Single guide RNA
SOE	Splice by Overlap Extension
Sth1 dcas9	*Streptococcus thermophilus* CRISPRi inactivated *cas9*
TB	Tuberculosis
Tm	Melting Temperature
US	Upstream
WT	Wild Type
XDR	Extensively Drug-Resistant
Zeo	Zeocin
Zeo^R	Zeocin Resistant/Zeocin Resistance Gene
Zeo^s	Zeocin Sensitive

List of Units & Symbols

bp	Base Pairs
CFU	Colony Forming Unit
° C	Degrees Celsius
g	Grams
h	Hour(s)
Kb	Kilobase
kV	Kilovolt
M	Molar
min	Minute(s)
mg	Milligram
mL	Millilitre
mm	Millimetre
mM	Millimolar
ng	Nanogram
nM	Nanomolar
nt	Nucleotide
%	Percentage
Ω	Resistance
s	Second(s)
µg	Microgram
µL	Microlitre
µM	Micromolar
V	Volt

Acknowledgements

Firstly, I would like to thank the best supervisor ever, Dr Garth Abrahams. There are not enough words to express my appreciation for your guidance and support throughout my academic journey. I am eternally grateful for your kindness and patience (especially your patience). Your combination of genius and humility remains a constant source of inspiration and these are two qualities I hold in the highest regard. It has been a privilege doing this research under your supervision. Thank you, thank you, thank you for everything.

Secondly, to my fellow lab mates in Lab 309, thank you for all your support and guidance. A special thank you to Ariana Watkins and Courtney Smit-Wright. Ari, I want to thank you for your continuous support, guidance and of course, all the ice cream adventures! Your work ethic is admirable, and your dedication inspires me to continually strive for improvement in my journey as a scientist. I appreciate you and your friendship. Courts, I am truly grateful for our newfound friendship and the impact it has had on my professional and personal growth. Thank you for all the Relish adventures and for making my last year at Rhodes one for the books!

Thirdly, a heartfelt appreciation goes out to my lab neighbours, Nomxolisi Mqwathi, Urisha Naidoo and Megan Starbuck. The countless conversations, shared experiences, and the laughter we've shared together has made my time at Rhodes more memorable and meaningful. Your friendship has left an indelible mark, and I am very lucky to have met you three.

Lastly, I would like to thank my parents as this would not have been possible without them. Thank you for being my pillar of strength throughout my academic journey. I am deeply grateful for your unwavering support, love, understanding, and sacrifices which have made it possible for me to reach this milestone. Thank you for being the best parents a child can only dream of having.

Chapter 1: Literature Review

1.1 General Introduction

Mycobacterium tuberculosis (*Mtb*) is an air-borne, facultative intracellular pathogen that causes the infectious disease tuberculosis (TB) in humans. Although significant financial and research investment has been made to identify and develop new antitubercular drugs and vaccines over the last several decades (Dartois & Rubin, 2022; Srivastava *et al*., 2023), TB remains one of the leading infectious causes of death worldwide each year. According to the most recent World Health Organisation (WHO) estimates, there were ~10.6 million new cases of TB in 2022, which resulted in ~1.3 million deaths (WHO, 2023). This makes TB the leading cause of death due to a bacterial pathogen globally and the second overall cause of death due to an infectious agent after COVID-19, which is caused by the viral pathogen SARS-CoV-2 (WHO, 2023). Of the ~1.3 million deaths associated with TB infection, ~167, 000 occurred in individuals also infected with HIV, making TB the leading cause of HIV/AIDS-associated deaths each year (WHO, 2023). Besides active TB cases, a quarter of the world's population is estimated to be infected with TB in a clinically asymptomatic or latent form (Houben & Dodd, 2016; WHO, 2023). These individuals carry a ~5 to 10% lifetime risk of progressing to active disease and consequently represent a large reservoir from which disease transmission can potentially originate (Behr *et al*., 2021; Tiemersma *et al*., 2011).

Despite the large global burden of disease, cases of active TB caused by drug-sensitive (DS) forms of *Mtb* can be treated with a chemotherapeutic regimen composed of four first-line drugs administered for a period of four to six months (WHO, 2023). While untreated TB can have a mortality rate of ~50%, this antitubercular regimen is effective in curing ~85% of all treated (WHO, 2023). The need to administer multiple drugs over a period of several months can, however, lead to the interruption or premature cessation of treatment. This, in turn, can promote the development and selection of *Mtb* strains that are genetically resistant to one or more first-line drugs. Treatment of drug-resistant (DR) *Mtb* strains requires the use of second-line antitubercular drugs, which are less effective and, therefore, less likely to have successful treatment outcomes. To improve the outcomes of treating *Mtb* infections, which often contain bacilli that are genetically drug-resistant and/or phenotypically unresponsive to drug treatment (Kloprogge *et al.*, 2022), requires the identification and validation of new and more effective drugs, together with their corresponding drug-targets. During this study, we investigated the requirement of the CA enzymes, CanA and CanB, for the growth and survival of model

mycobacterial species, *Msm*, with the ultimate goal of validating CA enzymes as potential drug targets in the related, pathogenic mycobacterial species, *Mtb*.

1.2 Classification and Taxonomy

Mtb is a member of the genus *Mycobacterium*, the sole genus within the family *Mycobacteriaceae* (Lory, 2014). Besides *Mtb*, the genus contains ~200 species (Tortoli *et al*., 2019) that are characterised as strictly aerobic, non-motile, non-spore-forming bacilli with sizes that range from 0.3 – 0.5 μm in diameter and 1.5 – 4.0 μm in length (Cook *et al*., 2009). Other distinguishing features of mycobacterial species include their relatively high G+C contents, which can range between 62 and 70% (Tortoli *et al.* 2019) and the presence of long-chain (C60-C90) fatty acids known as mycolic acids in their cell envelopes (Barry *et al*., 1998; Cook *et al*., 2009). The cell envelope consists of four layers, which include (i) the plasma or inner membrane, (ii) the arabinogalactan-peptidoglycan (AGP) complex, (iii) a mycolic acid layer that is covalently linked to the underlying AGP complex, and (iv) an external capsule-like layer composed of (glyco)lipids, lipoglycans and lipoproteins (Jankute *et al*., 2015; Kalscheuer *et al*., 2019). The mycolic acid and capsular layer form the inner and outer leaflets of the mycobacterial outer membrane (or mycomembrane), respectively (Daffé & Marrakchi, 2019; Jackson, 2014). The hydrophobic, lipid-rich nature of the mycobacterial cell envelope serves as an effective barrier to the entry of many small molecules encountered in the natural or host environment, conferring it with increased resistance to a variety of chemical stresses, antibiotics and immune system effectors (Batt *et al*., 2020; Dulberger *et al*., 2020).

Given its medical significance as the causative agent of TB in humans, *Mtb* is the most extensively studied mycobacterial species. Several mammalian species other than humans (e.g., cattle, horses, deer, antelopes, pigs, elephants, carnivores and aquatic mammals) are susceptible to infection with *Mtb* (Cvetnić *et al*., 2018; Lory, 2014). The bacterium is adapted to cause disease in human hosts, however, and is not a significant cause of natural infection in other animals. There are also no known environmental reservoirs for *Mtb,* and infection is, therefore, almost exclusively acquired from infected human hosts. Like *Mtb*, the *Mycobacterium (M.)* species *M. africanum* and *M. canetti* are obligate, human host-adapted pathogens. The number of TB cases attributable to these mycobacterial species is relatively limited, however, and are restricted primarily to West Africa and the Horn of Africa, respectively (Cirillo *et al*., 2021; Gagneux, 2018). The following *Mycobacterium* species are capable of causing TB-like disease but display a tropism for mammalian species other than humans. These include *M. bovis* (cattle), *M. microti (rodents)*, *M. pinnipedii (seals, sea lions)*,

M. caprae (goats), *M. suricattae (meerkats)*, *M. oryx (oryx)*, *M. mungi (mongoose)* (Lory, 2014; Tortoli, 2019). Despite possessing differences in their host range, geographic distribution, and pathogenicity, the human and animal-adapted mycobacterial species display >99.9% genetic similarity at the nucleotide level and are thought to share a clonal ancestor (Cirillo *et al*., 2021; Gagneux, 2018). They are also all characterised by their relatively slow growth rates (e.g., one cell division every 18-54 h) and are referred to as slow-growing mycobacteria (SGM). Based on their similarity to *Mtb* and each other, these pathogenic mycobacterial species are referred to as the "*Mycobacterium tuberculosis* complex" or MTBC. Besides the members of the MTBC, pathogenic mycobacterial species also include *M. leprae* and *M. lepromatosis,* the causative agents of leprosy in humans (Lory, 2014). These organisms are obligate intracellular pathogens that possess reduced genomes and are, therefore, unable to replicate independently of their hosts, which includes humans and armadillos. (Lory, 2014).

In contrast to the medically important organisms listed above, the majority of mycobacterial species exist as saprophytes in the natural or built environment, or as the symbionts or commensals of animals (Lory, 2014). Environments in which these species are typically found include, amongst others, soil or dust, salt or fresh water bodies, water distribution systems, on or within domestic and wild animals, plant surfaces or tissues, or within various amoebae, ciliates or protozoa (Briancesco *et al*., 2014; Cvetnić *et al*., 2018). These mycobacterial species are varyingly referred to as "environmental", "atypical", or "non-tuberculosis" mycobacteria" (NTM) (Turenne, 2019). Most of the species classified as NTM are non-pathogenic, which include, amongst others, *M. aurum*, *M. phlei,* and *M. terraei* (Pavlik *et al*., 2022). Other NTM are the frequent causes of opportunistic infections in humans or other animals, particularly those with compromised immunity (Pereira *et al*., 2020). These NTM include members of the *M. avium* complex (MAC) and *M. abscessus*. While some NTM, such as members of the *M. avium* complex (*M avium and. M. intracellurare*), are classified as SGM, others, such as *M. smegmatis* (*Msm*) and *M. phlei* have relatively fast growth rates (one cell division every 3-4.5 h, respectively) and are consequently referred to as fast-growing mycobacteria (FGM) (Kim *et al*., 2013).

Due to its non-pathogenic nature, fast growth rate, high transformation efficiency, and availability of genetic tools, *Msm* is often used as a model organism to elucidate the biology of both non-pathogenic and pathogenic members of the *Mycobacterium* genus (Sparks *et al*., 2023; T, Sundarsingh *et al*., 2020). A high degree of conservation of genes and gene function also exists across the genus. Approximately 96% of the genes identified as essential in *Msm*

have orthologues in *Mtb*, for instance, of which 90% are also essential in *Mtb* (Sparks *et al*., 2023). Studies on the physiological role(s) of genes or their gene products in *Msm* can, therefore, often provide insights into the function of its orthologues in *Mtb*. Given its utility as a model organism, *Msm* served as the primary mycobacterial species used in this study.

1.3 TB Pathogenesis

1.3.1 The *Mtb* infectious process and the host environment

As discussed in the preceding section, humans are the natural reservoirs of *Mtb* and the organism is primarily transmitted from infected to susceptible human hosts (Guinn & Rubin, 2017). *Mtb* is transmitted when an uninfected individual inhales aerosolised droplets expelled by an individual with active pulmonary TB through coughing, sneezing or vocalisation (Patterson & Wood, 2019). Following inhalation, the aerosolised droplets pass through the upper respiratory tract and land in the terminal air sacs, called alveoli, within the lungs (Lerner *et al*., 2015). *Mtb* is initially recognised by lung-resident macrophages called alveolar macrophages (AMs) using pattern recognition receptors (PRRs) such as Toll-like receptors (TLRs) and C-type lectin receptors (CLRs) present on the macrophages (Ravesloot-Chávez *et al*., 2021). These receptors engage with *Mtb* pathogen-associated molecular patterns (PAMPS), which trigger the phagocytic uptake of *Mtb* by the AMs, as well as the secretion of pro-inflammatory cytokines and chemokines that recruit other components of the innate immune system to the site of infection (Bussi & Gutierrez, 2019; Lovewell *et al*., 2021). Following phagocytosis of *Mtb*, infected AMs then cross the alveolar epithelium and migrate into the lung interstitium (Cohen *et al*., 2018). In some instances, infected individuals may launch an innate immune response of sufficient magnitude to clear the infection before it progresses any further (Chandra *et al*., 2022). In the absence of bacterial clearance, *Mtb* can interfere with the phagolysosomal maturation pathway and inhibit phagosome-lysosome fusion, which promotes bacterial growth and survival within the intracellular environment (Pisu *et al*., 2021). Ongoing bacterial replication results in the lysis of the infected macrophages and release of the bacilli into the extracellular space. Here, the released bacilli can infect a variety of phagocytic cells, such as macrophages, neutrophils, and dendritic cells, which are recruited to the site of infection (Chandra *et al*., 2022). The phagocytic uptake of *Mtb* by dendritic cells triggers their maturation into antigen-presenting cells. These cells travel to the draining lymph nodes, where they present *Mtb*-specific antigens to antigen-specific T-cells, resulting in their activation and proliferation (Ravesloot-Chávez *et al*., 2021). The activated T-cells subsequently migrate to the initial site of infection, where they attempt to limit the progression and dissemination of infection by recruiting additional cells of the innate (e.g., macrophages, neutrophils) and

adaptive (B and T lymphocytes) immune system, as well as fibroblasts. This facilitates the formation and maturation of cellular aggregates around the infected area, resulting in the formation of a granuloma (Chandra *et al*., 2022). Granulomas form part of a host's defence against foreign substances that, during *Mtb* infection, serve as a protective structure that "walls off" bacteria to limit their ongoing growth and spread to other body sites (Saunders & Cooper, 2000). Granuloma formation in *Mtb*-infected individuals takes many shapes and forms. TB is often associated with the formation of caseous granulomas, where the cells in the central region of the granuloma have undergone necrotic cell death. This process results in a core composed of cell debris, often exhibiting a soft-cheese-like consistency known as caseum (Lenaerts *et al*., 2015; Cronan, 2022). Various types of necrotic granulomas exist, such as fibrotic granulomas (surrounded by a fibrotic rim), calcified granulomas (necrotic core is mineralised) and suppurative granulomas (necrotic core is invaded by neutrophils). *Mtb* infection is also associated with the formation of cellular or non-necrotising granulomas, characterised by the absence of a central necrotic core and the bacteria reside intracellularly (Mattila *et al*., 2013). Contrary to the previous understanding of the granuloma as an exclusively host-protective structure, recent studies have shown that mycobacteria enhance the formation of granulomas as a defensive mechanism against the host's immune system, which *Mtb* has evolved to exploit for their own expansion and dissemination (Davis & Ramakrishnan, 2009; Cronan *et al*., 2016). It is important to note that these distinct granuloma types can be present in one infected host (Lin *et al*., 2009).

There are three possible outcomes following granuloma formation. Firstly, when there is an effective adaptive immune response, the infection can be eliminated, leaving behind a calcified granuloma (Chandra *et al*., 2022). Secondly, if the immune system can achieve control but not clear the infection completely, latent TB is achieved, whereby the bacilli remain dormant or quiescent within the granuloma. Lastly, from this point, some individuals proceed to active TB disease, either directly after primary infection or after reactivation from true latent infection, which generally happens in cases of immunosuppression. This is accompanied by a change in the structure of the granuloma and the presence of caseum, which can facilitate more rapid *Mtb* growth. The central region of the caseum can liquify, creating an even more favourable environment for growth (Rahlwes *et al*., 2023). *Mtb* can then disseminate, spreading beyond the lungs via the lymphatic or circulatory system to other parts of the body (Lerner *et al*., 2020; Rahlwes *et al*., 2023). **Figure 1.1** below depicts the potential outcomes following Mtb infection.

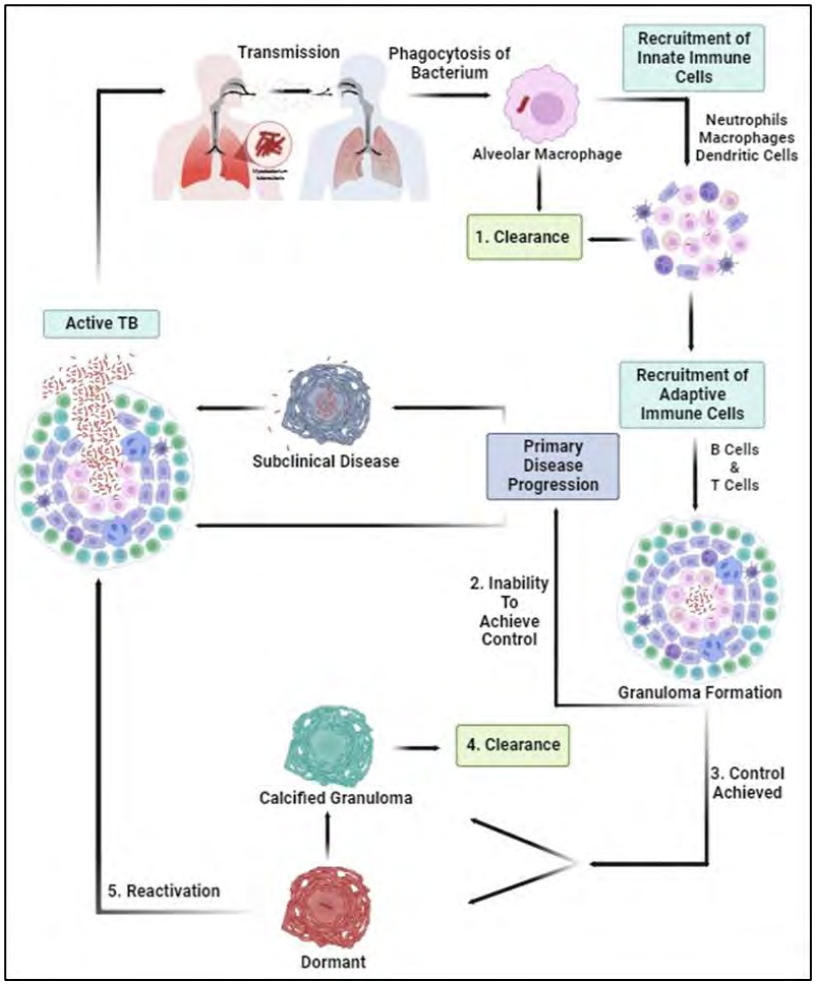

Figure 1.1: Schematic representation of the multiple outcomes following *Mtb* infection. Adapted from Chandra *et al*., 2022. The infection cycle is initiated with the emission of aerosolised droplets carrying bacilli from a person with active TB and subsequent inhalation by an uninfected person. The first host cells that *Mtb* encounters are alveolar macrophages. These macrophages phagocytose the bacteria and, in turn, produce cytokines and chemokines, which stimulate the inflammatory response and facilitate the recruitment of additional innate immune cells such as tissue-resident macrophages, neutrophils, and dendritic cells. These innate immune cells transport the bacteria from the lung epithelial to deeper tissues. This results in the activation, proliferation, and recruitment of additional innate and adaptive immune cells, such as B and T cells, which surround the bacteria to initiate granuloma formation. There are four possible outcomes: **1) Clearance:** The host's innate response can immediately eliminate the bacteria. **2) Inability to achieve control**: In instances where the immune system fails to control bacterial replication, primary disease can occur, resulting in progression to active TB. Active TB may also be preceded by a subclinical phase that eventually progresses to the active form of disease. **3) Control**: This results in encapsulation of the bacteria within a granuloma, followed by clearance or reactivation. **4) Clearance:** Upon encapsulation of the bacteria, the immune system eliminates bacilli, a calcified granuloma forms, and the infection is cleared. If the infection is not cleared, the bacteria may remain dormant or quiescent within the granuloma, and latent TB (LTBI) occurs. **5) Reactivation:** In cases of immunosuppression, the immune system fails to contain the bacteria during latent infection, reactivation occurs and progresses to active TB (Blomgran *et al*., 2012; Chackerian *et al*., 2002; Ernst, 2012; Kang *et al*., 2011; Stuck *et al*., 2022).

1.3.2 Forms of TB disease

TB can present as a spectrum of diseases ranging from asymptomatic infection to life-threatening disease (Barry *et al*., 2009; Pai *et al*., 2016). It is, however, important to note that individuals can move in both directions of this spectrum of disease (Barry *et al*., 2009; Richards *et al*., 2023). There are five states that an individual who has ever encountered *Mtb* may be classified into. Eliminated TB infection is when an individual with prior exposure to *Mtb* has either successfully cleared the infection by the innate and/or acquired immune responses or has been cured through adequate treatment with anti-TB drugs. The presence of live *Mtb* is no longer detectable in this person, although immunological indications of a previous infection(s) may remain (Drain *et al*., 2018). Latent TB infection (LTBI) is an infection with viable *Mtb* successfully suppressed by the immune system, whereby the bacteria remain dormant (Stuck *et al*., 2022). There is no anticipated progression to active TB disease in the near future, provided there is no significant immunological compromise (Drain *et al*., 2018). It is an asymptomatic and non-transmissible state (Barry *et al*., 2009; Pai *et al*., 2016). Currently, there is a lack of a diagnostic to confirm LTBI or quantify its microbiological load. The only diagnostics available to infer LTBI are based on T-cell responses to *Mtb* or Mtb-like antigens (e.g., due to vaccination with BCG) (Dheda *et al*., 2014; Drain *et al*., 2018). Incipient TB infection refers to infection with viable *Mtb*. It is likely to progress to active disease in the absence of intervention. At this stage, it has not manifested clinical symptoms, radiographic abnormalities, or microbiological evidence consistent with active disease. Subclinical TB is a disease where viable *Mtb* does not cause clinical symptoms typically associated with TB disease but can cause other abnormalities that may be identified using existing radiological or microbiological assays (Drain *et al*., 2018). It is an asymptomatic but transmissible state (Dowdy *et al*., 2013; Pai *et al*., 2016). Therefore, individuals with subclinical TB are much less likely to be tested for TB, making them a reservoir nearly invisible to passive monitoring or case detection (Esmail *et al*., 2018). Active TB disease is when viable *Mtb* causes clinical TB-related symptoms with radiographic abnormalities and microbiological evidence consistent with active TB. It is present in a symptomatic and transmissible state (Barry *et al*., 2009; Pai *et al*., 2016). A way in which active TB disease can occur is from a primary infection when the immune system is unable to defend against initial infection. Another way is if, during LTBI, the immune system is unable to contain the *Mtb* within the granuloma, and they overwhelm the body's immune system; this is referred to as reactivation. The most common form of active TB is reactivation TB, which represents 90% of all cases (MacPherson *et al*., 2020). Following infection, the likelihood of developing active TB is highest within the first two years; however,

the manifestation of the active disease typically occurs several years later in most patients (Jilani *et al*., 2022).

1.3.3 Mtb host cell niches

Mtb is known to inhabit several micro-environments within the host over the course of infection, including phagocytic cells and granulomas (Baker *et al*., 2019). Although these environments are unfavourable for bacterial proliferation and viability, *Mtb* has developed many mechanisms that provide resistance to bacterial eradication, enabling it to persist inside infected hosts for prolonged periods. During pathogenesis, *Mtb* will encounter environments with low pH, hypoxia, restricted carbon sources, low nutrient availability and oxidative and nitrosative stressors (Berney & Berney-Meyer, 2017). Understanding how *Mtb* regulates its growth rate in response to environmental cues encountered during infection provides insight into the physiology that makes *Mtb* a successful and difficult-to-treat pathogen (Baker *et al*., 2014).

Mtb has a unique ability to survive within macrophages and use it for replication. Following phagocytosis, *Mtb* resides in a vacuolar compartment with low pH, reactive oxygen and nitrogen species (ROS and RNS, respectively), antimicrobial peptides and lysosomal hydrolases (Yang *et al*., 2012). *Mtb* is able to subvert or neutralise host defences early in the phagosome maturation pathway through the use of a vast array of molecules and strategies. Depending on the activation status of macrophages, the pH of the surrounding environment is dynamic and subject to change (Yates *et al*., 2005). The vacuole in non-activated macrophages is slightly acidified (~ pH 6.4) and contains limited lysosomal contents. When macrophages are activated by interferon-gamma (IFN-γ), the phagosomal maturation process proceeds, enabling the delivery of *Mtb* to a highly acidified phagolysosome (~ pH 4.5), which is rich in antimicrobial peptides and compounds (Baker *et al*., 2019). As part of their antimicrobial activity, the activated macrophage produces two notable enzymes: the phagocyte oxidase complex (phox) and inducible nitric oxide synthase (iNOS). The phagocyte oxidase complex, often referred to as NADPH oxidase, is a multi-subunit enzyme that generates ROS such as superoxide ($O_2^{\bullet-}$), hydrogen peroxide (H_2O_2) and hydroxyl radicals (Sies & Jones, 2020). ROS can cross the membranes of bacterial pathogens, damaging a variety of their cellular components, such as nucleic acids, proteins and cell membranes, leading to growth inhibition or cell death (Nguyen *et al*., 2017). Activation of phagocytic cells by IFN-γ induces the activity of iNOS, which is an enzyme that catalyses the oxidation of L-arginine to L-citrulline and nitric oxide (NO) (MacMicking *et al*., 1997; Bogdan, 2015). NO can also form other RNS such as

nitrite (NO_2^-), dinitrogen trioxide (N_2O_3), nitrogen dioxide (NO_2) and peroxynitrite ($ONOO^-$). RNS, like ROS, also interfere with cellular components of pathogens, such as damaging nucleic acids and inhibiting enzyme function, leading to growth inhibition or cell death (Ehrt & Schnappinger, 2009; Schairer *et al*., 2012).

IFN-γ-activated macrophages are crucial in controlling mycobacterial infections and rely on the production of toxic oxidative radicals as previously described. However, the antimicrobial effect of IFN-γ is not the only contributor. Activated macrophages also have the ability to restrict the growth of intracellular pathogens by depriving them of essential nutrients and carbon sources. Over time, *Mtb* has evolved to exploit a specialised set of metabolic pathways to utilise host-derived nutrients and carbon sources within macrophages to meet its energy and biosynthetic demands (Pandey & Sassetti, 2008). By consensus, fatty acids, as opposed to carbohydrates such as glucose, are proposed to be the preferred primary carbon source for *Mtb* during infection (Chang & Guan, 2021). Examples of fatty acids utilised by *Mtb* as carbon sources are cholesterol, palmitic acid and oleic acid. Fatty acids are oxidised through β-oxidation to produce acetyl-coenzyme A (CoA), a key metabolite in cellular energy production. Acetyl-CoA feeds into the tricarboxylic acid (TCA) cycle to generate adenosine triphosphate (ATP) (Munoz-Elias & McKinney, 2006). Additionally, acetyl-CoA is a precursor for amino acids and lipids, which are essential for bacterial growth and replication (Ke *et al*., 2000). The TCA cycle, also known as the Krebs cycle or citric acid cycle, is central to energy production and synthesis of biosynthetic precursors in aerobic organisms. Prior to initiation of the TCA cycle, glycolysis occurs where glucose is broken down into pyruvate, ATP and NADH. Pyruvate is then decarboxylated to form acetyl-CoA, which enters the TCA cycle (Choi *et al*., 2021). Both pyruvate and its immediate glycolytic precursor, phosphoenolpyruvate (PEP), can be carboxylated to form the TCA intermediate, oxaloacetic acid (OAA).

Similar to the environment of phagolysosomes, *Mtb* also encounters a harsh environment within granulomas. The pH within granulomas ranges between 5.0 and 7.2, with 5.5 being the median pH (Kemker *et al*., 2017; Baker *et al*., 2019). Under environments of hypoxia, such as that found in the centre of caseating granulomas, *Mtb*'s levels of ATP are decreased but maintained at a constant low level (Kumar *et al*., 2011). Macrophages accumulate lipid droplets under hypoxia, and it has been shown that *Mtb* can access these host-derived lipid droplets, which serve as energy sources (Daniel *et al*., 2011). Additionally, granulomas lack mature vasculature, which limits the delivery of nutrients to *Mtb* (Qualls & Murray, 2015). In response to these stresses, *Mtb* can alter its metabolism to enter a state of dormancy, which allows viable

bacteria to persist in a non-replicating and -dividing state until conditions are more favourable until growth is restored (Wayne & Hayes, 1996).

Mtb is also exposed to a wide range of CO_2 concentrations during its infectious cycle, which could impact bacterial growth and physiology. During transmission in aerosols or respiratory droplets, *Mtb* is exposed to relatively low CO_2 concentrations [atmospheric CO_2 concentrations ~0.035% (v/v)]. Following entry into the physiological environment of the lung, the CO_2 concentrations are high [~5% (v/v)] due to the generation of CO_2 during aerobic respiration in their mammalian hosts. The CO_2 concentration in the large proximal airways can change dramatically during the respiratory cycle, however, with the CO_2 concentration reaching that of ambient air (~0.035% v/v) during inspiration and 5% during expiration (2–4 sec) (Cochrane *et al*., 1982). Outside of the lung, most cell types and compartments have a similar CO_2 concentration of ~5% (Thornell *et al.* 2018). At physiological pH's, the conversion of CO_2 into HCO_3^- is favoured, however, so that HCO_3^- is the predominant form of Ci found in cells and bodily fluids, with concentrations of ~15 and 25 mM found in red blood cells (pH 7.2) and blood, respectively (pH 7.4) (Cummins *et al*., 2020; Geers & Gros, 2000). Epithelial cells that line the respiratory, gastrointestinal, and genitourinary systems also secrete HCO_3^--containing fluids, where concentrations can reach levels up to 140 mM. For pathogenic microbes, the presence of elevated levels of CO_2 and HCO_3^- relative to the environment may serve as a signal of the host environment, triggering altered expression profiles, including for those encoding functions relating to metabolism and virulence. Infection with *Mtb* can also obstruct airways, leading to elevated CO_2 concentrations [up to 20% (v/v)] in the lung, a factor known to stimulate cough responses that promote bacterial transmission (Hanacek *et al*., 2003; Ruhl *et al*., 2020). While elevated CO_2 concentrations (2 to 5% v/v) have long been recognised to promote the growth of *Mtb* under certain nutritional conditions, such as when grown on fatty acids or in the absence of biotin (Schaefer *et al*., 1955; Middlebrook & Cohn 1958; Cohn *et al*., 1960), its precise effects on mycobacterial physiology and metabolism have not been extensively investigated. This topic, therefore, warrants further study.

1.4 Prevention and Treatment of TB

While several vaccine candidates are currently being tested for their ability to prevent TB infection or disease, the Bacille Calmette–Guérin (BCG) vaccine remains the only currently licensed TB vaccine (Srivastava *et al*., 2023). BCG is a live, attenuated *M. bovis* strain developed in the early 20th Century by serial, *in vitro* passage of the bacterium by Albert Calmette and Camille Guérin (Calmette & Guérin, 1920). The BCG vaccine is usually

administered to new-borns or infants via the intradermal route and confers protection against pulmonary, miliary, and meningeal TB in these population groups (Fatima *et al*., 2020; Mangtani *et al*., 2014; Martinez *et al*., 2022). This protection conferred by the BCG vaccine wanes by adolescence or early adulthood, however, and does not prevent active pulmonary TB in adults, who are the primary drivers of TB transmission (Fatima *et al*., 2020; Mangtani *et al*., 2014; Martinez *et al*., 2022). The vaccine also does not provide protection against reactivation and progression to active TB in individuals with LTBI, who serve as significant reservoirs of disease (Fatima *et al*., 2020). Since it is a live, attenuated vaccine, BCG vaccination is also contra-indicated in certain immune-suppressed populations (e.g. HIV-infected individuals and/or pregnant females), further limiting its usefulness. Despite these shortcomings, BCG is still widely used due to its ability to confer protection against TB disease between infancy and adolescence, coupled with its affordability and safety profile (Fatima *et al*., 2020). Newer vaccines that confer protection to all populations at risk of contracting or developing TB disease are, however, needed.

The preferred "short-course" regimen for treating adults with active DS forms of TB consists of an intensive phase consisting of the four first-line drugs, isoniazid (H), rifampin (R), pyrazinamide (Z), and ethambutol (E) taken for two months, followed by a continuation phase of H and R taken for an additional four months (Belknap & Haas, 2018). This regimen is relatively affordable (~US$20 dollars per patient) and results in the cure of ~85% of TB patients, when taken as prescribed (WHO, 2023). Treatment with either rifampin (or rifapentine) and/or isoniazid for 3 to 9 months can, furthermore, be used to prevent the reactivation of *Mtb* and progression to active, pulmonary TB in individuals latently infected with DS-TB (Sterling *et al*., 2020). While the DS-forms of active and latent TB can be treated successfully, the emergence and spread of DR *Mtb* strains remain a critical issue. Drug resistance in *Mtb* develops primarily via genetic mutation of chromosomal genes that (i) encode the immediate target of the drug, (ii) activate pro-drugs to their active form, or (iii) act as efflux pumps. These mutations can reduce the susceptibility or confer complete resistance to one or more first-line drugs. Several factors are thought to contribute to the emergence of DR-TB, including the extended length of antitubercular therapy, the adverse effects that arise following prolonged use of certain first-line drugs, and the lack of drug tolerance amongst some patient groups (Dartois & Rubin, 2022; Tiberi *et al*., 2022). These factors often lead to patients discontinuing treatment, which encourages the development and selection of DR *Mtb* following

exposure to sub-therapeutic doses of one or more antitubercular drug(s) (Dartois & Rubin, 2022; Tiberi *et al*., 2022).

DR-TB can be classified as either (i) mono-resistant TB, which are *Mtb* strains resistant to either isoniazid or rifampin, (ii) multidrug-resistant TB (MDR-TB), which is caused by *Mtb* strains resistant to both isoniazid and rifampin, (iii) pre-extensively drug-resistant TB (pre-XDR-TB), caused by MDR or RR *Mtb* strains that have acquired additional resistance to either a fluoroquinolone (WHO, 2022) or injectable drugs such as amikacin, capreomycin, and kanamycin (CDC, 2022), and (iv) extensively drug-resistant TB (XDR-TB), caused by pre-XDR *Mtb* strains that have acquired additional resistance to at least one "Group A" drug, which include moxifloxacin (M), levofloxacin (L), bedaquiline (B) and linezolid (L) (WHO, 2022; CDC, 2022). Historically, treatment for MDR- and XDR-TB was composed of 5 to 7 second-line drugs, which are often less effective when compared to those containing first-line drugs. The treatment of DR-TB consequently often needs to be administered for extended periods (18 to 24 months) to ensure a relapse-free cure, which is more expensive (≥US$ 1000 per patient) and produces more side effects than those used to treat DS-TB. While shorter treatment regimens comprised of bedaquiline, pretomanid, linezolid and/or moxifloxacin (BPaLM) have recently been developed for the treatment of MDR- and XDR-TB (Conradie *et al.*, 2020), concerns remain about its long-term efficacy, cost-effectiveness in resource-limited settings, and emergence of drug resistance. The difficulty in treating drug-resistant TB, coupled with the threat it poses to public health and health security, highlights the need to identify new drugs and drug targets to combat this challenge (Lu *et al*., 2019).

1.5 Carbonic anhydrases

1.5.1 Introductions to carbonic anhydrases

Carbonic anhydrases (CAs) are a family of metalloenzymes that catalyse the reversible hydration of carbon dioxide (CO_2) to form bicarbonate (HCO_3^-), a weak base, and protons (H^+), a strong acid, as depicted below (Smith & Ferry, 2000; Supuran, 2016):

$$CO_2 + H_2O \rightleftarrows HCO_3^- + H+$$

The reaction catalysed by CA enzymes is necessary for several important physiological functions that occur in living organisms, including respiration, photosynthesis, dissolved inorganic carbon (Ci) assimilation, pH homeostasis, and CO_2/ HCO_3^- transport (Smith & Ferry, 2000). In the absence of CA activity, bicarbonate formation depends on the rate of spontaneous CO_2 hydration, as well as the environmental concentration of CO_2. While CO_2 is relatively soluble in aqueous solutions, its rate of hydration or dehydration at atmospheric CO_2

concentrations and physiological pH values is low, with catalytic rates (kcat) of ~1 ´ 10^{-1} and 5 ´ 10^{1} s^{-1} for the forward and reverse reactions, respectively (Supuran, 2016). Unless grown at elevated CO_2 concentrations, such as those found physiologically, this rate is often too low to fulfil the cellular requirements of most organisms. To overcome this limitation, most life forms employ CAs to catalyse the hydration of CO_2 (or the reverse dehydration reaction, depending on cellular needs) to achieve catalytic rates (kcat) ranging from 1´ 10^{5} to 10^{7} s^{-1}. CAs, therefore, expedite the ability of organisms to maintain essential metabolic processes that depend on either CO_2 or HCO_3^-, as well as those involved in the maintenance of cellular pH homeostasis via HCO_3^- or H^+ buffering (Smith & Ferry, 2000; Supuran, 2016). Organisms that lack CA activity are, therefore, usually capnophiles that require high environmental CO_2 availability (Merlin *et al*., 2003; Ueda *et al*., 2012). Other organisms may, however, employ HCO_3^- or other types of dissolved Ci transporters to meet their metabolic needs.

1.5.2 Classification of Enzymatic Mechanism of Carbonic Anhydrases

The CA superfamily of enzymes is ubiquitous in nature and can be found in representative organisms from all three domains of life (Aspatwar *et al*., 2022; Capasso & Supuran, 2015; Smith & Ferry, 2000; Smith *et al*., 1999). At present, eight gene families of CAs have been identified within the CA superfamily, which is designated by the Greek alphabet letters α, β, γ, δ, ζ, η, θ, ι (Capasso, 2023). The eight CA families are phylogenetically unrelated and possess low sequence and structural similarity to each other. The reaction mechanism employed by each CA family is, however, highly conserved in all eight families, and the metal-binding and active site residues display similar geometries. Since the distribution of some CA superfamily members is limited to specific domains or kingdoms, the CA families are thought to have arisen independently and have developed similar functions and mechanisms through a process of convergent evolution (Aspatwar *et al*., 2022; Capasso & Supuran, 2015; Smith & Ferry, 2000; Smith *et al*., 1999). As metalloenzymes, the CAs are dependent on the presence of metal-ion cofactors in their catalytic site for activity (Capasso, 2023; Nocentini *et al*., 2023; Smith & Ferry, 2000). The metal-ion cofactors (e.g., Zn^{2+}) present in CAs are essential for the coordination of water (H_2O) (**Figure 1.2,** 1), which serves as one ligand in the reaction. Once the oxygen atom of H_2O is coordinated with the positively charged metal-ion cofactor (Zn^{2+}-H_2O), it is deprotonated to form a hydroxide ion (Zn^{2+}-OH^-) (**Figure 1.2,** 2). The OH^- subsequently initiates a nucleophilic attack on the carbonyl group of incoming CO_2 (**Figure 1.2,** 3), converting it into HCO_3^- (**Figure 1.2,** 4**;** Zn^{2+}- HCO_3^-), which is subsequently released

from the enzyme. The cofactor subsequently binds to another H_2O molecule to repeat the catalytic cycle.

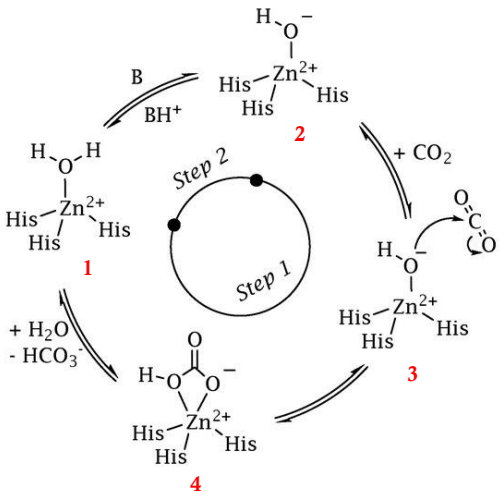

Figure 1.2. The catalytic mechanism employed by α-class CA-enzymes (Adapted from (Nocentini *et al*., 2023))

The majority of CAs, including the α-, β-, δ-, η- and θ-families, use Zn^{2+} as the metal-ion cofactor. Other CA-families can utilise metal ions other than Zn^{2+}, including Fe^{2+}, Co^{2+}, Cd^{2+}, or Mn^{2+} (Capasso, 2023; Supuran, 2016). The γ-CAs, for instance, use $Fe^{2+,}$ although they are also active with either Zn^{2+} or Co^{2+}, albeit to a lesser degree. The ζ-CAs, by contrast, display similar levels of activity with either Cd^{2+} or Zn^{2+} as a cofactor. Surprisingly, while the ι-class CA from some organisms appears to utilise Zn^{2+} as a cofactor, more recently identified representatives display activity without the need for a metal cofactor (Del Prete *et al*., 2020; Hirakawa *et al*., 2021). Irrespective of the precise cofactor, the metal ions in the catalytic site of CA-enzymes are usually coordinated by a combination of several active site amino acids. In the α-, γ- δ- and θ-class CAs, the cofactor is coordinated by three His residues, with the fourth coordination site of the metal cofactor occupied by a water molecule (H_2O) or hydroxide ion (OH^-) (see **Figure 1.2**). In the β- and ζ-class CAs, the role of the three His-residues is replaced by one His and two Cys residues, or two His and one Gln residue in the η-class CAs.

Besides differences in their primary amino acid sequence, characteristic folds, tertiary structures, and preference for metal-ion cofactors, the CA classes are also known to vary in their oligomerisation state (Capasso, 2023; Supuran, 2016). The α-class CAs are typically active as monomers and less often dimers. The β-class CAs are active either as dimers, tetramers, or octamers, and the γ-class as trimers. While the θ-class CAs are structurally similar to the β-class CAs, no information is currently available regarding their oligomerisation state, or that of members of the more recently identified δ-, ζ- and η- and ι-class CAs.

1.5.3 Natural Distribution of Carbonic Anhydrases

Members of the CA-superfamily have been identified in all three domains of life, including lower and higher eukaryotes, as well as prokaryotes within the Bacterial and Archaeal domains (Aspatwar *et al*., 2022; Capasso & Supuran, 2015; Smith & Ferry, 2000; Smith *et al*., 1999). While some prokaryotic species such as *Ricketsia, Chlamydia, Mycoplasma, Treponema* species have been found to lack identifiable homologs of CA enzymes, the majority are symbionts or obligate pathogens that possess reduced genomes and inhabit host-cell niches with high concentrations of CO_2/ HCO_3^- (or biosynthetic products derived from HCO_3^-), which negate the need for CA activity (Capasso & Supuran, 2015; Merlin *et al*., 2003; Ueda *et al*., 2012). As shown in **Figure 1.3**, the α-CAs are encoded in the genomes of animals, green plants, yeast and other fungi, algae, protozoa, and bacteria (Aspatwar *et al*., 2022). The CAs found in mammals all belong to the α-CA gene family, with ~15 different isoforms having been identified to date (Aspatwar *et al*., 2022). These isoforms typically possess different cellular functions, localisation, and expression profiles. The β-CAs are found in prokaryotic bacterial and archaeal species, as well as eukaryotic fungi, algae, green plants, protozoans, and invertebrates such as arthropods and nematodes. The γ-CAs have, likewise, been found in both bacterial and archaeal species, as well as plants and some protists, such as diatoms and protozoans. The δ-, ζ- η-, and θ-CAs, by contrast, appear to be restricted mainly to either diatoms or protozoans, while representatives of the ι-CAs have, to date, only been identified in some bacterial and diatom species.

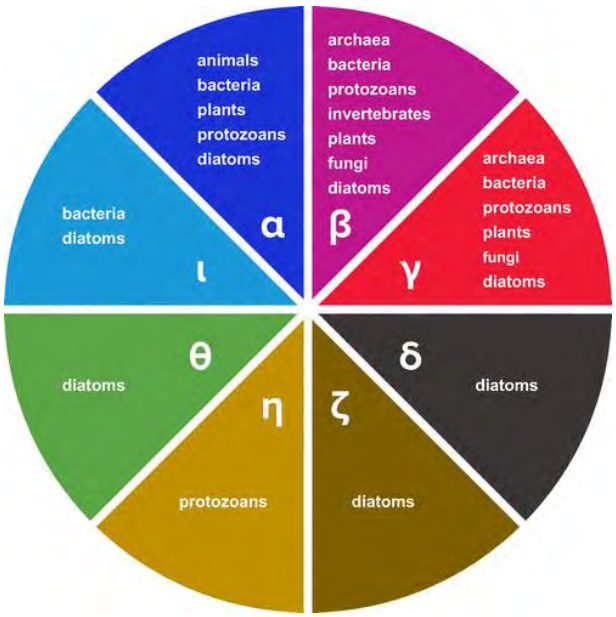

Figure 1.3 Natural Distribution of Carbonic Anhydrases amongst organisms comprising the three domains of life (adapted from Aspatwar *et al*., 2022).

1.5.4 Physiological roles of CAs in microbes

The reactants of CA-catalysed reactions (CO_2, HCO_3^- and H^+) play important roles in a variety of biological processes (Casey, 2006; Supuran, 2024, 2018; Tresguerres *et al*., 2010). In the presence of CA activity, CO_2 can be rapidly converted into its hydrated form, HCO_3^-, which rapidly dissociates into HCO_3^- and H^+ (Tresguerres *et al.,* 2010). At physiological pH values, HCO_3^- is consequently present at concentrations 20× higher than CO_2. As a gas, CO_2 is highly soluble in aqueous solutions and lipids, and can diffuse across the biological membranes of most cells, organelles, and vacuoles relatively easily. CO_2 is also the product of aerobic respiration and is usually present in significant amounts within metabolically active, aerobically grown cells (Merlin *et al.*, 2003). For many metabolic reactions, such as those catalysed by biosynthetic carboxylase enzymes, Ci needs to be present as HCO_3^- to be utilised (Supuran, 2018). To prevent the loss of CO_2 from cells (or the lumen of cellular vacuoles and organelles), CO_2 must be converted to HCO_3^-. While HCO_3^- is soluble in aqueous solutions, it is negatively charged and also has low solubility in lipids (Casey, 2006; Tresguerres *et al*., 2010). HCO_3^- is, therefore, unable to cross biological membranes without the aid of dedicated HCO_3^- transporters. The activity of CAs is therefore important to retain Ci, which may otherwise be lost as CO_2 from the cytoplasm or other compartments (e.g., periplasm, chloroplasts, carboxysomes) of cells (Tresguerres *et al*., 2010; Supuran 2024). In general, the requirement for CA-activity in bacterial species is limited to environments with low CO_2 concentrations, where the quantity of HCO_3^- formed spontaneously is below the levels needed to meet the metabolic demands of the cells. These include CO_2 concentrations commonly found in the atmosphere or in marine or freshwater environments. At high CO_2 concentrations, such as those encountered physiologically, CA activity is often dispensable, since sufficient quantities of HCO_3^- is formed spontaneously.

As discussed above, CAs often act to ensure an adequate supply of HCO_3^- for use as substrates in downstream reactions. One such group of enzymes are the bicarbonate-dependent carboxylases (BDC), which are required for the biosynthesis of several important metabolites, including intermediates of the TCA cycle, amino acids, nucleotides, and fatty acids (Mitsuhashi *et al*., 2004; Merlin *et al*., 2003; Supuran, 2016). Two BDCs that utilise HCO_3^- as a substrate are Pyruvate Carboxylase (PC) and Phosphoenolpyruvate (PEP) Carboxylase (PEPC), which are responsible for the anaplerotic replenishment of the TCA intermediate, oxaloacetate (OAA), from pyruvate and PEP, respectively (Chegwidden *et al*., 2000; Supuran, 2018/6). Given OAAs central role in metabolism, the activities of CAs, PC and PEPC are thought to

regulate flux through several central metabolic pathways. These include the TCA cycle, glycolysis, and gluconeogenesis, as well as the synthesis of the Asp-family amino acids, which are derived from OAA (i.e., Asp, Thr, Lys, Met, Ile). Other notable BDC enzymes include (i) the *purE*-encoded 17hosphor-ribosyl aminoimidazole (AIR) carboxylase, which catalyses the carboxylation of AIR to 17hosphor-ribosyl aminoimidazole-carboxylic acid in the *de novo* purine biosynthesis pathway; (ii) the *carAB*-encoded carbamoyl phosphate (CP) synthetase, which catalyse the carboxylation of ATP to form carboxyl-phosphate, for *de novo* biosynthesis of arginine, citrulline, ornithine and pyrimidines, (iii) the *accABCD* encoded acetyl-CoA carboxylase (ACC), which catalyses the conversion of acetyl-CoA to malonyl-CoA, the first committed step in FA biosynthesis, and (iv) propionyl-CoA carboxylase (PCC), which catalyses the carboxylation of propionyl-CoA to methyl malonyl-CoA.

In addition to providing HCO_3^- for carboxylation reactions, many autotrophic microbes employ CAs to ensure an adequate supply of CO_2 for use in photosynthesis, particularly in CO_2-limiting, alkaline, aquatic environments where the majority of Ci exists primarily as HCO_3^-, which cannot freely diffuse into cells (Badger, 2003; Casey, 2006; DiMario *et al.*, 2018). The CAs of microbes that inhabit these environments (e.g., algae, diatoms, cyanobacteria) can exist as extracellular CAs (eCAs) in the cell wall or periplasmic space, or as intracellular CAs (iCAs) in the cell's cytoplasm, or membranes or lumen of photosynthetic organelles such as chloroplasts or cyanobacterial carboxysomes (DiMario *et al.*, 2018). The eCAs function primarily to convert environmental HCO_3^- to CO_2 close to the plasma membrane. This facilitates CO_2 diffusion into the cytoplasm of the cell, where it can serve as a substrate for ribulose-1,5-bisphosphate carboxylase/oxygenase (RubisCO), which catalyses the fixation of CO_2 to ribulose-1,5-bisphosphate (RuBP) that is subsequently converted to two molecules of 3-phosphoglycerate (Badger, 2003). eCAs also function to recover leaked CO_2 from the cell and convert it to HCO_3^-, thereby preventing the loss of Ci. Other photosynthetic microbes possess Ci transporters, which they use to import HCO_3^- directly into the cytoplasm of cells (Price, 2011). Their iCAs then convert the imported HCO_3^- to CO_2 for subsequent CO_2 fixation by RubisCO-containing organelles.

Some microbes such as *Vibrio cholerae* and *Helicobacter pylori* can, depending on the localisation of the enzyme, use CAs to modulate the pH of the extracellular or intracellular environment (Kostiuk *et al*., 2023; Marcus *et al*., 2005). iCAs can buffer the intracellular pH through the production or utilisation of HCO_3^-, which either produces or consumes protons to increase or decrease the pH, respectively (Smith & Ferry, 2000). eCAs located in the periplasm

or cell surface can, by contrast, modulate the pH found within the periplasm space or extracellular environment, respectively. Some microbes possess multiple CAs, which can be used to modulate pH in both intracellular and extracellular locations. *Leishmania major* uses its iCA (LmCA1) to reduce its cytoplasmic pH by consuming protons using HCO_3^- as a substrate (Pal *et al*., 2017). This produces H_2O and CO_2, which is released from the cell. The organism then uses its periplasmic eCA (LmCA2) to convert the released CO_2 back into HCO_3^-, which is transported back into the cell's cytoplasm for reuse by LmCA1 using an HCO_3^- transporter.

1.5.5 Carbonic Anhydrases in Mtb

Mtb has three CAs that belong to the β-CA gene family and are encoded by the Rv3588c, Rv1284 and Rv3273 genes, respectively (Aspatwar *et al*., 2019). For the purposes of this study, the CA-encoding genes will be referred to as *Mtb canA* (Rv3588c), *canB* (Rv1284) and *canC* (Rv3273c), respectively, and their encoded gene products, *Mtb* CanA, CanB and CanC. The CanA, CanB, and CanC polypeptides contain 207, 163 and 761 aa residues, respectively (Covarrubias *et al*., 2005). All three *Mtb* CAs display features characteristic of the β-family of CAs, including all of the conserved active-site Cys and His residues that coordinate the Zn^{2+} cofactor. While CanA is thought to function as a cytoplasmic enzyme, both CanB and CanC have been shown to associate with the plasma membrane following fractionation and may, therefore, function as surface-associated enzymes (de Souza *et al.*, 2011). The three CA enzymes have been purified as recombinant enzymes in *E. coli* and display Zn-dependent CA activity in biochemical assays performed *in vitro* (Nienaber *et al*., 2015; Aspatwar *et al*., 2018). The CanA enzyme displays the greatest similarity (% identity; % similarity) to the extensively characterised and widely distributed β-CA enzymes of *E. coli* (*Ec*CanA, 213 aa) and other bacterial species, many of which have been shown to be essential for bacterial growth and/or survival at low, but not high CO_2 concentrations (Capasso & Supuran, 2015; Merlin *et al*., 2003; Ueda *et al*., 2012). The recombinant CanA enzyme displays the highest catalytic activity for CO_2 hydration reaction among the three *Mtb* CAs (Carta *et al.,* 2009), leading to the proposal that it may serve as the primary CA in *Mtb* under standard, aerobic growth conditions (Carta *et al.,* 2009). Based on the results of genome-wide essentiality screens, the requirement for CanA activity for *Mtb* growth *in vitro* and *in vivo* is, however, equivocal. Using transposon mutagenesis, the *canA* (Rv3588c) gene was classified as non-essential for the *in vitro* growth of *Mtb* during growth on both rich (Minato *et al.,* 2019) and minimal 7H10 agar medium (Sassetti *et al.,* 2003; Lamichhane *et al.,* 2003; DeJesus *et al.* 2017, Bosch *et al.,* 2021). The

gene was, by contrast, classified as essential for growth on both glycerol and cholesterol-containing medium in the genome-wide essentiality screen by Griffin *et al.,* (2011). CanA activity was also shown to be required for the growth of *Mtb* in C57BL/6J mice (Sassetti & Rubin, 2003), suggesting that the enzyme is required for virulence. Using CRISPRi-based approaches, two recent studies demonstrated that a *canA* knockdown (KD) mutant is attenuated *in vitro* and following infection of murine macrophages, supporting the idea that the enzyme's activity is required for the growth and/or survival of *Mtb* cells (Dechow *et al*., 2022; Degiacomi *et al*., 2023).

The *Mtb* CanB displays lower enzymatic activity than either CanA or CanC when assayed under standard (aerobic) conditions (Carta *et al*., 2009; Nishimoria *et al*., 2010). The enzyme was subsequently shown to be regulated in a redox-dependent manner, which reduces its activity when assayed aerobically (Nienaber *et al*., 2015). Following exposure to oxidising conditions, an active site Cys residue (Cys^{35}) forms a disulphide bond with a non-active site Cys residue (Cys^{61}), which leads to the loss of the enzymes Zn^{2+}-ion and catalytic activity (Nienaber *et al*., 2015). The redox-dependent loss of CanB activity was shown to be reversible, however, and could be regained following exposure to reducing conditions. Since the hydration of CO_2 results in the production of protons, the authors proposed that the regulation of CanB activity may provide the cell with a means of increasing or decreasing the pH under reducing or oxidative conditions, respectively (Nienaber *et al*., 2015). To date, this mode of regulation has been demonstrated for the recombinant CanB enzyme assayed *in vitro* and its physiological relevance, if any, for the growth of *Mtb in vitro* or *in vivo* remains unknown. Like CanA, CanB activity has been shown to be dispensable for the growth of *Mtb in vitro* (Lamichhane *et al.,* 2003; DeJesus *et al.,* 2017, Minato *et al.,* 2019; Bosch *et al.,* 2021), but essential in others (Sassetti *et al.,* 2003). CanB mutants are also attenuated during infection of C57BL/6J mice (Sassetti & Rubin, 2003), although no attenuation was observed for a *Mtb canB* CRISPRi-KD strain during infection of macrophages *ex vivo* (Dechow *et al.,* 2022).

The 764 aa CanC is the largest of the three mycobacterial CAs. The protein is comprised of two domains: (i) an N-terminal transmembrane domain composed of 11 predicted transmembrane helices at its N-terminus (aa 121–414) and (ii) a β-CA domain (aa 571–741) at its C-terminus (Nishimori *et al*., 2009). The N-terminal domain displays similarity to the SulP permease family of proteins, which are involved in the transport of inorganic anions. The linkage of the SulP-like domain to a functionally active β-CA domain has led to the suggestion that CanC may play a role in promoting the transport of HCO_3^- across the plasma membrane,

as has been observed in other bacterial species (Price *et al.,* 2004; Du *et al*., 2014; Rose & Bermudez, 2016). In contrast to CanA and CanB, which have orthologues present in both slow- and fast-growing mycobacterial species, including *Msm*, CanC orthologues are limited to a number of species, the majority of which are pathogenic members of the MTBC or NTM (e.g. *Mtb*, *M. africanum, M. bovis, M. avium, M. abseccus)*. This raises the possibility that CanC may play a specialised role in ensuring the survival of mycobacterial strains within environments encountered during infection of their human or animal hosts. The genetic inactivation of CanC, however, has no effect on the growth and survival of *Mtb* following infection of macrophages (Dechow *et al.,* 2022) or mice (Sassetti & Rubin, 2003). Multiple studies have also failed to reveal a phenotype associated with *canC* inactivation during growth *in vitro* (Sassetti *et al.,* 2003; Lamichhane *et al.,* 2003; DeJesus *et al.,* 2017, Minato *et al.,* 2019; Bosch *et al.,* 2021). The precise physiological role of the CanC enzyme in mycobacterial species, therefore, remains unclear.

1.6 Motivation

As discussed above, CAs are a widely distributed family of enzymes that have been shown to mediate a wide variety of roles in different microbial species. While the three *Mtb* CAs have been characterised with regard to their structure, biochemical activity and inhibition by small molecules (Covarrubias *et al*., 2005; Nishimori *et al*., 2010; Carta *et al*., 2009; Nienaber *et al*., 2015; Apsatwar *et al*., 2019), their exact role(s) in the physiology and metabolism of *Mtb* have not been established to date. The essentiality of the CA enzymes for the growth of *Mtb in vitro* and *in vivo,* and hence their usefulness as potential drug targets, has not been unequivocally established. The MSMEG_6082 and MSMEG_4985 genes of *Msm* are predicted to encode 206 and 163 aa proteins with 72% (85%) and 79% (89%) identity (similarity) to the *Mtb* CanA (207 aa) and CanB (163 aa) enzymes, respectively. To gain a better understanding of the role(s) of CanA and CanB enzymes in the physiology of mycobacterial species, we used a genetic approach to examine the essentiality of the putative *Msm* CanA and CanB under various environmental conditions relevant to CA function. This was accomplished by completing the experimental objectives listed below.

1.7 Experimental Aims and Objectives

1. Generate *Msm canA* (MSMEG_6082) and *canB* (MSMEG_4985) knockdown (KD) strains using CRISPR interference (CRISPRi).
2. Determine the essentiality of the *canA* and *canB* genes for *Msm* growth and survival by examining the effects of gene silencing under different environmental conditions relevant to the known functions of CA enzymes (e.g. low and high CO_2 concentrations, different pH values).
3. Determine the essentiality of the *Msm canA* (MSMEG_6082) and *canB* (MSMEG_4985) genes by generating knockout (KO) strains using mycobacterial recombineering.
4. Compare the growth of the WT *Msm* with that of the *canA* and *canB* KO strains (if viable) to validate the results obtained using the KD mutants.

Chapter 2: Materials and Methods

2.1 Bacterial Strains

All bacterial strains and plasmids used in this study are listed in **Table 2.1**. *E. coli* Mach1 and Top10 cells were obtained from ThermoFisher Scientific and used for the routine cloning, isolation and/or maintenance of plasmids. The electroporation-proficient *Msm* mc^2155 strain (Snapper *et al*., 1990) was utilised for all mycobacterial work, including the generation of the KD and KO mutants. All chemicals and reagents used in this study are listed in the **Supplementary Material, Table A1**.

2.2 Bacterial Growth Conditions

All *E. coli* strains were routinely grown in liquid Lysogeny Broth (LB) [1% Tryptone, 0.5% Yeast Extract, and 1% NaCl (w/v)] under aerobic conditions with shaking (180 rpm), or on solid LB Agar medium (LA) [LB broth, 1.5% agar (w/v)]. Unless otherwise specified, cells were grown at 37 °C. Where applicable, antibiotics were added to the following final concentrations: ampicillin (Amp) at 100 μg/mL, hygromycin (Hyg) at 200 μg/mL, kanamycin (Kan) at 50 μg/mL and zeocin (Zeo) at 100 μg/mL.

M. smegmatis mc^2155 (wild-type [WT]) and mutant strains were routinely grown under aerobic conditions at 37 °C in Middlebrook 7H9 medium (BD Difco) supplemented with 0.2% (v/v) glycerol, 0.2% (w/v) glucose, 0.85% (w/v) NaCl and 0.05% (v/v) Tween 80 or on solid Middlebrook 7H10 agar supplemented with 0.5% (v/v) glycerol, 0.2% (w/v) glucose and 0.85% (w/v) NaCl, unless otherwise specified. Where applicable, antibiotics were added to the growth medium at the following final concentrations: Hyg at 50 μg/mL, Kan at 25 μg/mL, Zeo at 12.5 μg/mL and (anhydrotetracycline) ATc at 200 ng/mL.

For the long-term storage and maintenance of the bacterial strains, cultures were grown to late exponential phase in either LB for *E. coli* or Middlebrook 7H9 medium for *Msm*. The culture was diluted 1:1 in 50% (v/v) glycerol, which served as a cryopreservant. The cells were left to equilibrate in the glycerol for 15 min at room temperature before transferring them to a -80 °C freezer. Working stocks of strains were prepared by transferring 10 μL of the frozen glycerol stocks onto the surface of appropriately supplemented Luria Agar (LA) (*E. coli* strains) or Middlebrook 7H11 agar plates (*Msm* strains), followed by streak-plating for single colonies. The plates were incubated at 37 °C for 16 h (*E. coli* strains) or 72 h (*Msm* strains) before being transferred to 4 °C or room temperature (RT) for short-term storage of up to 2 or 4 weeks, respectively. Single bacterial colonies present on the plates were used to start liquid cultures for bacterial growth assays, as described in **Section 2.8.1**.

Table 2.1 Bacterial strains and plasmids used and generated in this study

STRAINS	GENOTYPE AND RELEVANT PHENOTYPES	SOURCE / REFERENCE
E. coli		
Mach1	Δ*rec*A1*398 end*A1 *F- φ80(lacZ)ΔM15 Δlac*X74 *hsd*R*(rK-mK+) ton*A	ThermoFisher Scientific
Top10	F- *mcr*A Δ(*mrr-hsd*RMS-*mcr*BC) Φ80*lacZ* ΔM15 Δ*lac*X74 *rec*A1 *ara*D139 Δ(*ara-leu*)7697 *gal*U *gal*K *rsp*L (STR^R) *end*A1 *nup*G	ThermoFisher Scientific
M. smegmatis		
***Msm* mc²155 (*Msm* WT)**	A high-frequency transformation (electroporation-proficient) *Msm* strain. Used as the WT strain in this study.	Snapper *et al*., 1990
***Msm* WT pLJR962**	*Msm* WT harboring pLJR962 in the L5 *attB* site.	This study
***Msm canA1* KD**	*Msm* WT harbouring pLJR962::*canA*_sgRNA1 in the L5 *attB* site. Kan^R	This study
***Msm canA2* KD**	*Msm* WT harbouring pLJR962::*canA*_sgRNA2 in the L5 *attB* site. Kan^R	This study
***Msm canA3* KD**	*Msm* WT harbouring pLJR962::*canA*_sgRNA3 in the L5 *attB* site. Kan^R	This study
***Msm canB1* KD**	*Msm* WT harbouring pLJR962::*canB*_sgRNA1 in the L5 *attB* site. Kan^R	This study
***Msm canB2* KD**	*Msm* WT harbouring pLJR962::*canB*_sgRNA2 in the L5 *attB* site. Kan^R	This study
***Msm canB3* KD**	*Msm* WT harbouring pLJR962::*canB*_sgRNA3 in the L5 *attB* site. Kan^R	This study
***Msm canB4* KD**	*Msm* WT harbouring pLJR962::*canB*_sgRNA4 in the L5 *attB* site. Kan^R	This study
***Msm canB5* KD**	*Msm* WT harbouring pLJR962::*canB*_sgRNA5 in the L5 *attB* site. Kan^R	This study
***Msm mmpL3* KD**	*Msm* WT harbouring pLJR962::*mmpL3*_sgRNA in the L5 *attB* site. Kan^R	This study
***Msm* WT pJV53hyg**	*Msm* WT harbouring pJV53hyg. Recombineering proficient *Msm* strain used to generate *canA* KO strain. Che9c genes 60-61. Hyg^R	This study
Msm* WT pJV53hyg L5::pMV306kan::*canA	*Msm* WT pJV53hyg harbouring pCanA, which expresses a second copy of the *canA* gene from its native promoter. Used to generate *canA* KO strain. Hyg^R Kan^R	This study
Msm* Δ*canA*::Zeo^R pJV53hyg L5::pMV306kan::*canA	Zeo^R-marked *canA* deletion mutant derived from *Msm* WT pJV53hyg L5::pMV306kan::*canA*. Hyg^R, Kan^R, Zeo^R	This study
Msm* Δ*canA*::Zeo^R L5::pMV306kan::*canA	Zeo^R-marked *canA* deletion mutant derived from *Msm* WT pJV53hyg L5::pMV306kan::*canA*. Hyg^R, Kan^R, Zeo^R	This study
Msm* Δ*canA*::Zeo^R L5::pMV306kan::*canA	Zeo^R-marked *canA* deletion mutant derived from *Msm* WT pJV53hyg L5::pMV306kan::*canA* Cured of the temperature-sensitive pJV53hyg. Kan^R Zeo^R	This study
Msm* Δ*canA* L5::pMV306kan::*canA	Unmarked *canA* deletion mutant derived from *Msm* Δ*canA*::Zeo^R L5::pMV306kan::*canA*. Cured of the temperature-sensitive pJV53hyg. Kan^R Zeo^R	This study
***Msm* WT pJV53kan**	*Msm* WT harbouring pJV53kan. Recombineering proficient *Msm* strain used to generate *canB* KO strain. Che9c genes 60-61. Used to generate *canB* KO strain. Kan^R	This study
***Msm* Δ*canB*::Zeo^R pJV53kan**	Zeo^R-marked *canB* deletion mutant derived from *Msm* WT pJV53kan. Kan^R, Zeo^R.	This study
***Msm* Δ*canB*::Zeo^R**	Zeo^R-marked *canB* deletion mutant derived from *Msm* Δ*canB*::Zeo^R. pJV53kan.- Cured of the temperature-sensitive pJV53kan. Zeo^R	This study
Msm* Δ*canB	Unmarked *canB* deletion mutant derived from *Msm* Δ*canA*::Zeo^R. Antibiotic sensitive.	This study
Msm* Δ*canB* L5::pMV306kan::*canB	*Msm* Δ*canB* harbouring **L5::pMV306kan::*canB***, which expresses the WT *canB* gene from its native promoter. Kan^R	This study

PLASMIDS	DESCRIPTION	SOURCE / REFERENCE
CRISPRi Vectors		
pLJR962	Low copy, integrative (L5) vector that expresses a *Sth*1 *dCas9* enzyme from an anhydrotetracycline (ATc)-inducible promoter, L5 Integrase, Kan^R	(Rock *et al*., 2017)
pLJR962::*canA* sgRNA1	Low copy, integrative (L5) vector that expresses a *Sth*1 *dCas9* enzyme and *Msm canA*_sgRNA1 from ATc-inducible promoters, L5 Integrase, Kan^R.	This study
pLJR962::*canA* sgRNA2	Low copy, integrative (L5) vector that expresses a *Sth*1 *dCas9* enzyme and *Msm canA*_sgRNA2 from ATc-inducible promoters, L5 Integrase, Kan^R.	This study
pLJR962::*canA* sgRNA3	Low copy, integrative (L5) vector that expresses a *Sth*1 *dCas9* enzyme and *Msm canA*_sgRNA3 from ATc-inducible promoters, L5 Integrase, Kan^R	This study
pLJR962::*canB* sgRNA1	Low copy, integrative (L5) vector that expresses a *Sth*1 *dCas9* enzyme and *Msm canB*_sgRNA1 from ATc-inducible promoters, L5 Integrase, Kan^R	This study
pLJR962::*canB* sgRNA2	Low copy, integrative (L5) vector that expresses a *Sth*1 *dCas9* enzyme and *Msm canB*_sgRNA2 from ATc-inducible promoters, L5 Integrase, Kan^R	This study
pLJR962::*canB* sgRNA3	Low copy, integrative (L5) vector that expresses a *Sth*1 *dCas9* enzyme and *Msm canB*_sgRNA3 from ATc-inducible promoters, L5 Integrase, Kan^R	This study
pLJR962::*canB* sgRNA4	Low copy, integrative (L5) vector that expresses a *Sth*1 *dCas9* enzyme and *Msm canB*_sgRNA4 from ATc-inducible promoters, L5 Integrase, Kan^R	This study
pLJR962::*canB* sgRNA5	Low copy, integrative (L5) vector that expresses a *Sth*1 *dCas9* enzyme and *Msm canB*_sgRNA5 from ATc-inducible promoters, L5 Integrase, Kan^R	This study
pLJR962::*mmpL3* sgRNA1	Low copy, integrative (L5) vector that expresses an *Sth*1 *dCas9* enzyme and *Msm mmpl3*_sgRNA from ATc-inducible promoters, L5 Integrase, Kan^R.	This study
Generation of Knock-Out Vectors		
pJV53kan	High copy number vector that encodes Che9c 60-61 under the control of an acetamidase promoter for mycobacterial recombineering, Kan^R.	(van Kessel & Hatfull, 2007)
pJV53hyg	High copy number vector that encodes Che9c 60-61 under the control of an acetamidase promoter for mycobacterial recombineering, Hyg^R.	This study
pML1342	High-copy number vector that integrates at the mycobacteriophage L5 site for mycobacterial gene switching, Hyg^R.	(Huff *et al*., 2010)
pML2714	A temperature-sensitive vector that expresses Cre recombinase for mycobacterial recombineering, Kan^R.	(Ofer *et al*., 2012)
pMSG360Zeo	Low copy number vector that contains a Zeo^R cassette flanked by two *lox*P sites for mycobacterial recombineering, Zeo^R.	(Barkan *et al*., 2010)
Generation of Complementation Vectors		
pMV306hsp	Low copy number, integrative vector, Kan^R.	(Zelmer *et al*., 2010)
pMV306kan::*canA*	*Msm canA* gene and its native promoter cloned into pMV306hsp, Kan^R.	This study
pMV306kan::*canB*	*Msm canB* gene and its native promoter cloned into pMV306hsp, Kan^R.	This study

2.3 Nucleic Acid Isolation, Purification, and Quantification

2.3.1 DNA Isolation, Purification, and Quantification

DNA from *E. coli* was isolated and purified using commercial kits according to the manufacturer's instructions. Genomic DNA (gDNA) was extracted using the GeneJet Genomic DNA Purification Kit (ThermoFisher Scientific). Plasmids were purified using the GeneJet MiniPrep Kit (ThermoFisher Scientific) or E.Z.N.A Plasmid DNA Mini Kit (Omega Bio-tek). PCR products and other linearised DNA fragments were purified using the GeneJet PCR Purification Kit (ThermoFisher Scientific). When necessary, DNA fragments were electrophoresed through 0.8% agarose gel using agarose gel electrophoresis (AGE) and removed by excision using a scalpel blade following visualisation using a blue light transilluminator (IORodeo; 470 nm). The DNA within the excised gel fragment was purified using the Silica Bead Gel Purification Kit (ThermoFisher Scientific).

2.3.2 RNA Isolation, Purification and Quantification

Msm was grown in 7H9 Middlebrook media to mid-exponential phase (OD_{600} ~0.6) and harvested by centrifugation at 2000 × g for 5 min at RT. The cell pellet obtained was resuspended in 1 mL TRIzol (ThermoFisher Scientific) or TRI Reagent (Zymo Research) and stored at -80 °C for later use. The cells were homogenised with 0.1 mm acid-washed glass beads (Sigma-Aldrich) in a BeadBug 3 Microtube Homogeniser (Benchmark Scientific) at 6000 rpm for 30 s (4 times with 30 s cooling intervals). The samples were centrifuged at 13, 400 × g for 2 min at 4 °C and the supernatant transferred into a clean tube containing an equal volume of 100% ethanol. The RNA included in the samples was purified using the Direct-zol RNA MiniPrep kit (Zymo Research). To eliminate any gDNA contamination, an on-column treatment with DNase I was performed as described by the manufacturer's protocol (Zymo Research), followed by treatment of the eluted nucleic acids with the Rapid Out DNA Removal Kit (ThermoFisher Scientific). The absence of gDNA contamination in RNA preparations was confirmed by the absence of PCR amplicons in reactions that had not been reverse transcribed into cDNA prior to performing semi-quantitative RT-PCR or quantitative PCR (qPCR) reactions.

2.3.3 Nucleic Acid Quantification

DNA and RNA concentrations were quantified by measuring the absorbance of samples at a wavelength of 260 nm using a Nanodrop ND-1000 Spectrophotometer (ThermoFisher Scientific). A conversion factor of 50 ng and 33 ng was used for single-stranded nucleic acids (RNA) or double-stranded nucleic acids (DNA), respectively. The purity of nucleic acids was determined by calculating the ratio of absorbances measured at 260/280 nm or 260/230 nm,

which serve as indicators of potential contamination with RNA or organic salts, respectively. The concentration of purified DNA fragments used to generate recombinant DNA molecules was confirmed by comparing the intensity of ethidium-bromide-stained DNA molecules with that of known quantities of DNA present in DNA ladders (**Supplementary Material, Figure B1**) following AGE and visualisation under ultraviolet (UV) light (**Section 2.7**, below).

2.4 General Recombinant DNA Procedures

All recombinant DNA and molecular biology techniques were performed according to standard protocols (Ausubel *et al*., 2003; Sambrook & Russell, 2001) unless otherwise specified. All restriction and modification enzymes, kits and reagents (**Appendix A**) were used as per the manufacturer's instructions, unless otherwise specified.

2.4.1 Restriction Endonuclease Digestion of DNA

Restriction endonuclease (RE) digestion of DNA was performed using Anza (ThermoFisher Scientific) or FastDigest (ThermoFisher Scientific) restriction endonuclease enzymes as per the manufacturer's instructions. Analytical restriction enzyme digests were performed using 1 µg of plasmid DNA, 1 µL of each restriction enzyme (10 U/µL), 1 × restriction enzyme buffer and ultrapure, nuclease-free dH_2O (Gibco) to a final volume of 30 µL. Preparative restriction enzyme digests were performed with 1 to 3 µg of plasmid DNA or PCR product, 1 µL of each restriction enzyme (10 U/µL) per 1 µg DNA, 1 × restriction enzyme buffer and ultrapure, nuclease-free dH_2O (ThermoFisher Scientific) to a final volume of 30 to 90 µL and incubated at 37 °C for 1 to 16 h. Following incubation, the samples were analysed using AGE (**Section 2.7**) and/or purified (**Section 2.4.1**) in order to prepare the samples for subsequent use in downstream applications.

2.4.2 Enzymatic Modification of DNA

All DNA modification processes were performed as per the manufacturer's instructions. In order to prevent re-ligation of plasmids following restriction enzyme digestion with blunt- or compatible sticky-ends, the plasmids were treated with FastAP Thermosensitive Alkaline Phosphatase (ThermoFisher Scientific). The reactions were performed by adding 1 × FastAP or RE buffer, 1 µL FastAP, 1 µg DNA, and ultrapure, nuclease-free dH_2O (ThermoFisher Scientific) in a final reaction volume of 20 µL and incubated at 37 °C for 15 min. The dephosphorylated vector was purified (**Section 2.2.1**) prior to its use in ligation reactions. The DNA fragments possessing sticky ends were converted to blunt-ended fragments through the use of the Anza DNA End Repair Kit (ThermoFisher Scientific). The reactions were carried out by combining 1 × Anza End Repair buffer, 1 µL Anza DNA End Repair Mix, 1 µg of DNA

and ultrapure, nuclease-free water to a final volume of 20 µL. The resulting mixture was incubated at 20 °C for 15 min and then purified for subsequent use in downstream applications. The PCR products that lacked 5'-phosphate groups were subjected to phosphorylation prior to being ligated into dephosphorylated vectors. This was achieved using the Anza T4 PNK 5' Phosphorylation Kit (ThermoFisher Scientific). The reactions were carried out by combining 1 × Anza PNK buffer, 1 µL Anza T4 PNK enzyme, 1 µg DNA, and ultrapure, nuclease-free dH_2O (ThermoFisher Scientific) to a final reaction volume of 20 µL. The reactions were incubated at 20 °C for 15 min followed by inactivation of PNK at 80 °C for 5 min. The phosphorylated vectors were used directly in ligation reactions.

2.4.3 Ligation Reactions

Cloning reactions of DNA fragments with sticky-ends were performed using a molar ratio of 3:1 (insert:vector) containing 10 ng of vector, the appropriate molar amount of the DNA insert, 10 µL Instant Sticky-End Ligase 2 × Master Mix (New England Biolabs), and the balance of the volume (to 20 µL) with ultrapure, nuclease-free dH_2O (Gibco). In certain instances, the commercial 2 × Master Mix was replaced with 2 µL T4 DNA ligase (ThermoFisher Scientific), 2 µL 10 × T4 DNA ligase buffer (ThermoFisher Scientific) and 6 µL nuclease-free dH_2O. Cloning reactions of DNA fragments with blunt-ends were performed using a molar ratio of 3:1 (insert:vector) containing 10 ng of vector, the appropriate molar amount of the DNA insert, 5 µL Anza T4 DNA Ligase Master Mix (4 ×) and the balance of the volume (to 20 µL) with ultrapure, nuclease-free dH_2O (Gibco).

2.5 PCR Amplification Procedures

The oligonucleotides used for plasmid construction, strain verification and real-time quantitative PCR can be found in **Table 2.2**. The sequence of oligonucleotides was based on that of the *Msm* mc^2155 genome (GenBank CP000480.1) and were manufactured by Inqaba Biotec (South Africa), ThermoFisher Scientific (UK) or Metabion (Germany). The Applied Biosystems SimpliAmp (ThermoFisher Scientific) or MultiGene Mini Personal (Labnet International) thermal cyclers were used to perform all PCR reactions.

2.5.1 Analytical PCR Reactions

Analytical PCR reactions were performed using Taq DNA Polymerase with commercially available 2 × PCR master mixes [KAPA Taq Ready Mix (Sigma) or Taq Master Mix (New England Biolabs)]. The PCR reactions were carried out in 25 µL reactions consisting of 12.5 µL of the 2 × Taq Master Mix, 0.3 µM of the forward and reverse primers, 2.5 µL DNA-containing solution, and 7.5 µL nuclease-free dH_2O. PCR was performed with the specified

thermocycling parameters which included: (i) initial denaturation at 95 °C for 4 min, (ii) denaturation at 95 °C for 30 s (repeated for a total of 30 cycles), (iii) annealing of the primers at the appropriate temperature for the specific primer pair being used for 30 s, (iv) extension at 72 °C for 45 s per kb and (v) a final extension at 72 °C for 7 min. The annealing temperatures were determined by calculating the melting temperatures (Tm) of the forward and reverse primers, in accordance with the guidelines provided by the manufacturer (**Table 2.3**).

2.5.2 Preparative PCR Reactions

The PCR amplification of DNA fragments for the purpose of generating recombinant plasmids or allelic exchange substrates (AES) was carried out using the Phusion High-Fidelity PCR Kit (ThermoFisher Scientific) as per the manufacturer's instructions. The PCR reactions were carried out in 50 µL consisting of 10 µL 5 × HF buffer, 0.3 µM forward and reverse primers, 200 µM deoxynucleotide triphosphates (dNTPs), 10 to 100 ng of template DNA, 0.5 µL of Phusion DNA polymerase, and the balance of the volume (to 50 µL) with nuclease-free dH_2O (ThermoFisher Scientific). To facilitate the amplification of genes that possess a high G+C content (>55%), the HF buffer was substituted with a 5 × GC buffer. Additionally, DMSO was added to a final concentration of 3% (v/v). PCR was performed with the specified thermocycling parameters which included (i) initial denaturation at 98 °C for a duration of 3 min; (ii) denaturation at 98 °C for 20 s (repeated for a total of 30 cycles); (iii) annealing of the primers was performed at the appropriate temperature for the specific primer pair being used, with a duration of 30 s; (iv) extension at 72 °C for 30 s per kb, and lastly, (v) a final extension at 72 °C for 7 min. The annealing temperatures were determined by calculating the melting temperatures (Tm) of the forward and reverse primers, in accordance with the guidelines provided by the manufacturer (**Table 2.3**).

2.5.3 Colony PCR Reactions

Colony PCR was used to confirm the construction of plasmids and mutant strains using cell lysates as described previously (Woodman *et al.*, 2016). For *E. coli*, the bacteria were grown in microcentrifuge tubes in 100 µL of LB supplemented with the necessary antibiotics and incubated at 37 °C for 4 to 16 h. The cells were harvested by centrifugation at 13, 400 × g for 1 min and the supernatant was discarded. The cell pellets were resuspended in 100 µL nuclease-free dH_2O and lysed by boiling at 100 °C for 10 min. The lysed cells were centrifuged at 13, 400 × g for 2 min to remove any cell debris. The DNA-containing supernatant was transferred to a sterile microcentrifuge tube and 2.5 µL used in 25 µL analytical PCR reactions as described above (**Section 2.4.2**). For *Msm*, bacterial colonies were resuspended in 200 µL nuclease-free

water containing 5% (v/v) Chelex 100 Resin (200-400 mesh, Bio-Rad) as described previously (Singer-Sam *et al.,* 1989). The resuspended cells were boiled at 100 °C for 10 min, centrifuged at 13, 400 × g for 2 min, and 2.5 µL used in 25 µL in analytical PCR reactions as described above (**Section 2.4.2**).

2.5.4 Reverse Transcriptase and Real-Time Quantitative PCR (qPCR)

First-strand cDNA synthesis was performed by reverse transcribing 250 ng of purified RNA **(Section 2.2.2)** using either the Superscript IV VILO Mastermix (ThermoFisher Scientific) or LunaScript RT Supermix (New England Biolabs). Semi-quantitative PCR reactions were carried out in 25 µL volumes using gene-specific primers and 2 µL cDNA as a template, as described previously (**Section 2.6.2**). Real-time quantitative PCR (qPCR) reactions were performed in 20 µL volumes containing 10 µL of the Luna Universal qPCR Master Mix (New England Biolabs), 0.5 µM of gene-specific forward and reverse primers (0.5 µL each) and 2 µL of cDNA as a template. qPCR reactions were performed using the Bio-Rad CFX96 Connect RT-PCR Detection System with the following conditions: (i) initial denaturation at 95 °C for 1 min; (ii) 40 cycles of denaturation at 95 °C for 15 s; (iii) annealing and extension at 60 °C for 30 s. The efficiency of all primer pairs were validated (90 to 110% efficiency) against a standard curve generated in qPCR reactions using 3 µL of a 10-fold dilution series of *Msm* gDNA (1 to 1 000 000 pg DNA) as a template. The gene expression levels were normalised relative to the *Msm sigA* gene and calculated using the 2-ΔCt or 2-ΔΔCt method (Livak and Schmittgen, 2001; Schmittgen and Livak, 2008).

Table 2.2 List of oligonucleotide primers used in this study

PRIMER NAME	PRIMER SEQUENCE (5'-3')	AMPLICON PROPERTIES / REGION TARGETED
Generation & Confirmation of *Msm* KD Mutants Using CRISPRi [a]		
pLJR-Seq-For	AAGCTCTCACCAACCGTG	Forward primer used to confirm successful cloning of sgRNAs into pLJR962.
pLJR-Seq-Rev	CTGCGTTATCCCCTGATTCTG	Reverse primer used to confirm successful cloning of sgRNAs into pLJR962.
canA-sgRNA1-For	**GGGA**GCACCTCGCCCTCGTCGAGC	Forward oligonucleotide used to generate *Msm canA*_sgRNA1.
canA-sgRNA1-Rev	**AAAC**GCTCGACGAGGGCGAGGTGC	Reverse oligonucleotide used to generate *Msm canA*_sgRNA1.
canA-sgRNA2-For	**GGGA**GCTCAACCCGGCCTTGCGTCCCA	Forward oligonucleotide used to generate *Msm canA*_sgRNA2.
canA-sgRNA2-Rev	**AAAC**TGGGACGCAAGGCCGGGTTGAGC	Reverse oligonucleotide used to generate *Msm canA*_sgRNA2.
canA-sgRNA3-For	**GGGA**GCTCAACCCGGCCTTGCGTC	Forward oligonucleotide used to generate *Msm canA*_sgRNA3.
canA-sgRNA3-Rev	**AAAC**GACGCAAGGCCGGGTTGAGC	Reverse oligonucleotide used to generate *Msm canA*_sgRNA3.
canB-sgRNA1-For	**GGGA**GCCACGTGCTTGCTGGGCGGCA	Forward oligonucleotide used to generate *Msm canB*_sgRNA1.
canB-sgRNA1-Rev	**AAAC**TGCCGCCCAGCAAGCACGTGGC	Reverse oligonucleotide used to generate *Msm canB*_sgRNA1.
canB-sgRNA2-For	**GGGA**GAACTCGTCGTCGGTGAACG	Forward oligonucleotide used to generate *Msm canB*_sgRNA2.
canB-sgRNA2-Rev	**AAAC**CGTTCACCGACGACGAGTTC	Reverse oligonucleotide used to generate *Msm canB*_sgRNA2.
canB-sgRNA3-For	**GGGA**GCCGCAGTCGGTGTGGTGGA	Forward oligonucleotide used to generate *Msm canB*_sgRNA3.
canB-sgRNA3-Rev	**AAAC**TCCACCACACCGACTGCGGC	Reverse oligonucleotide used to generate *Msm canB*_sgRNA3.
canB-sgRNA4-For	**GGGA**GGCCTCACCGTCGCCGAGGC	Forward oligonucleotide used to generate *Msm canB*_sgRNA4.
canB-sgRNA4-Rev	**AAAC**GCCTCGGCGACGGTGAGGCC	Reverse oligonucleotide used to generate *Msm canB*_sgRNA4.
canB-sgRNA5-For	**GGGA**GAGGATGATCTCCTTGGTGC	Forward oligonucleotide used to generate *Msm canB*_sgRNA5.
canB-sgRNA5-Rev	**AAAC**GCACCAAGGAGATCATCCTC	Reverse oligonucleotide used to generate *Msm canB*_sgRNA5.
mmpL3-sgRNA1-For	**GGGA**GCGACAGACTGGCTGCCCTCGTC	Forward oligonucleotide used to generate *Msm mmpL3*_sgRNA
mmpL3-sgRNA1-Rev	**AAAC**GACGAGGGCAGCCAGTCTGTCGC	Reverse oligonucleotide used to generate *Msm mmpl3*_sgRNA.
Generation & Confirmation of the *Msm* KO Mutants [b]		
pKMZeo-For	GCATGGTGGCCCGGTATA	Forward primer for the amplification of the Zeo^R cassette from pMSG360Zeo.
pKMZeo-Rev	CCGAAATCCGGTACAGTTCGA	Reverse primer for the amplification of the Zeo^R cassette from pMSG360Zeo.
canA-US-For	ACCATGTCGAGATCGCG	Forward primer for the amplification of the US fragment of the *Msm canA* gene.
canA-US-Rev	**TATACCGGGCCACCATGC**CGCTGCCACAGGATTTGA	Reverse SOE primer for the amplification of the US fragment of the *Msm canA* gene. 5' end is complementary to pKMZeo-For (underlined).
canA-DS-For	**TCGAACTGTACCGGATTTCGG**GGCGATATCGGCGAAGTC	Forward SOE primer for the amplification of the DS fragment of the *Msm canA* gene. 5' end is complementary to pKMZeo-Rev (underlined).
canA-DS-Rev	ATCGCCGACGACGTACTC	Reverse primer for the amplification of the DS fragment of the *Msm canA* gene.
canB-US-For	TACTCGGTGGAGACCGTG	Forward primer for the amplification of the US fragment and for confirming allelic exchange in the *Msm canB* knockout mutant.
canB-US-Rev	**TATACCGGGCCACCATGC**CGCCAGGTACTGATCAGTG	Reverse SOE primer for the amplification of the US fragment of the *Msm canB* gene. 5' end is complementary to pKMZeo-For (underlined).

canB-DS-For	**<u>TCGAACTGTACCGGATTTCGG</u>**AAGCTCGCCGAGGTCAC	Forward SOE primer for the amplification of the DS fragment of the *Msm canB* gene. 5' end is complementary to pKMZeo-Rev (underlined).
canB-DS-Rev	ACCGGTTCCGACGTGATG	Reverse primer for the amplification of the DS fragment and for confirming allelic exchange in the *Msm canB* knockout.
Zeo-Check-For	CATGACCGAGATCGGCGA	Forward Zeo^{R} cassette specific primer for confirming allelic exchange in the *Msm canA* and *canB* knockout mutants.
Zeo-Check-Rev	GTGTCAGTCCTGCTCCTC	Reverse Zeo^{R} cassette specific primer for confirming allelic exchange in the *Msm canA* and *canB* knockout mutants.
***Msm*-canA-For**	TTGTGCTGTCGCGCAACAC	Forward gene-specific primer for confirming allelic exchange in *Msm canA* knockout mutant.
***Msm*-canA-Rev**	AGGTGCCCGGACCGATCG	Reverse gene-specific primer for confirming allelic exchange in *Msm canA* knockout mutant.
***Msm*-canA-Comp-For**	CGACCGAGCGCAACGCGTGCACCATGTCGAGATCGCGC	Forward primer used for amplifying the *Msm canA* gene and its native promoter.
***Msm*-canA-Comp-Rev**	TAACTACGTCGACATCGATATCGGGATCCCGAGCTGCTG	Reverse primer used for amplifying the *Msm canA* gene and its native promoter.
***Msm*-canB-Comp-For**	CGACCGAGCGCAACGCGTGCTGGCGTACTCGGTGGAGA	Forward primer used for amplifying the *Msm canB* gene and its native promoter.
***Msm*-canB-Comp-Rev**	TAACTACGTCGACATCGATAGTGTCGATGTCACTGCAG	Reverse primer used for amplifying the *Msm canB* gene and its native promoter.
Hyg-For	CAGTAATACAAGGGGTGTTATGACACAAGAATCCCTGTTAC	Forward primer used to confirm successful transformation of pML1342 into *Msm* strains.
Hyg-Rev	AACCAATTAACCAATTCTGAATCAGCTAGAGGGGGCG	Reverse primer used to confirm successful transformation of pML1342 into *Msm* strains.
RT-PCR & Real-Time qPCR		
***Msm*-SigA-RTF**	CATCTCGCTGGACCAGACC	Forward primer used to amplify a 100 bp *Msm sigA* (*mysA/MSMEG_2758*)-specific amplicon.
***Msm*-SigA-RTR**	TCGAGCAGCGTGAACGACAC	Reverse primer used to amplify a 100 bp *Msm sigA* (*mysA/MSMEG_2758*)-specific amplicon.
canA-RTF	GCTCGGGTCGATCGAATA	Forward primer used to amplify a 90 bp, *Msm canA*-specific amplicon.
canA-RTR	GAAAGCGTCGCCTTGAC	Reverse primer used to amplify a 90 bp, *Msm canA*-specific amplicon.
canB-RTF	GATCATCCTCATCCACCACA	Forward primer used to amplify a 90 bp, *Msm canB*-specific amplicon.
canB-RTR	GCCCATTCGGGTTTGATG	Forward primer used to amplify a 90 bp, *Msm canB*-specific amplicon.

[a] Sticky end tails compatible with the pLJR962 BsmBI cleavage are underlined.
[b] Complementary regions are underlined.

Table 2.3 Expected PCR product sizes following amplification of plasmids and WT or mutant strains with the indicated primer pair

PRIMER PAIR	RELEVANT GENE / ALLELE	EXPECTED PCR PRODUCT LENGTH
Generation & Confirmation of *Msm* KD Mutant Using CRISPRi		
pLJR962-Seq-For **pLJR962-Seq-Rev**	Region of PLJR962 containing insertion site for sgRNA's	450 bp **(Figure C1.4)**
canA-sgRNA-For **pLJR962-Seq-Rev**	*canA* sgRNA 1 and portion of pLJR962.	250 bp **(Figure C1.3)**
canA-sgRNA-For **pLJR962-Seq-Rev**	*canA* sgRNA 2 and portion of pLJR962.	250 bp **(Figure C1.3)**
canA-sgRNA-For **pLJR962-Seq-Rev**	*canA* sgRNA 3 and portion of pLJR962.	250 bp **(Figure C1.3)**
canB-sgRNA-For **pLJR962-Seq-Rev**	*canB* sgRNA 1 and portion of pLJR962.	250 bp **(Figure C1.3)**
canB-sgRNA-For **pLJR962-Seq-Rev**	*canB* sgRNA 2 and portion of pLJR962.	250 bp **(Figure C1.3)**
canB-sgRNA-For **pLJR962-Seq-Rev**	*canB* sgRNA 3 and portion of pLJR962.	250 bp **(Figure C1.3)**
canB-sgRNA-For **pLJR962-Seq-Rev**	*canB* sgRNA 4 and portion of pLJR962.	250 bp **(Figure C1.3)**
canB-sgRNA-For **pLJR962-Seq-Rev**	*canB* sgRNA 5 and portion of pLJR962.	250 bp **(Figure C1.3)**
Generation & Confirmation of *Msm* KO Mutant		
pKMZeo-For **pKMZeo-Rev**	pMSG360Zeo Zeo^R gene flanked by two *loxP* sites	740 bp **(Figure 3.3.1 A; Figure 3.4.1 A)**
canA-US-For **canA-US-Rev**	*Msm* WT *canA* US region	540 bp **(Figure 3.3.1 A)**
canA-DS-For **canA-DS-Rev**	*Msm* WT *canA* DS region	480 bp **(Figure 3.3.1 A)**
canA-US-For **canA-DS-Rev**	*canA* AES	1, 760 bp **(Figure 3.3.1 B)**
canA-For **canA-Rev**	*Msm* WT *canA* *Msm* Δ*canA*::comp::Zeo^R *Msm* Δ*canA*::comp	2, 088 bp **(Figure 3.3.2 & Figure 3.3.3)** 2, 200 bp **(Figure 3.3.2 & Figure 3.3.3)** 1, 500 bp **(Figure 3.3.3)**
Generation & Confirmation of *Msm* KO Mutant (Continued)		
canA-US-For **Zeo-Check-Rev**	*Msm* WT Δ*canA* *Msm* Δ*canA*::comp::Zeo^R	No PCR product expected. **(Figure 3.3.2)** 1 177 bp **(Figure 3.3.2)**
Zeo-Check-For **canA-DS-Rev**	*Msm* WT Δ*canA* *Msm* Δ*canA*::comp::Zeo^R	No PCR product is expected. **(Figure 3.3.3)** 683 bp **(Figure 3.3.2)**
canB-US-For **canB-US-Rev**	*Msm* WT *canB* US region	522 bp **(Figure 3.4.1 A)**
canB-DS-For **canB-DS-Rev**	*Msm* WT *canB* DS region	514 bp **(Figure 3.4.1 A)**
canB-US-For **canB-DS-Rev**	*canB* AES	1, 776 bp **(Figure 3.4.1 B)**
canB-US-For **canB-DS-Rev**	*Msm* WT *canB* *Msm* Δ*canB*::Zeo^R	1, 477 bp **(Figure 3.4.2)** 1, 776 bp **(Figure 3.4.2)**
canB-US-For **Zeo-Check-Rev**	*Msm* WT *canB* *Msm* Δ*canB*::Zeo^R	No PCR product is expected. **(Figure 3.4.2)** 1, 159 bp **(Figure 3.4.2)**
Zeo-Check For **canB-DS-Rev**	*Msm* WT *canB* *Msm* Δ*canB*::Zeo^R	No PCR product is expected. **(Figure 3.4.2)** 717 bp **(Figure 3.4.2)**
canA-CompP-For **canA-CompP-Rev**	*Msm* WT *canA* with its natural promoter	1, 346 bp **(Figure C 2.1)**
canB-CompP-For **canB-CompP-Rev**	*Msm* WT *canA* with its natural promoter	1, 251 bp **(Figure C2.1)**

2.6 Agarose Gel Electrophoresis

Agarose gels [0.8% or 2% (w/v)] were made using TopVision Agarose Tablets (ThermoFisher Scientific) in 1 × TAE buffer (40 mM Tris, 20 mM acetic acid, 1 mM EDTA, pH 8.0). To facilitate the visualisation of DNA, ethidium bromide (EtBr; 0.5 µg/mL) was added to the agarose. The samples were loaded into the gel using 6 × TriTrack Loading Dye (ThermoFisher Scientific). The sizes of DNA fragments were estimated by comparing their migration to that of those contained in the 1 kb GeneRuler Plus or GeneRuler 50 bp DNA Ladders from ThermoFisher Scientific (**Appendix Figure B1**). Gels were electrophoresed at 80 to 100 V for 45 to 60 min using a Mini-Sub Cell GT horizontal Electrophoresis Chamber (Bio-Rad) and a Universal PowerPac Power Supply (Bio-Rad). The gels were observed UV light utilising a ChemiDoc XRS+ Imaging System (Bio-Rad). Digital images were captured using the associated software (Image Lab, Bio-Rad).

2.7 Bacterial Transformation

DNA was introduced into *E. coli* or *Msm* by heat shock of chemically competent cells or electroporation of electrocompetent cells, respectively, followed by selection of antibiotic-resistant transformants on solid media supplemented with antibiotics as described below.

2.7.1 Preparation of Chemically Competent Cells

Large-scale preparation of chemically competent *E. coli* cells (>100 mL) was performed as described by Inoue *et al.* (1990). *E. coli* cultures were initiated in 5 mL LB as described in **Section 2.1**, incubated at 37 °C for 8 h and diluted 1:100 into 125 mL LB. The cultures were incubated at 18 °C until the OD_{600} reached ~0.55. The cells were transferred onto ice for 10 min and centrifuged at 2 500 × g for 10 min at 4 °C (Megafuge 1.0R, Heraeus). The supernatant was discarded and the pellet resuspended in 40 mL of ice-cold Inoue transformation buffer (55 mM $MnCl_2$, 15 mM $CaCl_2$, 250 mM KCl, 10 mM PIPES (pH 6.7). The cells were centrifuged at 2 500 × g for 10 min at 4 °C and the supernatant discarded. The cell pellet was then resuspended in 10 mL of ice-cold Inoue transformation buffer supplemented with 0.75% (v/v) DMSO and stored on ice for an additional 10 min. The cells were either used immediately or aliquoted into smaller volumes and stored at -80 °C for later use.

2.7.2 Transformation of Chemically Competent Cells

The introduction of DNA into chemically competent *E. coli* cells was achieved by the addition of ligation reactions (1 to 5 µL) or plasmid DNA (1 to 50 ng) to 50 µL of chemically competent cells in pre-chilled 1.5 mL microcentrifuge tubes. The samples were combined and mixed by aspiration and incubated on ice for 10 min, followed by the addition of 950 µL pre-warmed LB. The samples were incubated at 37 °C for 1 h followed by centrifugation at 13, 400 × g for

1 min. The cell pellets were resuspended in 50 µL LB and streak-plated onto the appropriate selective medium. The plates were incubated at 37 °C overnight and antibiotic-resistant transformants were subsequently selected for further analysis.

2.7.3 Preparation of Electrocompetent *Msm* Cells

Electrocompetent *Msm* cells were prepared as described previously (Goude *et al.,* 2015). *Msm* cultures were initiated in 5 mL 7H9 medium as described in **Section 2.1** and incubated at 37 °C until saturated. The culture was diluted 1:100 into 100 mL of pre-warmed 7H9 medium and incubated at 37 °C until an OD_{600} of ~0.6 was reached. The culture was chilled on ice for 1.5 h and the cells harvested by centrifugation at 4000 × g for 10 min. The supernatant was discarded and the resulting cell pellet washed three times with 25 mL ice-cold 10% (v/v) glycerol. Following the final wash step, the cell pellet was resuspended in 2 mL 10% (v/v) glycerol, and either used immediately or stored in aliquots at -80 °C for later use.

For the generation of *Msm* mutants by recombineering, electrocompetent *Msm* harbouring pJV53 were prepared as previously described (van Kessel & Hatfull, 2007). *Msm* (pJV53) was inoculated into 5 mL 7H9 medium and grown at 37 °C until saturated. The culture was diluted 1:100 into 100 mL pre-warmed 7H9 medium supplemented with 0.2% (w/v) succinate, grown until an OD_{600} of ~0.6 and acetamide was then added to a final concentration of 0.2% (w/v) to induce expression of the pJV53-encoded Che9c 60-61 proteins. The culture was grown at 37 °C for an additional 3 h, harvested, and washed three times with 25 mL ice-cold 10% (v/v) glycerol. Following the final wash step, the cell pellet was resuspended in 2 mL 10% (v/v) glycerol and either stored at -80 °C or immediately used for electroporation.

2.7.4 Electroporation of Electrocompetent *Msm* Cells

Plasmid DNA (100 to 800 ng) was combined with 400 µL of electrocompetent *Msm* cells and placed on ice for 10 min. The mixture was transferred to a pre-chilled 0.2 cm electroporation cuvette (ThermoFisher Scientific). The cuvettes were placed in a GenePulser Xcell Electroporator (Bio-Rad) and subjected to pulsing using the following parameters: 2.5 kV, 25 µF, 1000 Ω. The cell suspension was combined with 1 mL pre-warmed 7H9 medium and incubated at 37 °C for 3 to 16 h to allow for the expression of the antibiotic resistance genes. The cells were harvested by centrifugation at 13, 400 × g for 1 min, resuspended in 100 µL 7H9 medium and plated on 7H10 or 7H11 medium supplemented with the appropriate antibiotics. The plates were incubated at 37 °C for 3 to 7 days and antibiotic-resistant transformants were selected for further analysis. Cells transformed with plasmids containing temperature-sensitive replicons were incubated at 30 °C to prevent plasmid loss under non-permissive conditions.

2.8 DNA Sequencing & Analyses

A compilation of the software programs used throughout this study is shown below in **Table 2.4**. The DNA inserts in recombinant plasmids were sent for sequencing to confirm that no mutations were present in PCR-amplified regions of recombinant plasmids. The sequencing was done by Iqaba Biotec using Sanger Sequencing with the BigDye Terminator v3.1 Cycle Sequencing kit. Snapgene was used to view, analyse and edit chromatograms (GSL Biotech).

Table 2.4 List of software programs used during this study

SOFTWARE	URL	REFERENCE
Bio-Rad CFX Manager	https://www.bio-rad.com/en-za/category/qpcr-analysis-software	Bio-Rad
GraphPad Prism 9.0	https://www.graphpad.com/scientific-software/prism/	GraphPad Software
SnapGene	https://www.snapgene.com/	GSL Biotech
SnapGene Viewer	https://www.snapgene.com/	GSL Biotech

2.9 Generation of Mutant Strains

2.9.1 Generation of Msm *canA* and *canB* CRISPRi Mutants

In order to conditionally silence the *Msm canA* and *canB* genes, a CRISPRi-based method was employed (Rock *et al*., 2017). To enable the expression of the single-guide RNA (sgRNA) molecules, we identified three and five dCas9 PAM sequences (NNRGAAR) located on the non-coding strand of the *Msm canA* (MSMEG_6082) and *canB* (MSMEG_4985) genes, respectively. Complementary oligonucleotides were designed and synthesised (Iqaba Biotec) using 18-22 bp sequences on the 5'-end adjacent to each of the identified PAMs which would produce sgRNA sequences complementary to the non-coding strand of each target gene when expressed from the ATc-regulated promoter in pLJR962. To facilitate cloning into BsmBI-digested pLJR962, GGGA and AAAC sequences were incorporated at the 5'-end of the oligonucleotides corresponding to the coding and non-coding strands of the *canA* and *canB* gene, respectively.

Following receipt, the non-phosphorylated primers were resuspended in nuclease-free dH_2O and diluted to a concentration of 100 µM. 10 µL of each primer was combined with 65 µL nuclease-free water, 10 µL 10 × T4 ligase buffer (with ATP), and 5 µL polynucleotide kinase (PNK; 1 U/ µL). The phosphorylation reaction was incubated at 37 °C for 30 min in a thermocycler. The reaction was then heated to 95 °C for 5 min to inactivate PNK and denature the sgRNA primers. The tubes were removed from the thermocycler and allowed to cool to RT slowly to facilitate annealing of the complementary oligonucleotides. The PCR tubes were

centrifuged and the annealed oligonucleotides diluted 1:200 dilution into nuclease-free water. The efficiency of annealing was monitored by subjecting 5 µL of the diluted double-stranded, annealed oligo alongside an equivalent amount of single-stranded primer on a 2% agarose gel. The annealed sgRNA oligos were subsequently cloned into pLJR962 using the Golden Gate Cloning method described by McNeil & Cook (2019). The reactions were set up by combining 2.5 µL annealed sgRNA oligonucleotides, 4.25 µL nuclease-free water, 1.25 µL uncut pLJR962 (20 ng/µL), 0.5 µL T4 DNA Ligase, 1 µL 10 × T4 Ligase Buffer, and 0.5 µL BsmBI. The reactions were then placed in a thermocycler and incubated for 30 cycles of (i) restriction enzyme digestion with BsmBI at 42 °C for 5 min followed by (ii) ligation at 16 °C for 5 min. This was followed by an extended incubation at 55 °C for 30 min to digest any uncut pLJR962, followed by inactivation of the BsmBI enzyme at 80 °C for 10 min. 2.5 µL of the Golden Gate reactions were then transformed into chemically competent *E. coli* Mach1 cells as described in **Section 2.6.2** and transformants selected on LB/Km plates after 16 h incubation at 37 °C. Plasmids were isolated for each of the CRISPRi constructs and the successful cloning of the annealed oligonucleotides confirmed by sequencing with primers pLJR962-Seq-For/pLJR962-Seq-Rev (**Table 2.3**), which anneal to complementary regions on either side of the BsmBI site used for cloning into pLJR962. The amplicons, pLJR962::*canA* sgRNA1, pLJR962::*canA* sgRNA2, pLJR962::*canA* sgRNA3, pLJR962::*canB* sgRNA1, pLJR962::*canB* sgRNA2, pLJR962::*canB* sgRNA3, pLJR962::*canB* sgRNA4, pLJR962::*canB* sgRNA5 and pLJR962::*mmpL3* sgRNA were submitted for Sanger sequencing and thereafter, transformed into electrocompetent *Msm* cells as described in **Section 2.6.4** and selected on 7H10/Kan plates. *Msm* cells transformed with the pLJR962 vector lacking an insert or targeting the essential *Msm mmpL3* gene were included as CRISPRi growth controls. The plates were incubated at 37 °C for 3 days and Kan^R transformants were selected for further genotypic and/or phenotypic analysis.

2.9.2 Generation of *Msm canA* and *canB* Knockout (KO) Mutants

For recombineering, allelic exchange substrates (AES) were generated by splice-by-overlap extension PCR (SOE-PCR), as described by Judd *et al*. (2021). DNA fragments of 540 and 480 bp upstream (US) and downstream (DS) of the *Msm canA* (MSMEG_6082) gene **(Figure 2.1)** or 522 and 514 bp US and DS of the *Msm canB* gene (MSMEG_4985) (**Figure 2.2**) were PCR amplified using the canA-US-For/canA-US-Rev and canA-DS-For/canA-DS-Rev or canB-US-For/canB-US-Rev and canB-DS-For/canB-DS-Rev as primer pairs (**Table 2.3**), respectively. To facilitate the generation of marked deletion mutants, the 3'- and 5'-ends of the *canA* and *canB* US and DS PCR products were designed to contain 22 bp regions of homology to 5'- and

3’-ends of the *loxP*-flanked Zeocin-resistance (Zeo^R) cassette from plasmid pMSG350Zeo (Barkan *et al*., 2010). The Zeo^R-cassette was amplified using the pKMZeo-For/pKMZeo-Rev primer pair (**Table 2.3**). Following the first-round PCR amplification of the Zeo^R-cassette and US and DS fragments, the template DNA was removed by restriction endonuclease digestion with 1 µL DpnI for 1 h at 37 °C. The PCR amplicons were subsequently purified and used in equimolar amounts (10 pM) in a second round of amplification with either the canA-US-For/canA-DS-Rev (for *canA*) and canB-US-For/canB-DS-Rev (for *canB*) as the forward and reverse primers. The 1,760 bp and 1,776 bp full-length AES for *canA* and *canB* were subsequently gel purified following AGE and electroporated into electrocompetent *Msm*::pJV53 cells.

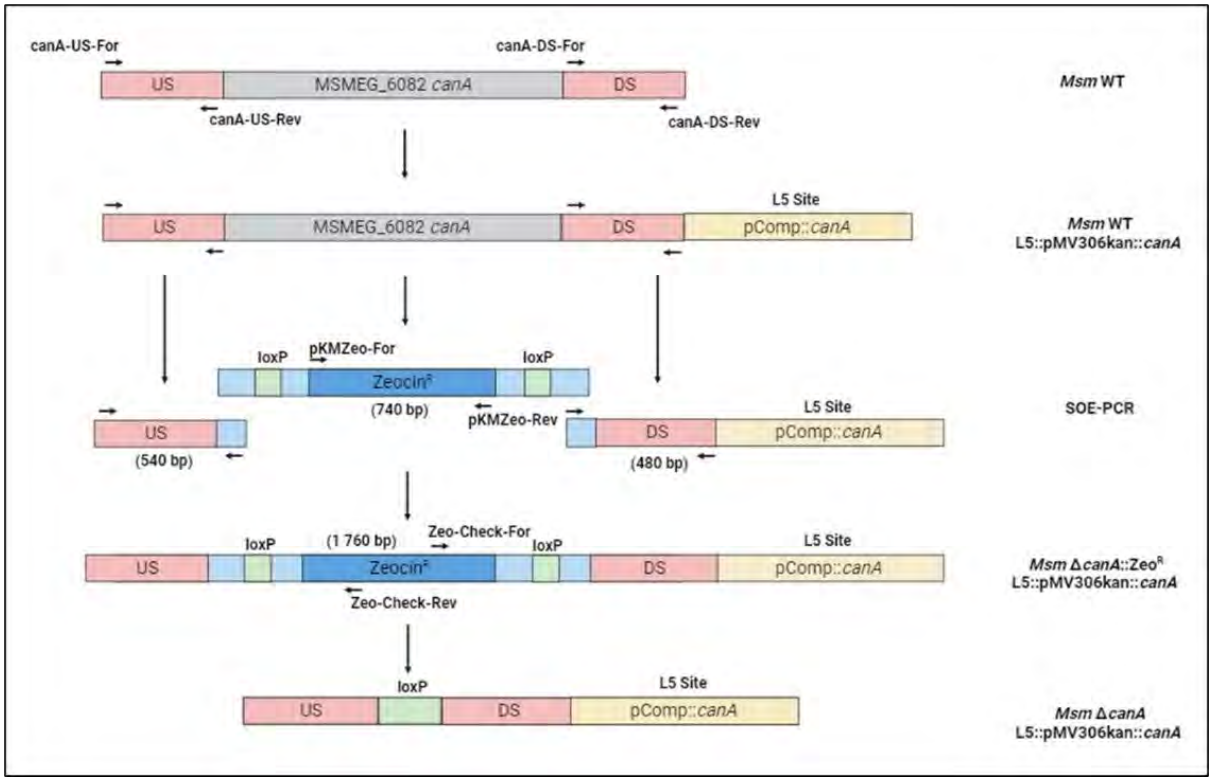

Figure 2.1 Schematic diagram illustrating the generation of the *Msm* Δ*canA* KO mutant. A *canA* specific allelic exchange substrate (AES) was generated by amplifying DNA fragments of 540 bp and 480 bp upstream (US) or downstream (DS) of the *canA* gene (pink boxes) using primer pairs (black arrows) canA-US-For/canA-US-Rev and canA-DS-For/canA-DS-Rev, respectively. The 740 bp Zeocin-resistance (Zeo^R) cassette from pMSG360Zeo (blue boxes) was amplified using primers pKMZeo-For/pKMZeo-Rev. The *loxP* sites flanking the Zeo-cassette are shown (green boxes). The three amplicons were purified, combined and spliced by SOE-PCR using the canA-US-For/canA-DS-Rev primers to generate the AES of 1,760 bp, which was subsequently introduced into *Msm* by electroporation. Replacement of the WT copy of the *canA* gene with the AES was only feasible in a *Msm* strain containing a second, functional copy of *canA*, integrated into the phage L5 *attB* site (yellow box)**.** Successful replacement of WT *canA* gene resulted in the generation of the marked *Msm* Δ*canA::*Zeo^R mutant. An unmarked *Msm* Δ*canA* mutant was generated by the Cre-recombinase mediated excision of the Zeo^R cassette from the Δ*canA::*Zeo^R mutant, leaving a *loxP*-scar sequence. The proper construction of the strain was confirmed by PCR and Sanger sequencing of the *canA* locus in the unmarked *Msm* Δ*canA* mutant. The location of all primers used are indicated by black arrows. The sizes of the fragments are indicated in base pairs (bp).

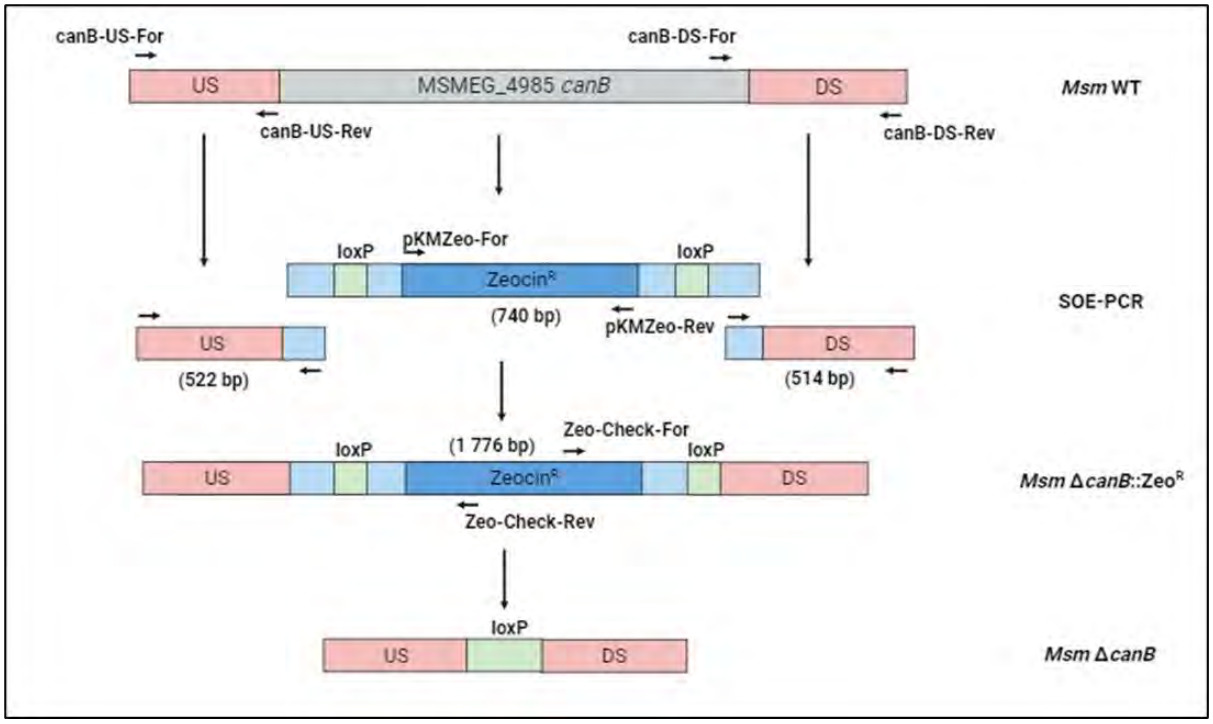

Figure 2.2 Schematic diagram illustrating the generation of the Δ*canB* KO mutant. A *canB* specific allelic exchange substrate (AES) was generated by amplifying DNA fragments of 522 bp and 514 bp upstream (US) or downstream (DS) of the *canB* gene (pink boxes) using primer pairs (black arrows) canB-US-For/canB-US-Rev and canB-DS-For/canB-DS-Rev, respectively. The 740 bp Zeocin-resistance (Zeo^R) cassette from pMSG360Zeo (blue boxes) was amplified using primers pKMZeo-For/pKMZeo-Rev. The *loxP* sites flanking the Zeo-cassette are shown (green boxes). The three amplicons were purified, combined and spliced by SOE-PCR using the canB-US-For/canB-DS-Rev primers to generate the AES of 1,776 bp, which was subsequently introduced into *Msm* by electroporation. Successful replacement of the WT copy of the *canB* gene with the AES resulted in the generation of the marked *Msm* Δ*canB::*Zeo^R mutant. An unmarked *Msm* Δ*canB* mutant was generated by the Cre-recombinase mediated excision of the Zeo^R cassette from the Δ*canB::*Zeo^R mutant, leaving a *loxP*-scar sequence. The proper construction of the strain was confirmed by PCR and Sanger sequencing of the *canB* locus in the unmarked *Msm* Δ*canB* mutant. The location of all primers used are indicated by black arrows. The sizes of the fragments are indicated in base pairs (bp).

2.9.3 Generation of Complementation Vectors

Plasmids for the genetic complementation were generated by PCR amplifying the coding sequences of the *Msm canA* and *canB* genes with its natural promoter using canA-Comp-For/canA-Comp-Rev and canB-Comp-For/canB-Comp-Rev primers, which were designed to contain the recognition sites for NotI and HindIII, respectively. Following amplification, the PCR products were purified, restricted with NotI and HindIII and ligated into the 4.3 kb fragment of pMV306hsp (Andreu *et al.*, 2010), which carries the Kan^R marker, to generate pMV306kan::*canA* and pMV306kan::*canB*. The ligation reactions were introduced into *E. coli* TOP10 chemically competent cells and transformants selected on LA/Kan medium. Kan^R

transformants were selected and analysed by colony PCR with gene-specific primers, as well as plasmid purification and restriction enzyme digestion to verify the successful construction of recombinant plasmids. The PCR amplified regions of recombinant plasmids were verified via Sanger sequencing as described in **Section 2.7**. Following confirmation, the pMV306kan::*canA* and pMV306kan::*canB* complementation constructs were electroporated into *Msm* WT (for generation of the *Msm* Δ*canA* KO mutant) or *Msm* Δ*canB*, respectively, for subsequent genotypic and phenotypic characterisation.

2.9.4 Gene Switching (L5 Allele Swaps)

The L5 integrating plasmid, pML1342 (Huff *et al.,* 2010), which carries the Hyg^R marker was used in L5 allele swap experiments (Pashley & Parish, 2003). The *canA* and *canB* genes were PCR amplified using the primer pairs canA-Comp-For/canA-Comp-Rev and canB-Comp-For/canB-Comp-Rev, respectively (**Table 2.3**). Following amplification with Phusion DNA polymerase, the PCR amplicons were phosphorylated with PNK, purified, and ligated into pML1342 digested with MssI to generate pML1342::*canA* and pML1342::*canB* (**Supplementary Material C.1**). The ligation reactions were introduced into *E. coli* TOP10 chemically competent cells, and transformants were selected on LA/Hyg medium following incubation overnight at 37 °C. Recombinant plasmids from Hyg^R transformants were verified by restriction enzyme digestion and DNA sequencing (**Supplementary Material, Figure C2.2**). The confirmed constructs were then electroporated into the genetically complemented *Msm* Δ*canA* L5::pMV306kan::*canA* strain for subsequent viability and antibiotic resistance profiling. **Figure 2.3 A, B, C, D** below depicts the three possible outcomes of the L5 allele swaps of the Kan^R pMV306kan::*canA* with the Hyg^R pML1342::*canA* and pML1342::*canB* (**Chapter 3, Figure 3.3.6**) plasmids.

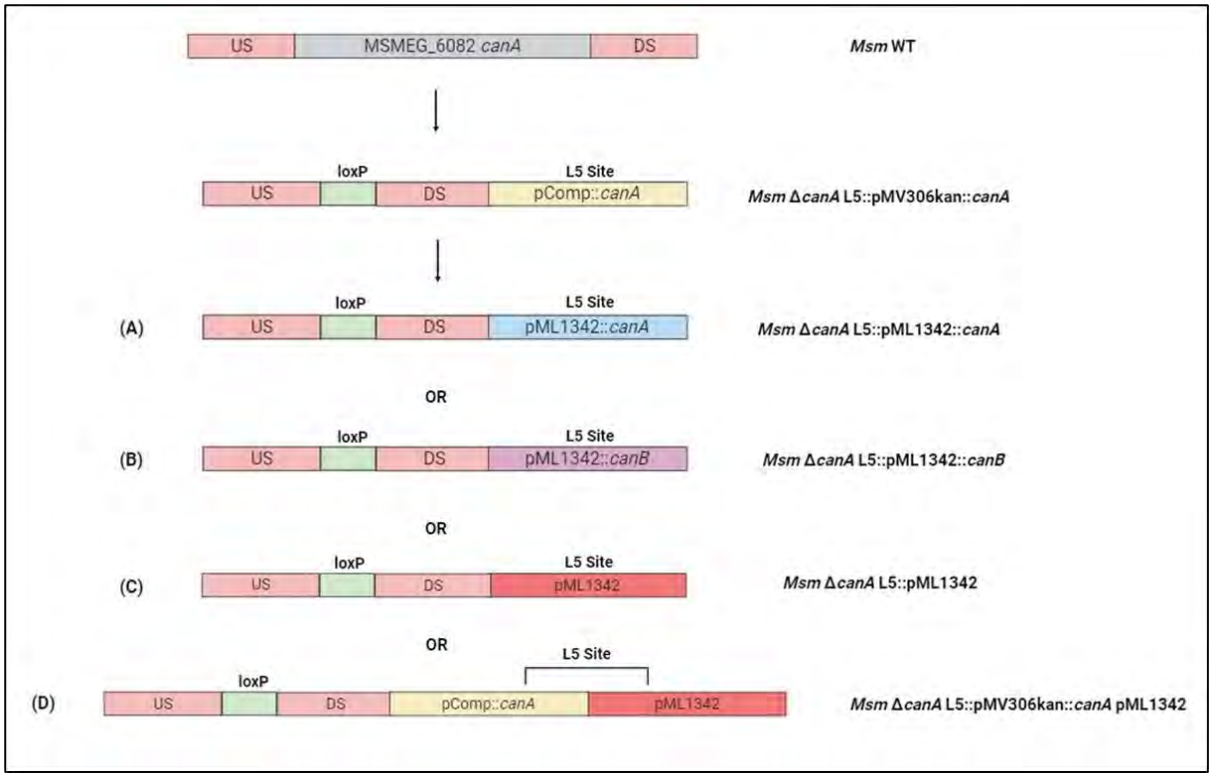

Figure 2.3. After a functional copy of *canA* was integrated into the L5 site of *Msm* WT using the Kan^R pMV306kan::*canA* (pComp::*canA;* yellow), the endogenous copy of *canA* (salmon) was inactivated by recombineering (**See Fig 2.1**). The ability of pML1342 (Hyg^R) containing *canA* (pML1342::*canA*; blue) or *canB* gene (pML1342::*canB*; purple), or just the parental pML1342 vector (red) to replace the original Kan^R pComp::can*A* vector was then examined following electroporation. In theory, pComp::*canA* could be replaced by any of the three plasmids to yield Hyg^R transformants as indicated in (**A**) pML1342::*canA* (**B**) pMl1342::*canB* or (**C**) pML1342. The original pComp::*canA* vector can also remain integrated at the L5 site, followed by integration of one of the three aforementioned vectors as indicated in (**D**) for pML1342. This would yield transformants that are both Kan^R and Hyg^R.

2.10 Growth Assays

2.10.1 Grow Assays in Liquid Medium

For growth assays, single colonies grown on 7H10 or 7H11 medium were inoculated into 5 ml of 7H9 media and incubated at 37 °C until saturated. The cultures were diluted 1:100 into 7H9 media and incubated at 37 °C overnight (~16 h). The OD_{600} of the cultures was measured and the cells diluted into fresh, pre-warmed 7H9 media to an initial OD_{600} of 0.05. The cultures were then incubated at 37 °C and the OD_{600} values measured at the specified time points indicated in the Results Section (**Chapter 3**). All absorbance readings were measured using the Jenway 6200 spectrophotometer and 1 cm path length semi-micro cuvettes (Lasec). When necessary, the cultures were diluted in 7H9 media to reduce the OD_{600} below 1.0 before

measuring the absorbance. The growth assays were performed using three independent biological replicate measurements for each sample.

2.10.2 Survival Assays in Liquid Medium

The cultures of *Msm* WT or mutant strains were started from single colonies and grown until saturation before dilution into 7H9 medium to an initial OD_{600} of 0.05. The cultures were grown to mid-exponential phase (OD_{600} of 0.4 to 0.6) and diluted to an OD_{600} of 0.01 in 7H9 media. When required, the growth medium for KD strains was supplemented with ATc (200 ng/mL) to silence gene expression, as specified in the Results (**Chapter 3**). Various concentrations of ATc were evaluated and a concentration of 200 ng/mL was selected and used, when required (**Supplementary Material, Figure D1**). Bacterial survival was quantified after 0, 3, 6, 9, 12 and 24 hrs, respectively. All strains were analysed using three biological replicates.

2.10.3 Biofilm Formation

Biofilm formation in *Msm* was performed as described by Ojha *et al*., (2015). *Msm* strains were grown to an OD_{600} of ~1.0 and diluted 1/1000 in 5 ml of biofilm media [modified M63 minimal media; 100 mM KH_2PO_4, 15 mM $(NH_4)_2SO_4$, 1.8 µM $FeSO_4 \cdot 7H_2O$, 0.1 mM $CaCl_2$, 0.1 mM $MgSO_4$, 0.5% casamino acids (w/v), 0.2% glucose (w/v), pH 7.2) in glass test tubes or 1 ml biofilm media in 24-well cell culture plates. Where required, the medium was supplemented with 200 ng/mL ATc to silence gene expression, as specified in the Results Section (**Chapter 3.5**). The cultures were incubated as static cultures (no shaking) at 30 °C for 5 days before biofilm formation was assessed.

2.10.4 Carbon Dioxide Assay

Msm strains grown to mid-exponential phase (OD_{600} of 0.4 to 0.6) were diluted to an OD_{600} of 0.01 in 7H9 medium. A 5 µL aliquot of the diluted cultures were spotted on the surface of 7H10 plates (**Section 2.1**) and streaked for single colonies. When required, the growth medium was supplemented with ATc (200 ng/mL) to silence gene expression, as specified in the Results Section (**Chapter 3.5**). The plates were incubated at 37 °C for 3 days either under low (0.03%) or high (5%) CO_2.

2.10.5 pH Assays

Msm strains grown to mid-exponential phase (OD_{600} of 0.4 to 0.6) were diluted to an OD_{600} of 0.01 in 7H9 medium. A 5 µL aliquot of the diluted cultures were streak-plated for single colonies on the surface of 7H10 plates (**Section 2.1**) whose pH levels were adjusted to 5.0 to 8.0 with 1 M NaOH or 1 M HCl. When required, the growth medium and assay plates were supplemented with ATc (200 ng/mL) to silence gene expression, as specified in the Results Section (**Chapter 3.5**). The plates were incubated at 37 °C for 3 days.

2.10.6 Nutritional Supplementation

Msm WT or mutant strains were grown to mid-exponential phase (OD_{600} of 0.4 to 0.6) and diluted to an OD_{600} of 0.01 in 7H9 medium. A 5 µL aliquot of the diluted cultures were placed on the surface of either non-supplemented 7H10 media (**Section 2.1**), or 7H10 media supplemented with metabolites listed in **Table 2.5**. When required, the growth medium and assay plates were supplemented with ATc (200 ng/mL) to silence gene expression, as specified in the Results Section (**Chapter 3.5**). The plates were incubated at 37 °C for 3 to 7 days.

Table 2.5 The concentrations of metabolites used in this study. All metabolites were filter sterilised using 0.22 µm filters and added to 7H10 media at the indicated concentrations after autoclaving.

METABOLITE	CONCENTRATION
Adenine	1 mM
Albumin Dextrose Saline (ADS)[a]	1×
Aspartic Acid	1 mM
Casamino Acids	0.2% (w/v)
Cholesterol	1 mM
Histidine	1 mM
Malic Acid	1 mM
Oleic Albumin Dextrose Complex (OADC)[b]	1×
Oleic Acid	0.06% (v/v)
Oxaloacetate	1 mM
Palmitic Acid	1 mM
Sodium Bicarbonate	10 mM
Sodium Pyruvate	1 mM
Succinate	1 mM
Tween 80	0.05% (v/v)
Uracil	1 mM

a: ADS = 5% bovine serum albumin fraction V (w/v), 2% dextrose (glucose) (w/v), 0.85% NaCl (w/v)
b: OADC = OADC enrichment; ADS, oleic acid (0.6 mL/L), catalase (0.003% w/v)

Chapter 3: Results

3.1 Generation and Characterisation of *Msm* KD Mutant Strains

To gain a better understanding of the physiological roles of the carbonic anhydrases (CAs) in *Msm*, the effect of silencing the expression of *Msm canA* and *canB* genes on the growth and survival of the organism was examined. Gene silencing was achieved using the CRISPR-interference (CRISPRi) system of Rock and colleagues (Rock *et al*., 2017; Wong & Rock, 2021), in which a deactivated Cas9 (dCas9) and single guide RNA (sgRNA) are expressed from two separate anhydrotetracycline (ATc) inducible promoters present on the L5-derived integrating CRISPRi vector, pLJR962 (Rock *et al*., 2017; **Supplementary Material, Figure C1.1**). To generate CRISPRi plasmids for silencing the expression of *canA* and *canB*, three sgRNA targeting sequences were generated for *canA* (canA_sgRNA1, 2 and 3; **Supplementary Material, Figure C1.2A**) and five for canB_sgRNA1, 2, 3, 4 and 5; **Supplementary Material, C1.2B**) and cloned into pLJR962, as described in **Chapter 2.9.1**. Once the generation of the recombinant plasmids had been confirmed by analytical PCR and Sanger sequencing (**Supplementary Material C1**), the plasmids targeting *canA* (designated pLJR962::*canA1*, pLJR962::*canA2*, pLJR962::*canA3*) or *canB* (designated pLJR962::*canB1*, pLJR962::*canB2*, pLJR962::*canB3,* pLJR962::*canB4*, pLJR962::*canB5*) were introduced into WT *Msm*. This resulted in the isolation of eight putative *Msm* "knock-down" (KD) mutant strains, which were designated *Msm canA1 KD*, *canA2 KD* or *canA3* KD (for *Msm* strains harbouring pLJR962::*canA1*, pLJR962::*canA2*, pLJR962::*canA3,* respectively) and *Msm canB1 KD*, *canB2 KD*, *canB3 KD, canB4 KD* and *canB5* KD (for *Msm* strains harbouring pLJR962::*canB1*, pLJR962::*canB2*, pLJR962::*canB3*, pLJR962::*canB3, and* pLJR962::*canB5,* respectively). For use as negative and positive growth controls, *Msm* strains harbouring the parental, control (PC) vector, pLJR962, or pLJR962::*mmpL3* were used, respectively (Wong & Rock, 2021). The PC vector lacks an sgRNA downstream of the plasmid's ATc-inducible promoter, while pLJR962::*mmpL3* harbours an sgRNA that mediates silencing of the growth essential *mmpL3* gene Rock *et al.,* 2017; McNeil & Cook, 2019). The growth of WT *Msm* pLJR962 should therefore be ATc-independent, while that of *Msm* pLJR962::*mmpL3* should be ATc-dependent with growth occurring in the absence, but not presence of ATc, which acts the inducer of *mmpL3* sgRNA expression.

3.2 Phenotypic Characterisation of the *canA* and *canB* Mutants

The three CA-encoding genes of *Mtb* have been shown to be dispensable for the organism's survival under standard, *in vitro* growth conditions (DeJesus *et al*., 2017; Dragset *et al*., 2019; Minato *et al*., 2019; Sassetti *et al*., 2001). To establish the essentiality of *Msm*'s two CA-

encoding genes, we first examined the growth of the *canA* and *canB* KD mutants on solid medium in the absence (-ATc) and presence (+ATc) of inducer (0 and 200 ng/mL ATc, respectively). As expected, the growth of the *Msm* pLJR962 control strain was not affected by ATc, with similar levels of growth occurring in both its absence and presence (**Figure 3.2.1 C** and **D,** respectively). Consistent with previous findings (Rock *et al*., 2017), the growth of the *Msm mmpL3* KD resembled that of the control strain in the absence of ATc (**Figure 3.2.1 C**) but was significantly reduced in its presence (**Figure 3.2.1 D**). The growth of *canA1, canA2 and canA3* KD mutants was, likewise, similar to that of the control strain in the absence of ATc but was reduced following induction of sgRNA expression in its presence (**Figure 3.2.1 B and D**). The degree of growth inhibition observed for the *canA* KDs correlated with the predicted strengths of the PAM sequence of the sgRNA harboured on each CRISPRi plasmid, with the greatest reduction of growth observed for the *canA1* KD mutant (predicted PAM strength = 0.83), followed by the *canA2* and *canA3* KD mutants (predicted PAM strengths = 0.8 and 0.47, respectively). The reduced growth observed for *canA* KD mutants following CRISPRi-mediated gene silencing suggests that CanA activity is essential for the growth of *Msm* during incubation on solid media at low CO_2 concentrations (~0.035% v/v). The growth of the five *canB* KD mutants, by contrast, resembled that of the WT *Msm* pLJR962 control strain and was not significantly different in plates supplemented with (**Figure 3.2.1 B and D**) or without (**Figure 3.2.1 A and C)** ATc. The lack of any visible growth defects in the five *canB* KD mutants following silencing of *canB* suggests that its gene product is dispensable for the growth of *Msm* under standard mycobacterial growth conditions (standard aeration with low CO_2). Taken together, our observations suggest that CanA is the primary CA responsible for catalysing bicarbonate formation from CO_2 at low CO_2 concentrations. CanB, by contrast, appears to be dispensable under these conditions and cannot compensate for the loss of CanA activity in the presence of ATc. This may, however, be due to a lack of *canB* expression or CanB enzymatic activity under the assay conditions used in these experiments.

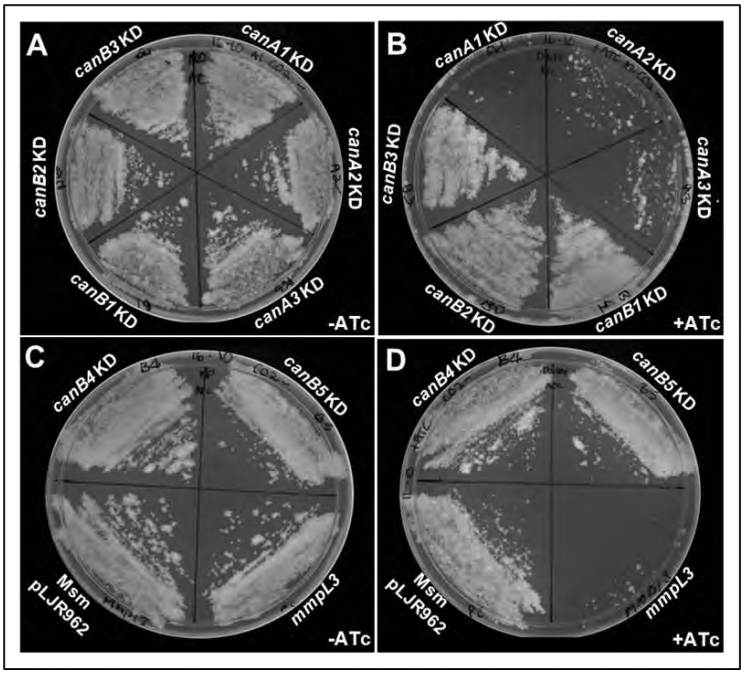

Figure 3.2.1 Survival of the *Msm* pLJR962 and the *canA* and *canB* KD mutants in the presence and absence of ATc. The *Msm* pLJR962, *Msm canA1-3*, *Msm canB1-5* and *Msm mmpL3* KD mutants were grown to mid-exponential phase, diluted to an OD_{600} of 0.1, and 10 µl spotted and streaked on 7H10 plates in either the absence (-ATc; 0 ng/mL) or presence (+ATc; 200 ng/mL) of ATc (shown in panels **A and C and B and D**, respectively) to induce gene silencing. The plates were incubated at 37 °C for 3 days before imaging.

To determine if the silencing of the *canA* gene also compromises the growth of the *Msm* in liquid medium, we compared the growth of ATc-treated and -untreated cultures of *Msm* pLJR962 and the *canA1* KD. As shown in **Figure 3.2.2**, the growth kinetics of the control *Msm* pLJR962 and *canA1* KD mutant strains was similar during the early stages of bacterial growth (i.e., lag and early exponential phase; 0 to 12 hrs) in both the ATc treated (+ATc) and untreated (-ATc) samples. While the growth of the untreated (-ATc) *canA1* KD mutant was similar to that of WT *Msm* pLJR962 during mid-to late-exponential (~12 – 20 hrs) and stationary phase (21 – 24 hrs) [**Figure 3.2.2,** purple (KD) and green (WT) curves, respectively], it was significantly reduced relative to the control when sgRNA expression was induced in treated (+ATc) cultures [**Figure 3.2.2,** blue (KD) and red (WT) curves, respectively**]**. These observations suggest that the activity of CanA is required for the *in vitro* growth of *Msm* in both solid and liquid formats. Similar to the results observed on solid media, ATc treatment did not affect the growth of the *canB* KD mutants strains during growth in liquid media (data not shown; see **Figure 3.7.1** for growth comparison of WT *Msm* and the Δ*canB* KO, however), supporting the idea that CanB activity is not required for the growth and/or survival of *Msm* under standard, laboratory growth conditions on either solid or liquid media.

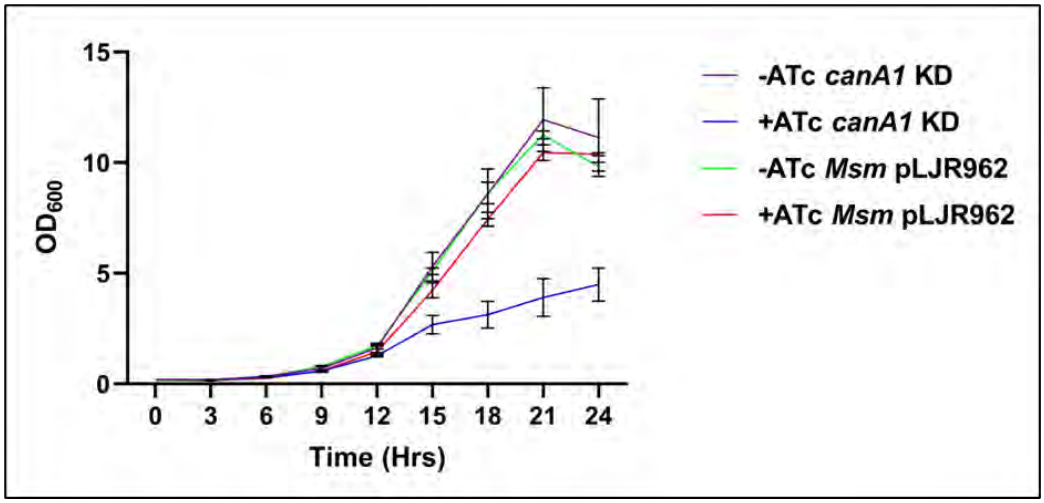

Figure 3.2.2. Growth kinetics of the WT *Msm* pLJR962 and *canA1* KD mutant in the presence and absence of ATc. The *Msm* pLJR962 control and *canA1* KD mutant strains were diluted to an OD_{600} of 0.05 in the absence (0 ng/mL; -ATc) and presence (200 ng/mL; +ATC) of ATc to induce gene silencing and incubated at 37 °C. Bacterial growth was determined by taking absorbance at OD_{600} measurements over 24 hrs at the indicated times. The average of three biological replicates is indicated with ± SD.

3.3 Expression Analysis of *canA* and *canB* in ATc-treated and Untreated KD Mutants

To confirm that ATc-treatment was effectively silencing the *canA* and *canB* genes in their respective KD mutants, the expression levels of the *canA* and *canB* genes were quantified by semi-quantitative reverse transcription PCR (RT-PCR; **Figure 3.3.1 and 3.3.2, respectively**) and quantitative real-time PCR (qPCR; **Figure 3.3.3 and 3.3.4, respectively**). For these experiments, the *canA1* and *canB1* KD mutants were used since they express the sgRNA with the highest predicted PAM strength for each gene. As shown in **Figure 3.3.1 and 3.3.2 (Lanes 4 and 5)**, both the *canA* and *canB* genes were expressed in a constitutive, ATc-independent manner in the WT *Msm* pLJR962 strain. The expression level of the *canA* gene was similar to that of the *Msm* pLJR962 strain, in ATc-untreated *canA1* KD cultures (**Figure 3.2.3 A and B, Lanes 2**). The expression of the *canA* gene was, however, below the level of detection in the *canA1* KD culture treated with ATc (**Figure 3.3.1 A, Lane 3)**. Similar observations were made for the *canB1* KD mutant (**Figure 3.3.2 A**). While *canB* was expressed at near wild-type levels in ATc-untreated *canB1* KD cultures (**Lane 2**), expression of the gene was undetectable in ATc-treated cultures (**Lane 3**). The expression of the control, *Msm sigA* (*MSM*EG_2758) housekeeping gene was, by contrast, similar in all samples analysed (**Figures 3.3.1 and 3.3.2 B)**. No amplicons were, furthermore, observed in the negative PCR control, which lacked a

DNA template (NC), or in the negative RT-PCR control, which contained RNA that had not undergone reverse transcription ("No RT Reactions"; **Figure 3.3.1 and 3.3.2 C and D**).

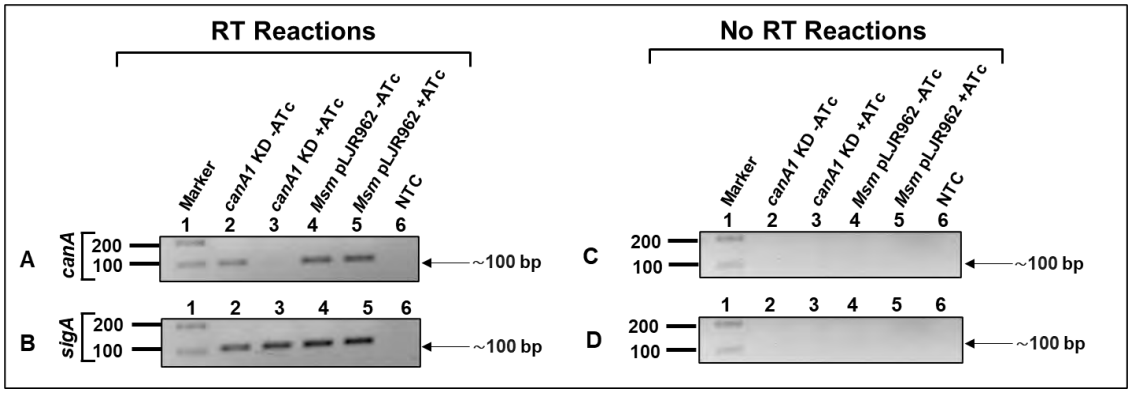

Figure 3.3.1. Semi-quantitative RT-PCR analysis of *canA* and *sigA* expression in the *canA1* KD strain. RNA obtained from each sample were reversed transcribed into cDNA and PCR amplified using either **A)** *canA* or **B)** *sigA* specific primers. 'No RT reactions' with the same primers were included to confirm the absence of gDNA contamination (**C** and **D**). The PCR products were electrophoresed on 2% (w/v) agarose at 80 V for 70 min. Figures (**A** and **B**) contain the RT reactions and panels (**C** and **D**) contain the No RT reactions. The cDNA used as a template in each reaction for **Figures A-D** was as follows: **Lanes 1:** Molecular Weight Marker; **Lanes 2:** *canA1* KD -ATc; **Lanes 3:** *canA1* KD +ATc; **Lanes 4:** *Msm* pLJR962 -ATc; **Lanes 5:** *Msm* pLJR962 +ATc; **Lanes 6:** No Template Control (NTC). Black arrows indicate the amplicons.

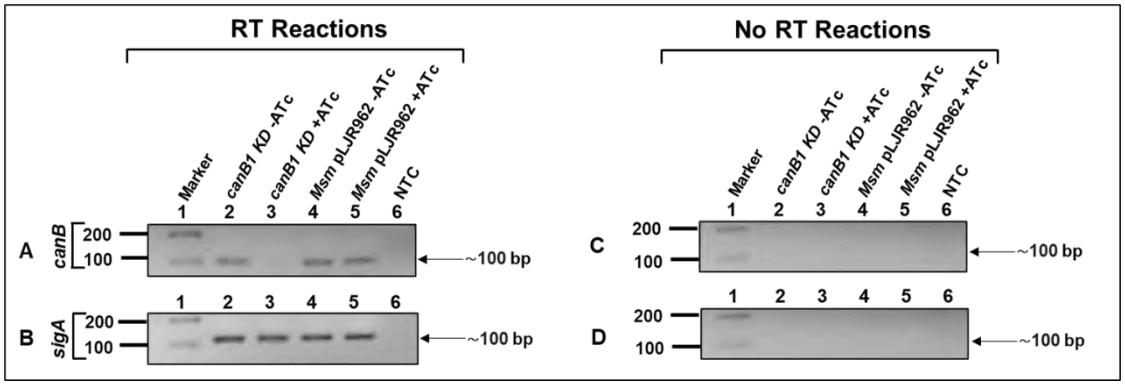

Figure 3.3.2. Semi-quantitative RT-PCR analysis of *canB* and *sigA* expression in the *canB1* KD strain. RNA obtained from each sample were reversed transcribed (RT) into cDNA and PCR amplified using either **A)** *canB* or **B)** *sigA* specific primers. 'No RT reactions' with the same primers were included to confirm the absence of gDNA contamination (**C** and **D**). The PCR products were electrophoresed on 2% (w/v) agarose at 80 V for 70 min. Figures (**A** and **B**) contain the RT reactions and panels (**C and D**) contain the No RT reactions. The cDNA used as a template in each reaction for **Figures A-D** was as follows: **Lanes 1:** Molecular Weight Marker; **Lanes 2:** *canB1* KD -ATc; **Lanes 3:** *canB1* KD +ATc; **Lanes 4:** *Msm* pLJR962 -ATc; **Lanes 5:** *Msm* pLJR962 +ATc; **Lanes 6:** No Template Control (NTC). Black arrows indicate the approximate sizes of the amplicons.

Using qRT-PCR, the expression of the *canA* and *canB* genes were found to be decreased >98% in the presence of ATc (relative to its absence) in their respective *canA1* **(Figure 3.3.3)** and

canB1 KD (**Figure 3.3.4)** mutants. The expression of these genes remained virtually unchanged in the WT *Msm* pLJR962 strain under the same conditions, however **(Figure 3.3.3 and 3.3.4)**.

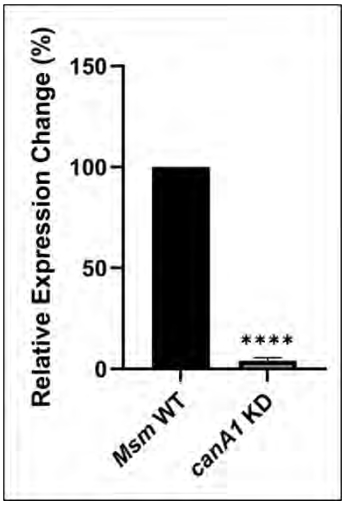

Figure 3.3.3. Relative expression levels of *canA* in the WT pLJR962 and *canA1* KD. *Msm* cultures were diluted to an OD_{600} of 0.1 and grown to the mid-exponential phase (OD_{600} ~0.8) before the isolation of total RNA from ATc-treated and -untreated cultures. Equivalent amounts of RNA were converted to cDNA and the relative expression levels of *canA* were determined using the 2-ΔΔCt method. Expression levels under different conditions were normalised to that of *sigA*. Statistical analysis was calculated using an ordinary on-way ANOVA test; **** denotes $p < 0.0001$.

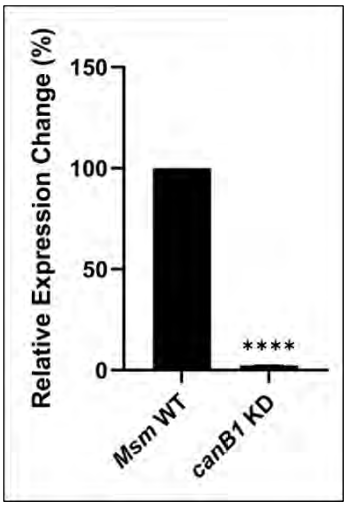

Figure 3.3.4. Relative expression levels of *canB* in the WT pLJR962 and *canB1* KD. *Msm* cultures were diluted to an OD_{600} of 0.1 and grown to the mid-exponential phase (OD_{600} ~0.8) before the isolation of total RNA from ATc-treated and -untreated cultures. Equivalent amounts of RNA were converted to cDNA and the relative expression levels of *canA* were determined using the 2-ΔΔCt method. Expression levels under different conditions were normalised to that of *sigA*. Statistical analysis was calculated using an ordinary on-way ANOVA test; **** denotes $p < 0.0001$.

Taken together, these findings indicate that the expression of the *canA* and *canB* genes are effectively silenced in the KD strains when cultured in the presence of ATc, making the *Msm*

canA1 and *canB1* KD mutants suitable for assessing the function(s) of the genes and their encoded gene proteins. The growth defects observed for the *canA1* KD mutant in both liquid and solid media (**Figure 3.2.1** and **3.2.2)** is, therefore, likely attributable to the silencing of the *canA* gene by ATc, as shown above (**Figure 3.3.1** and **3.3.3**). The *canB1* KD mutant, by contrast, did not display any growth defects under similar conditions, despite effective silencing of *canB* expression (**Figure 3.3.2** and **3.3.4**). The lack of any observable growth defects for the *canB1* KD mutant in the presence of ATc (**Figure 3.2.1)** is, therefore, not due to the inefficient silencing of the *canB* gene expression (e.g., due to poor sgRNA design or selection) under the growth conditions used. Taken together, these observations indicate that the activity of CanA is required for the growth of *Msm* at low CO_2 concentrations. The activity of CanB, by contrast, appears to be dispensable. The reasons for the constitutive expression of *canB* is currently unknown. The synthesis or activity of the encoded CanB enzyme may, however, be regulated by a post- transcriptional or -translational mechanism. The enzymes activity may, therefore, only become apparent under a specific environmental condition, where CanA activity is either absent or insufficient to support bacterial growth and/or survival.

3.4 Expression of *canA* and *canB* in Response to Environmental CO_2 Concentrations

To determine whether either of the CA-encoding genes are regulated by the environmental CO_2 concentration, the expression of *canA* and *canB* was compared following growth in liquid media at low and high CO_2 concentrations using RT-PCR and qPCR. As shown in **Figure 3.4.1 A**, the *canA* gene was expressed at both low and high CO_2 concentrations, with similar quantities of *canA*-specific transcripts detected under both conditions. The *canB* gene was, likewise, expressed at both low and high CO_2 concentrations (**Figure 3.4.1 B**). Like *canA,* equivalent amounts of *canB* transcripts were detected at both CO_2 concentrations examined. The expression profiles of *canA* and *canB* was confirmed by qRT-PCR **(Figure 3.4.2)**, where no significant differences in the relative expression levels of *canA* or *canB* at high vs. low CO_2 concentrations were observed. The constitutive and near equivalent levels of *canA* expression at low and high CO_2 concentrations suggests that CanA activity may be required for mediating the formation of HCO_3^- for cellular metabolism at both low and high CO_2 concentrations. While the pattern and expression levels of *canB* was found to be similar to that of *canA*, only the latter appears to be essential for *Msm* growth at either low or high CO_2 concentrations **(Chapter 3.1 and 3.2).**

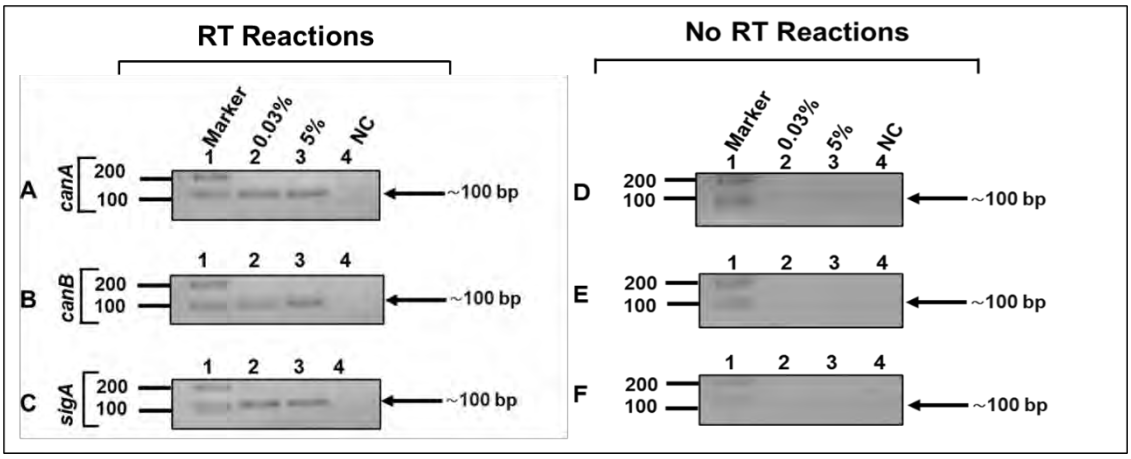

Figure 3.4.1. Semi-quantitative RT-PCR analysis of *canA* and *canB* expression in WT *Msm* at low and high CO_2 concentrations. RNA samples isolated from *Msm* grown at either 0.03 or 5% CO_2 were reversed transcribed into cDNA and the presence of *canA*, *canB* or *sigA* transcripts detected by PCR using primers specific for each gene. RNA samples that were not reverse transcribed were included as controls to confirm the absence of gDNA contamination (No RT reactions). Amplicons were electrophoresed on 2% (w/v) agarose at 80 V for 70 min and imaged under UV light. The cDNA used as a template in each reaction were as follows: (**A, B and C**) contain the RT reactions and figures (**D, E and F**) contain the No RT reactions. Each reaction was performed in triplicate. **Lanes 1:** Molecular Weight Marker; **Lanes 2:** *Msm* WT at 0.03% CO_2; **Lanes 3:** *Msm* WT at 5%; **Lanes 4:** Negative Control (NC) RT reaction. Black arrows indicate the sizes of the DNA fragments.

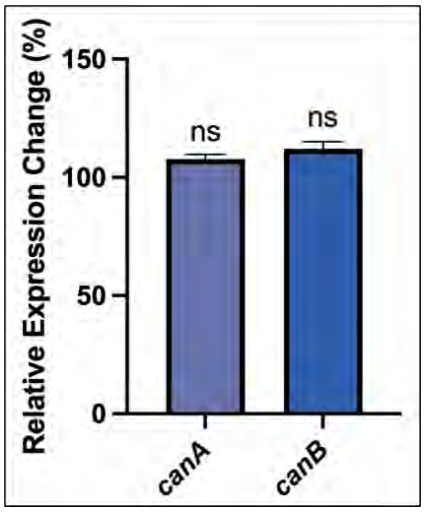

Figure 3.4.2. Relative expression levels of *canA* and *canB* in the *Msm* WT at in WT *Msm* at low and high CO_2 concentrations. *Msm* cultures were diluted to an OD_{600} of 0.1 and grown to the mid-exponential phase (OD_{600} ~0.8) before the isolation of total RNA. Equivalent amounts of RNA were converted to cDNA and the relative expression levels of *canA* and *canB* were determined using the 2-ΔΔCt method. Expression levels were normalised to *sigA* and the values depicted represent the percentage of *canA* or *canB* transcripts, relative to WT *Msm*. Statistical analysis was calculated using an ordinary one-way ANOVA test; ns denotes 'not significant'.

3.5 Nutritional Complementation of the *canA* and *canB* KD Mutants

HCO_3^- is required for the activity of several carboxylase enzymes involved in the biosynthesis of metabolites that include intermediates of central metabolic pathways (e.g. pyruvate, oxaloacetate), amino acids, fatty acids, and nucleotides (Aguilera *et al.,* 2005; Burghout *et al.,*

2010; Merlin *et al.,* 2003). Microbes that lack CA activity typically display a requirement for growth at high CO_2 concentrations given their inability to generate sufficient HCO_3^- to support cellular metabolism at atmospheric (low) CO_2 concentrations (Merlin *et al.,* 2003). To examine whether the growth phenotypes associated with *canA* gene silencing is due to reduced HCO_3^- formation, we next examined whether the growth defect of the ATc-treated *canA* KD strains could be rescued by incubation at either (i) high CO_2 concentrations or (ii) supplementation with 10 mM HCO_3^-. As previously demonstrated, the three *canA* KD mutants displayed severe growth defects when grown on solid media at low CO_2 concentrations in the presence, but not absence of ATc (**Figure 3.5.1 A** and **B**). While incubation at high CO_2 concentrations had no effect on the growth of the KD mutants in the absence of ATc (**Figures 3.5.1 A** vs. **E**), their growth was significantly improved in the presence of ATc (**Figures 3.5.1 B** vs. **F**).

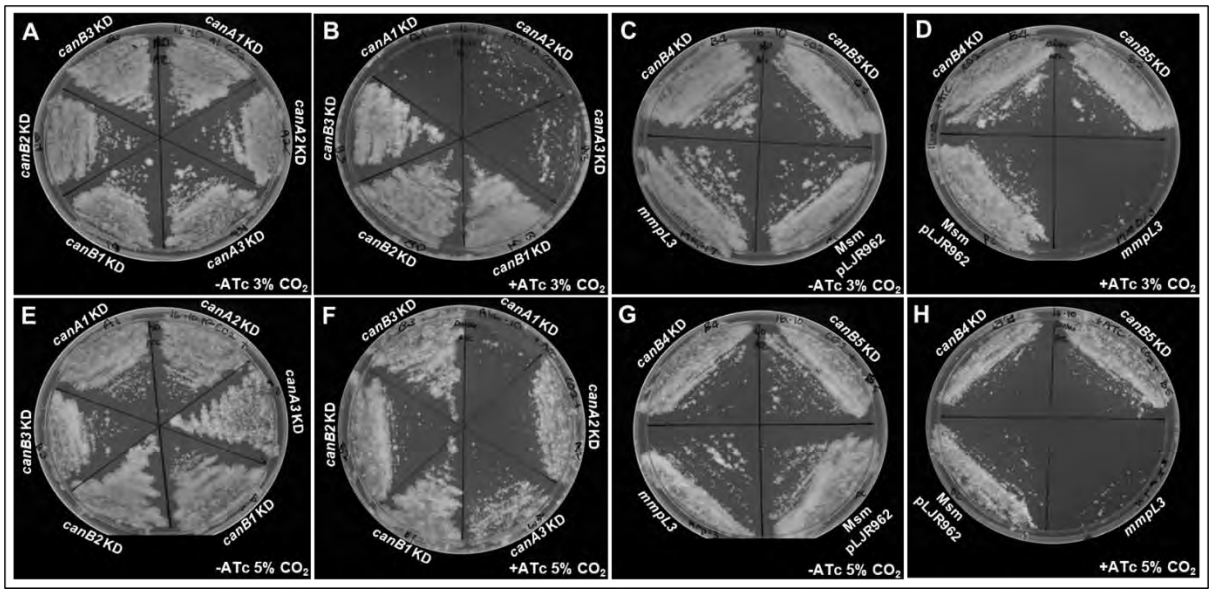

Figure 3.5.1. Comparison of the growth of *canA* and *canB* KD mutants on solid growth media in the presence and absence of ATc at 0.03% and 5% CO_2 levels. The indicated strains were prepared and plated as described in **Figure 3.2.1.** Plates in the upper panels (**A, B, C, D**) and lower panels (**E, F, G, H**) were incubated at low (0.03%) or high (5%) CO_2 concentrations, respectively. Plates in the panels **A, C, E and G** were not supplemented with ATc (-ATc), while plates in the panels **B, D, F and H** were supplemented with ATc (+ATc). The plates were grown at 37 °C and images were taken after 3 days.

The growth promoting effect of incubation at high CO_2 concentrations was, however, more pronounced in the *canA2* and *canA3* KD mutants than the *canA1* KD mutant (**Figure 3.5.1 B** and **F**). This may be due to the presence of higher, basal levels of CanA in the former two KD strains, given the weaker sgRNAs used in their construction, enabling their growth to be more easily rescued than the *canA1* KD. Due to more efficient gene silencing, the ATc-treated *canA1* KD may require CO_2 concentrations higher than 5% to be rescued. As shown in **Figure 3.5.2**, the growth of the ATc-treated *canA* KD mutants could also be improved by direct supplementation with 10 mM HCO_3^- (**B** vs. **F**). Similar to our observations with CO_2, this effect was more pronounced for the *canA2* and *canA3* KDs, than for the *canA1* KD. Neither CO_2 nor HCO_3^-supplementation was observed to affect the growth the *canB* KD mutants, or the growth of ATc-untreated cells **Figures 3.5.1** and **3.5.2)**.

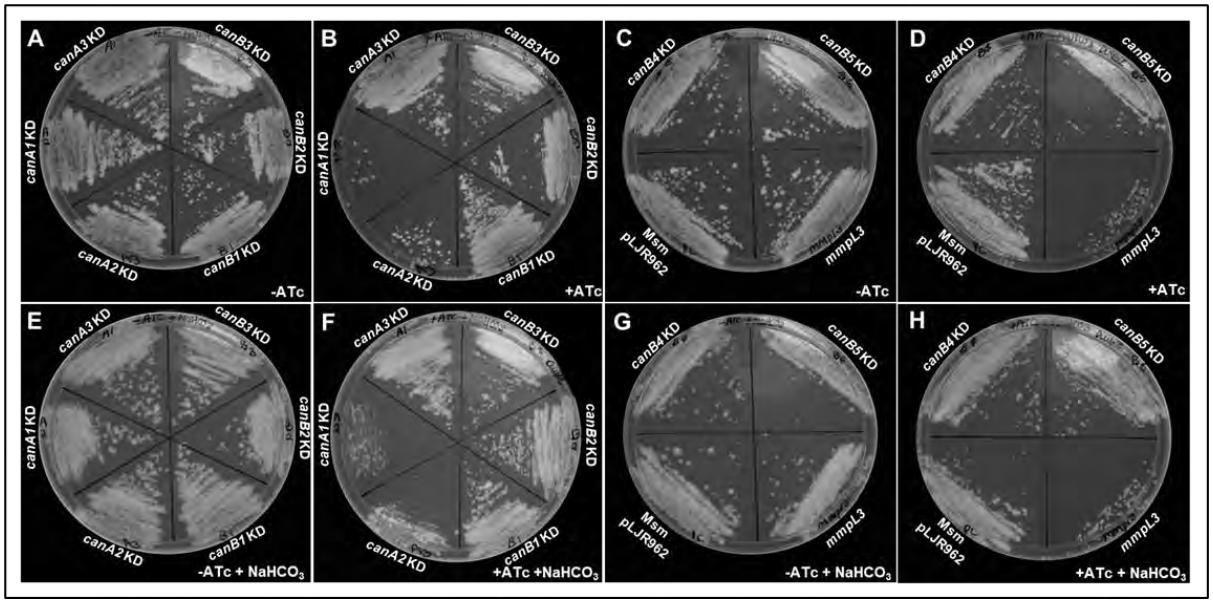

Figure 3.5.2. Examination of the effect of bicarbonate supplementation on the growth of the *canA* and *canB* KD mutants on solid growth media in the presence and absence of ATc. The indicated strains were prepared and plated as described in **Figure 3.2.1.** Plates in the upper panels (**A, B, C, D**) and lower panels (**E, F, G, H**) lacked or contained 10 mM $NaHCO_3$, respectively. Plates in the panels **A, C, E and G** were not supplemented with ATc (-ATc), while plates in the panels **B, D, F and H** were supplemented with ATc (+ATc). The plates were grown at 37 °C and images were taken after 3 days.

To examine whether growth of the *Msm canA1* KD mutant could be similarly rescued by supplementation with the end-products of HCO_3^--dependent carboxylation reactions, we compared the effects of gene silencing on solid media supplemented with metabolites previously shown to rescue the growth of CA-deficient microbes. As shown in **Figure 3.5.3**, supplementation with the TCA intermediates malate (**A, B**), oxaloacetate (**C, D**), pyruvate (**E,**

F), or succinate (**G, H**) could not rescue the growth defect of the ATc-treated *canA1* KD mutant. Supplementation with the amino acid aspartate (**I, J**), which is more stable than its TCA intermediate precursor, oxaloacetate, also had no effect on bacterial growth.

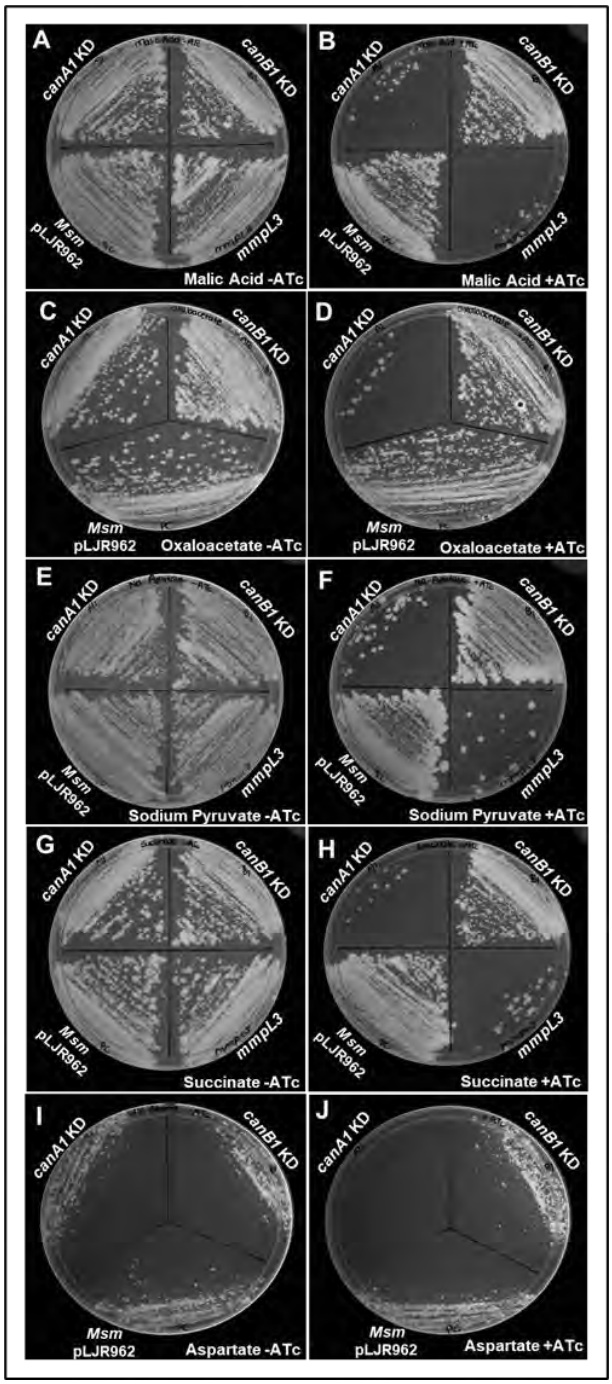

Figure 3.5.3. Effect of supplementation with TCA intermediates or aspartate on the growth of the *canA1* and *canB1* KD mutants in the presence and absence of ATc. *Msm* strains were grown as described in **Figure 3.1.1** and plated on solid medium in ATc's absence (left panels, **A, C, E, G** and **I**; -ATc) or presence (right panels, **B, D, F, H** and **J;** +ATc). The solid medium was supplemented with the following metabolites **A and B:** malate; **C and D**: oxaloacetate **E and F**; pyruvate; **G and H**: succinate; **I and J:** aspartate. The plates were incubated at 37 °C and images were taken after 3 days.

While supplementation with the pyrimidine, uracil, had no effect on the growth of CanA-depleted cells (**Figure 3.5.4 C** and **D**), supplementation with the purine, adenine, could partially rescue the growth of the *canA* KD strains (**Figure 3.5.4 A** and **B**).

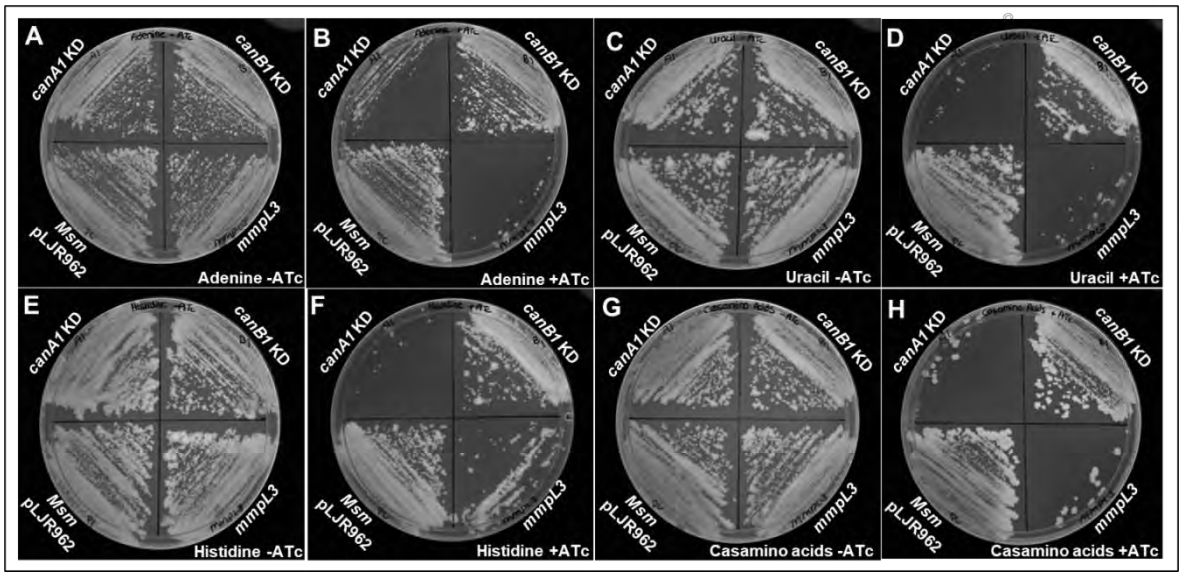

Figure 3.5.4. Effect of supplementation with nucleotides or casamino acids on the growth of the *canA1* and *canB1* KD in the presence or absence of ATc. *Msm* strains were grown as described in **Figure 3.1.1** and plated on solid medium in ATc's absence (left panels, **A, C, E and G**; -ATc) or presence (right panels, **B, D, F and H;** +ATc). The solid medium was supplemented with the following metabolites **A and B:** adenine; **C and D**: uracil **E and F**; histidine; **G and H**: casamino acids. The plates were grown at 37 °C and images were taken after 3 days.

Supplementation with OADC enrichment (BD) and ADS (albumin-dextrose-saline) did not alleviate the growth defect of the ATc-treated *canA* KD mutant (**Figure 3.5.5 A - D**). Since ACC catalyses the bicarbonate-dependent formation of malonyl-CoA from acetyl-CoA during fatty acid (FA) biosynthesis, we next examined the effect of FA supplementation of the growth the KD mutants. Supplementation with saturated, unsaturated, and branched FAs in the form of palmitate (P), oleate (O) and cholesterol (C), respectively [supplied together with ADS as PADS, OADS, CADS, respectively] had no effect on the growth of ATc-treated *canA1* KD cells (relative to the similarly treated *mmpL3* mutant) (**Figure 3.5.5 E - J**). Supplementation with both oleate and palmitate (OPADS) also had no effect on the growth of *canA* KD (**Figure 3.5.5 M** and **N**). The ability of FAs to rescue the growth of the ATc-treated *canA* KD was, however, partially improved when glucose was omitted from the media (OPAS) (**Figure 3.5.5 K** and **L**). This observation suggests that CA activity may be required to generate HCO_3^- for anaplerotic carboxylation reactions required to replenish TCA intermediates such as oxaloacetate during gluconeogenic growth on FAs.

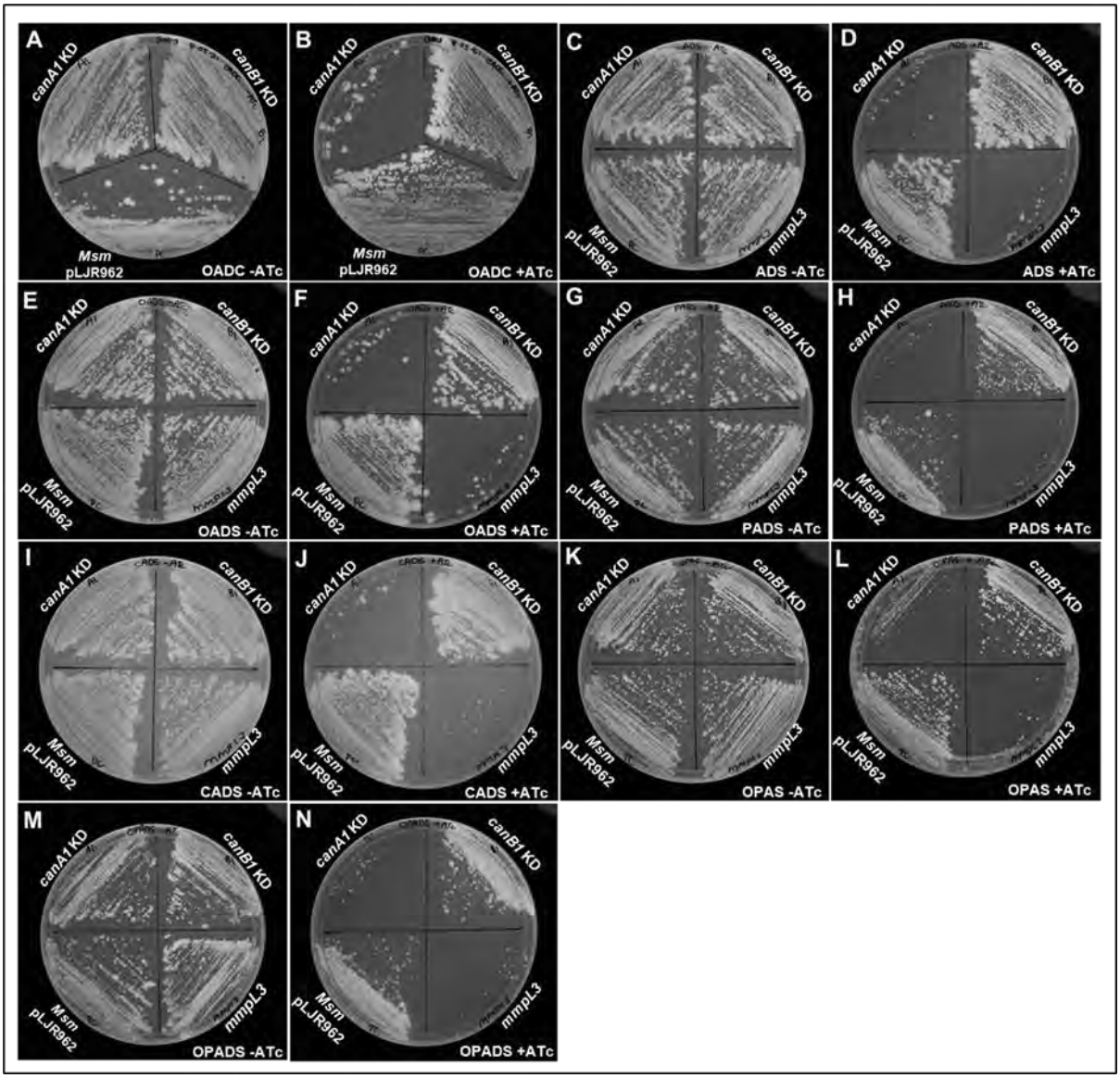

Figure 3.5.5. Effect of supplementation with fatty acids on the *canA1* and *canB1* KD in the presence or absence of ATc. Plates in the first and third columns (**A-M and C-K**) were grown without ATc (-ATc) and plates in the second and fourth columns (**B-N and D-L**) were grown in the presence of ATc (+ATc). Plates in panels **A and B** were grown in the presence of OADC. Plates in panels **C and D** were grown in the presence of ADS. Plates in panels **E and F** were grown in the presence of OADS. Plates in panels **G and H** were grown in the presence of PADS. Plates in panels **I and J** were grown in the presence of CADS. Plates in the panels **K and L** were grown in the presence of OPAS. Plates in the panels **M and N** were grown in the presence of OPADS. plates were grown at 37 °C and images were taken after 3 days.

We next examined whether a mixture of the end-products of HCO_3^--dependent carboxylases could rescue the growth of the ATc-treated *canA1* KD mutant. As shown in **Figure 3.5.6**, the growth of the KD mutant was significantly improved following incubation on LBsmeg (**Figure 3.5.6 C** and **D**), a rich source of sugars, purines, pyrimidines, vitamins and amino acids (Sezonov *et al*., 2007), as well as on 7H10 media supplemented with a combination of the metabolites shown to improve the growth of the *canA* KD above (**Figure 3.5.6 A and B vs E** and **F**). This observation suggests that the loss of CanA activity may inhibit the biosynthesis of the end-products of several different HCO_3-dependent carboxylation reactions. The growth defects observed for the *Msm* when CanA activity is reduced or eliminated may, therefore, be due to the absence of multiple, essential metabolites that rely on CA activity for formation.

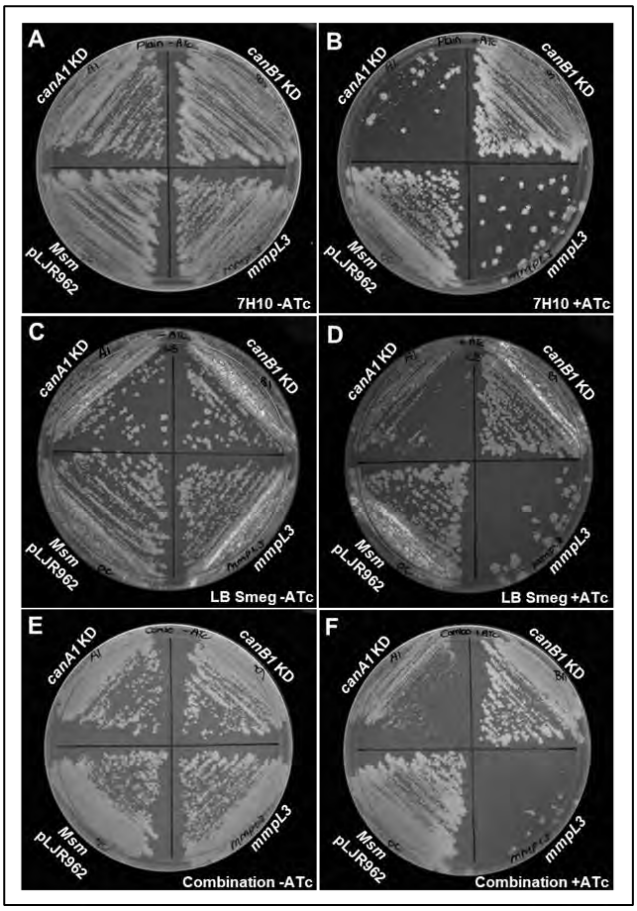

Figure 3.5.6. Effect of nutritional supplementation on the growth of the *canA1* and *canB1* KD in the presence or absence of ATc. Plates in the first column (**A-G**) were grown in the absence of ATc (-ATc) and plates in the second column (**B-H**) were grown in the presence of ATc (+ATc). Plates in the panels **A and B** were grown on plain 7H10 media. Plates in the panels **C and D** were grown on plain LB Smeg media. Plates in the panels **E and F** were grown on 7H10 plates containing a combination of several carbon, amino acid, fatty acids, TCA intermediates sources. The plates were grown at 37 °C and images were taken after 3 days.

3.6 Construction of Msm Δ*canA* and Δ*canB* Deletion Mutants

The results presented in the previous sections suggest that the *canA* gene is essential for *Msm* growth at both low and high CO_2 concentrations (i.e., 0.035 and 5%). Although the *Msm canB* gene was shown to be expressed under both low and high CO_2 concentrations (**Figure 3.4.2**), the CanB enzyme appears to be dispensable and unable to compensate for the loss of CanA under the conditions examined in this study thus far. To confirm these findings, we next attempted to genetically inactivate the *Msm canA* (**Chapter 3.6.1** below) and *canB* (**Chapter 3.6.2** below) genes by replacing the native, chromosomal copies of the genes with a zeocin-resistance (Zeo^R) cassette. The ZeoR-marked *canA* and *canB* genes were constructed by PCR amplification of DNA fragments homologous to the 5′- and 3′-ends of each gene [referred to as upstream (US) and downstream (DS) fragments] followed by their "splicing" to a *loxP*-flanked Zeo^R-cassette using overlap-extension PCR. The allelic exchange substrates (AES) thus generated were introduced into *Msm* to generate marked and unmarked Δ*canA* and Δ*canB* deletion mutants as described below.

3.6.1 Generation of a Marked and Unmarked Δ*canA* Deletion Mutant

For *canA*, PCR of the 5′- and 3′-ends of the gene resulted in the formation of amplicons of ~540 (**Figure 3.6.1 A, Lane 2**), and 480 bp (**Figure 3.6.1 A, Lane 3**), which correspond to the predicted sizes of the *canA* US and DS fragments, respectively (**Table 2.3**). The fragments were purified and subsequently spliced to the ~740 bp *loxP*-flanked Zeo^R cassette (**Figure 3.3.1 A, Lane 4**) that had been PCR amplified from pMSG360-Zeo (Barkan *et al*., 2010) using splice-by-overlap-extension PCR (SOE-PCR). This resulted in the amplification of a ~1,760 bp (**Figure 3.6.1 B, Lane 2**) product, which was purified and used as the linear allelic exchange substrate (AES) to genetically inactivate the *canA* gene. For this, the purified *canA*::Zeo^R AES was electroporated into the WT *Msm* (pJV53kan) strain (van Kessel & Hatfull, 2008), followed by plating and selection on 7H10 agar supplemented with zeomycin (7H10/Zeo). Despite repeated attempts, no Zeo^R transformants could be obtained in the WT genetic background, even after prolonged periods of incubation (<10 days) in either low or high CO_2 environments. Since our previous results suggested that the *canA* gene is essential for the viability of *Msm,* even when incubated at high CO_2 concentrations (**Figure 3.5.1**), we next examined whether the *canA* gene could be inactivated in a genetically complemented *Msm* strain that expresses a second copy of the *canA* gene from the phage L5 integration site. For this, we generated and used the *Msm* pJV53hyg L5*::*pMV306kan::*canA* strain, which expresses a second copy of the *Msm canA* gene from its native promoter *Msm* in the L5 integrations site, (**Chapter 2.9.4**), as a recipient strain

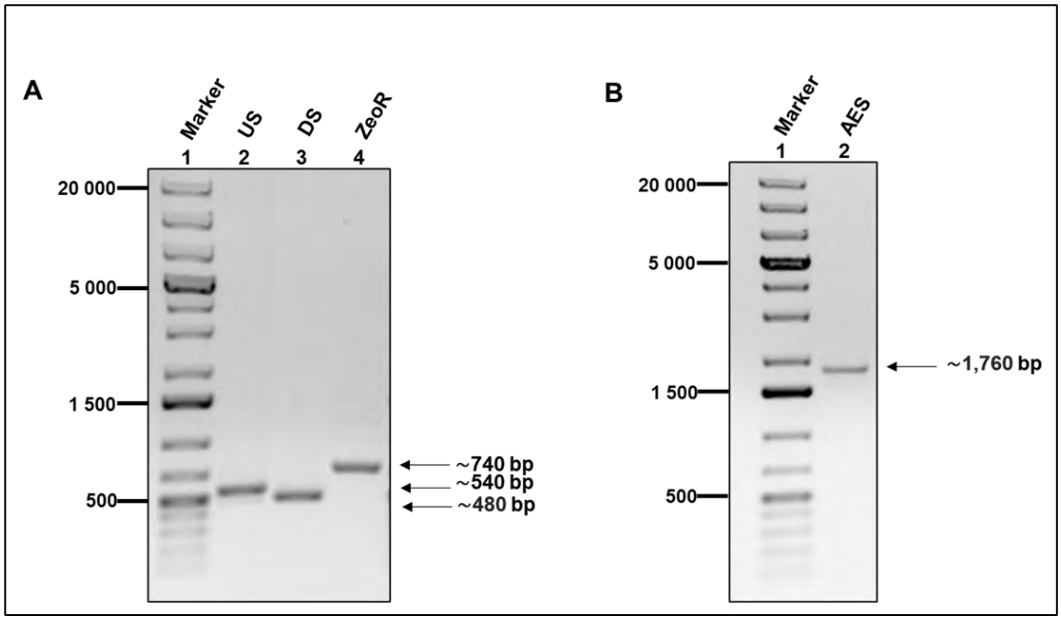

Figure 3.6.1. (A) Agarose gel confirming the successful amplification of the *canA* upstream fragment (US), downstream fragment (DS) and zeocin-resistance cassette (Zeo^R) fragment. (A) PCR reactions were performed using WT *Msm* gDNA (for US and DS fragments) or pMSG360Zeo (for the Zeo^R cassette) and the canA-US-For and canA-US-Rev (for US fragment), canA-DS-For and canA-DS-Rev (for DS fragment) and pKMZeo-For and pKMZeo-Rev (for Zeo^R). The PCR products were electrophoresed on 0.8% (w/v) agarose at 80 V for 50 min and imaged under UV light. **Lane 1:** Molecular Weight Marker; **Lane 2:** *canA* US fragment; **Lane 3:** *canA* DS fragment; **Lane 4:** Zeo^R cassette. **(B) Agarose gel confirming the successful generation of an allelic exchange substrate (AES).** The PCR reaction was initially performed using the purified US, DS and Zeo^R DNA and fragments and the flanking canA-US-For and canA-DS-Rev added after 10 cycles. The PCR product was electrophoresed on 0.8% (w/v) agarose at 80 V for 50 min. **Lane 1:** Molecular Weight Marker; **Lane 2:** Allelic Exchange Substrate (AES). Black arrows indicate the size of the predicted PCR amplicon.

Similar to the results obtained for WT *Msm* pJV53kan above, no Zeo^R transformants could be obtained following introduction of the *canA*::Zeo^R AES into a WT *Msm* pJV53hyg control strain. Numerous Zeo^R transformants could, however, be obtained in the genetically complemented *Msm* L5*::*pMV306kan::*canA* pJV53hyg strain. To confirm that the native copy of the *Msm canA* gene had been replaced in the isolated Zeo^R transformants, the genotype of the putative, marked Δ*canA*::Zeo^R mutants was analysed by PCR using *canA*- and/or Zeo^R-cassette-specific primers (**Figure 3.6.2**). Amplicons of ~2,200 (**Figure 3.6.2; Lane 2**), 1,177 (**Figure 3.6.2; Lane 3**) and 683 bp (**Figure 3.6.2; Lane 4**) were obtained from the putative *Msm* Δ*canA*::Zeo^R mutant when using the indicated *canA*- or Zeo^R-cassette specific primers, which is consistent with the sizes expected following replacement of the WT *Msm canA* allele with the inactivated *canA*::Zeo^R cassette **(Table 2.2).** The forward and reverse *canA* primers used for the genotypic analysis were designed to anneal either upstream or downstream of the

primers used to amplify the *canA*::Zeo^R AES or the pMV306kan::*canA* complementation vector, thereby allowing the native *Msm canA* locus to be differentiated from the *canA* allele present in the L5 integration site, or those that may have arisen from illegitimate recombination of the *canA*::Zeo^R AES into the *Msm* chromosome. For the WT *Msm* strain, an amplicon of ~2,088 bp was obtained when using the *canA*-specific primers (**Figure 3.6.2, Lane 5**), which is consistent with the size expected for the endogenous copy of the *Msm canA* gene when using these primers **(Table 2.2).** As expected, no amplicons were obtained from WT *Msm* strain when using either of the Zeo^R-cassette specific primers (**Figure 3.6.2, Lanes 6 and 7**). The observation that genetic inactivation of *canA* was only possible when a second copy of the gene was supplied *in trans* supports the idea that *canA* is essential for the viability of *Msm*, supporting our earlier findings with the *canA* KD mutants.

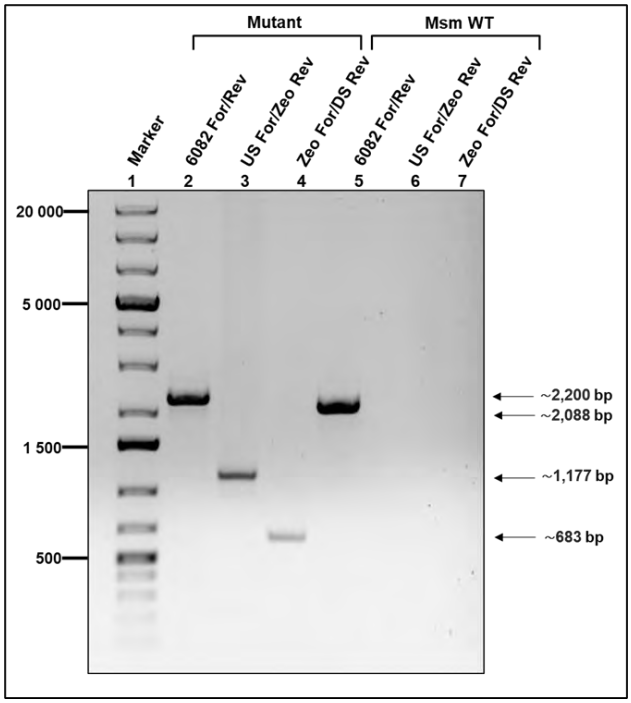

Figure 3.6.2. Agarose gel confirming the genotype of the putative *Msm* Δ*canA*::Zeo^R mutant. PCR reactions were performed using gDNA from *Msm* WT or a representative Δ*canA*::Zeo^R mutant using primers canA-US-For2 and canA-DS-Rev2 (6082 For/Rev), canA-US For and Zeo-Check-Rev (US-For/Zeo^R-Rev) and Zeo-Check-For and canA-DS-Rev (Zeo^R-For/DS-Rev). The PCR products were electrophoresed on a 0.8% agarose gel at 80 V for 50 min and visualised under UV light. The gDNA used as a template in the PCR reactions were as follows: **Lane 1:** Molecular Weight Marker; **Lanes 2-4:** Δ*canA*::Zeo^R mutant; **Lanes 5-7:** *Msm* WT gDNA. Black arrows indicate the approximate sizes of the predicted PCR amplicons.

To generate an unmarked *Msm* Δ*canA* deletion mutant, the *loxP*-flanked Zeo^R cassette was subsequently removed from the marked, genetically complemented *Msm* Δ*canA*::Zeo^R L5*::*pMV306kan::*canA* mutant by Cre-mediated recombination, as described in **Chapter 2.9.2**. The loss of the Zeo^R-cassette was confirmed by analytical PCR using the *canA*-specific primers described above (**Figure 3.6.3**). Amplicons of ~2,088 and 2,200 bp were obtained from the WT and Δ*canA*::Zeo^R pComp::*canA* strains, respectively (**Figure 3.6.3 Lanes 1 and 2**). An amplicon of ~1,500 bp was, by contrast, obtained from the unmarked Δ*canA* mutant (**Figure 3.6.3, Lane 3**), which is consistent with the excision of the ~700 bp Zeo^R-cassette from the *canA* gene **(Table 2.2).** DNA sequencing of the purified amplicon subsequently confirmed the removal of the Zeo^R-cassette and deletion of 193 codons (codons 10 to 200 of the *canA* gene in the newly generated, genetically complemented *Msm* Δ*canA* L5*::*pMV306kan::*canA* deletion mutant.

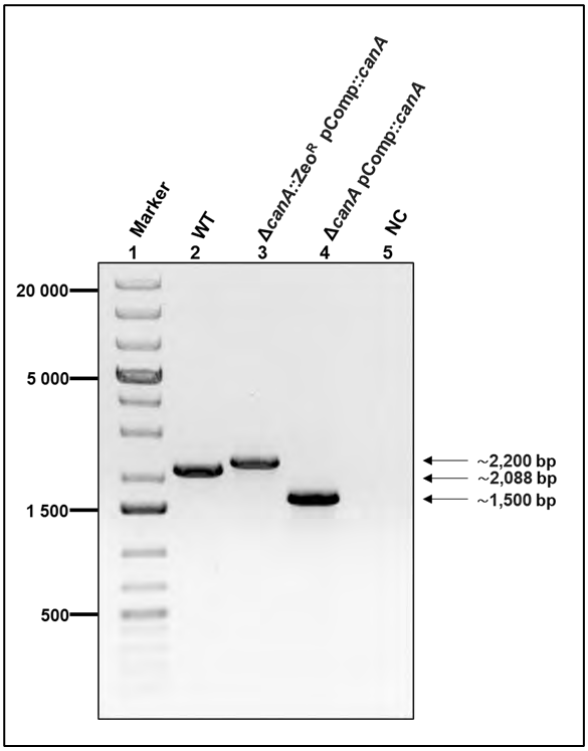

Figure 3.6.3. Agarose gel confirming the generation of the unmarked (A) *Msm* Δ*canA* deletion mutants. PCR reactions were performed using genomic DNA isolated from the **(A)** WT, Δ*canA*::Zeo^R pComp::*canA* using primers 6082-For and 6082-Rev. The PCR products were electrophoresed on 0.8% (w/v) agarose at 80 V for 50 min. The gDNA used as a template in the PCR reactions were as follows: **Lane 1:** Molecular Weight Marker; **Lane 2:** *Msm* WT gDNA; **Lane 3:** *Msm* Δ*canA*::Zeo^R pComp::*canA* gDNA; **Lane 4:** *Msm* pComp::*canA* gDNA; **Lane 5:** No DNA, negative control. Black arrows indicate the sizes of the predicted PCR amplicons.

As a final confirmation of the essentiality of the *Msm canA* gene, we attempted to replace the pMV306kan::*canA* vector in the *Msm* Δ*canA* L5*::*pMV306kan::*canA* strain with either (i) an empty L5 integrating vector, pML1342 [which confers resistance to Hyg as opposed to Km (Huff *et al.,* 2010)] or (ii) pML1342 harbouring a functional copy of either *canA* (pML1342::*canA*) or *canB* (pML1342::*canB*) (see **Figure 2.3** and **Supplementary Material C2**). The replacement of pMV306kan::*canA* via this mechanism ("L5 allele switching"; Pashley and Parish, 2003) can produce three different outcomes (see **Figure 2.3**): (i) replacement of pMV306kan::*canA* with either the parental pML1342 vector or one encoding an inactive CA enzyme would result in the formation of Hyg^R cells that are non-viable under standard growth conditions and therefore unable to survive on 7H10 agar plates, (ii) replacement of pMV306kan::*canA* with pML1342 encoding a functional CA enzyme would result in the formation of viable, Hyg^R [but kanamycin sensitive (Km^S)] transformants on 7H10 agar plates, (iii) site-specific recombination of pML1342 or its *canA*- or *canB*-encoding derivatives adjacent to the original, L5 integrated pMV306kan::*canA* plasmid would result in the formation of viable, Hyg^R Km^R transformants (Pashley and Parish, 2003; Wu *et al.,* 2019).

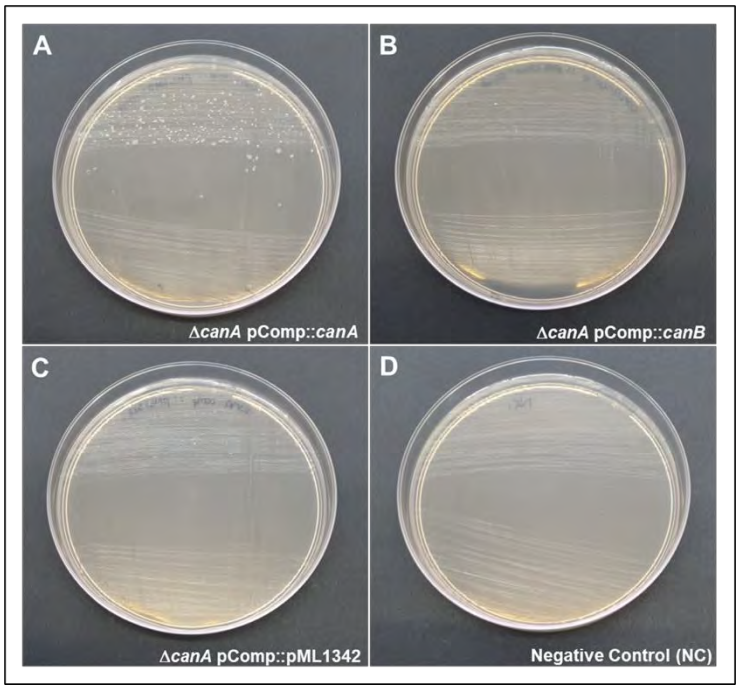

Figure 3.6.4. Demonstration of the essentiality of *Msm canA* using L5 allele swaps. The Hyg^R-conferring L5 integrating plasmids pML1342::*canA*, pML1342::*canB* gene and empty parental vector, pML1342 were introduced into Km^R *Msm* Δ*canA* L5::pMV306kan::*canA* (pComp::canA) cells and Hyg^R transformants selected on 7H10/Hyg agar plates. After 5 days of incubation at 37 °C, Hyg^R transformants transformed with either **(A)** pML1342::*canA*, **(B)** pML1342::*canB*, **(C)** pML1342 were identified and replica plated to determine their antibiotic-resistance profiles. **(D)** Untransformed *Msm* pComp::*canA* cells served as a negative control (NC).

Following the introduction of pML1342::*canA* into the *Msm* Δ*canA* L5::pMV306::*canA* strain, numerous Hyg^R transformants were obtained following selection on 7H10/Hyg agar plates (**Figure 3.6.4 A**). Replica plating of representative Hyg^R transformants revealed that these transformants were comprised of both Hyg^R Km^S and Hyg^R Km^R cells, with the former category of transformants representing cells in which pMV306kan::*canA* was replaced by pML1342::*canA* (data not shown). The number of transformants obtained following the introduction of either the parental pML1342, or pML1342::*canB* vector, was ~10 to 100-fold lower when compared with pML1342::*canA* (**Figure 3.6.4 B and C**). All the transformants arising from these two electroporation reactions were, moreover, shown to be comprised exclusively of Hyg^R Km^R transformants, indicating that they had not lost the original pMV306kan::*canA* vector. Taken together, our findings confirm that the *Msm canA* gene is essential for cellular viability since neither the endogenous gene (**Chapter 3.3.1**), nor the copy present on the pMV306kan::*canA* complementation plasmid could be lost, unless replaced with another functional, CA-encoding gene such as that contained on the pML1342::*canA* in these experiments. Our inability to obtain Hyg^R Km^S transformants following introduction of a second copy of the *canB* gene on the pML1342::*canB* plasmid, further supports the idea that the CanB enzyme is inactive under the assay conditions used in this study.

3.6.2 Generation of a Marked and Unmarked Δ*canB* Deletion Mutant

To generate a marked *Msm* Δ*canB* mutant, we used a similar approach to that described for *canA* above (see **Figure 2.2**). The 5′- and 3′-ends of the *canB* gene were first amplified producing amplicons of ~522 and 514 bp (**Figure 3.6.5, Lanes 3 and 4**), which correspond to the predicted sizes of the *canB* US and DS fragments, respectively (**Table 2.3**). The amplicons were purified and spliced to the Zeo^R cassette (**Figure 3.6.5, Lane 4**), as described for *canA*, resulting in the production of an amplicon of 1,776 bp that was used as the linear AES to genetically generate the marked *ΔcanB*::Zeo^R mutant (**Figure 3.6.5, Lane 2**).

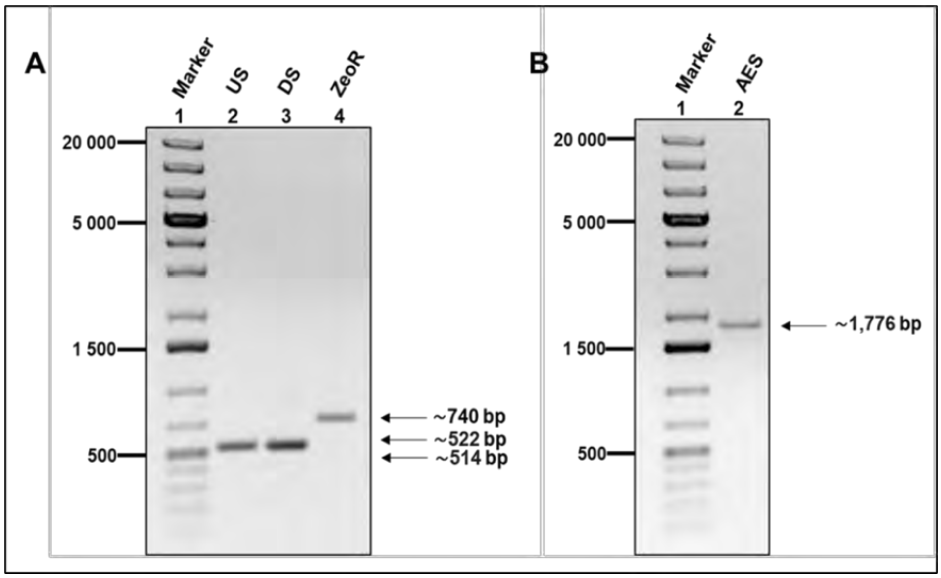

Figure 3.6.5. Agarose gel confirming the successful amplification of the *canB* upstream fragment (US), downstream fragment (DS) and zeocin-resistance cassette (Zeo^R) fragment. (A) PCR reactions were performed using WT *Msm* gDNA (for US and DS fragments) or pMSG360Zeo (for the Zeo^R cassette) and the canB-US-For and canB-US-Rev (for US fragment), canB-DS-For and canB-DS-Rev (for DS fragment) and pKMZeo-For and pKMZeo-Rev (for Zeo^R). The PCR products were electrophoresed on 0.8% (w/v) agarose at 80 V for 50 min and imaged under UV light. **Lane 1:** Molecular Weight Marker; **Lane 2:** *canB* US fragment; **Lane 3:** *canB* DS fragment; **Lane 4:** Zeo^R cassette. **(B) Agarose gel confirming the successful generation of an allelic exchange substrate (AES).** The PCR reaction was initially performed using the purified US, DS and ZeoR DNA and fragments and the flanking canB-US-For and canB-DS-Rev added after 10 cycles. The PCR product was electrophoresed on 0.8% agarose at 80 V for 50 min. **Lane 1:** Molecular Weight Marker; **Lane 2:** Allelic Exchange Substrate (AES). Black arrows indicate the size of the predicted PCR amplicon.

Once generated, the *canB* AES was introduced into WT *Msm* harbouring pJV53kan, as described for the *canA* AES above. In contrast to the results observed for *canA*, numerous Zeo^R transformants were obtained following selection on 7H10/Zeo agar medium following incubation at both low and high CO_2 concentrations. The genotype of the putative Δ*canB::*Zeo^R deletion mutants was analysed by PCR (**Figure 3.6.6**). Amplicons of ~1,776 (**Figure 3.6.6, Lane 2**), 1,159 (**Figure 3.6.6, Lane 3**) and 717 bp (**Figure 3.6.6, Lane 4**), which correspond to the predicted sizes for a *Msm* Δ*canB*::Zeo^R mutant **(Table 2.3),** were identified when using the indicated *canB*- and/or the Zeo^R-cassette-specific primer pairs. An amplicon of ~1,477 bp was identified for *Msm* WT (**Figure 3.6.6, Lane 5**), by contrast. which is expected for strains harbouring the endogenous *Msm canB* gene. As for *canA*, no amplicons were detected in the WT background when using primers specific for the Zeo^R-cassette (**Figure 3.6.6, Lanes 6 and 7**), given the absence of the Zeo^R marker from the genome of WT *Msm*.

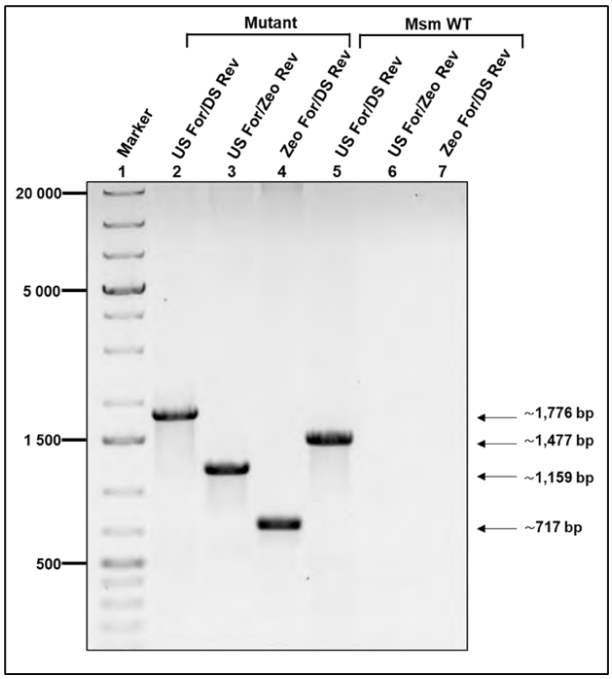

Figure 3.6.6. Agarose gel confirming the genotype of the putative *Msm* Δ*canB*::Zeo^R mutant. PCR reactions were performed using genomic DNA isolated from *Msm* WT or putative *canB*::Zeo^R mutant using primers canB-US-For and canB-DS-Rev (US-For/DS-Rev), canB-US For and Zeo-Check-Rev (US-For/Zeo^R-Rev) and Zeo-Check-For and canB-DS-Rev (Zeo^R-For/DS-Rev). The PCR products were electrophoresed on 0.8% agarose at 80 V for 50 min. The gDNA used as a template in the PCR reactions were as follows: **Lane 1:** Molecular Weight Marker; **Lanes 2-4:** Δ*canB*::Zeo^R; **Lanes 5-7:** *Msm* WT gDNA. Black arrows indicate the sizes of the predicted PCR amplicons.

Following removal of the Zeo^R-cassette by Cre-mediated recombination, the genotype of the unmarked *Msm* Δ*canB* mutant was confirmed by PCR. As shown in **Figure 3.6.7, Lane 4,** an amplicon of ~1,125 bp was produced for the putative unmarked Δ*canB* mutant. This contrasts with amplicons ~1,477 and 1,776 bp obtained for the WT and marked Δ*canB*::Zeo^R mutant *Msm* strains (**Figure 3.6.7, Lanes 2 and 3, respectively**). These observations are consistent with the removal of Zeo^R cassette in the unmarked Δ*canB* mutant. Subsequent DNA sequencing of the Δ*canB* amplicon confirmed the removal of the Zeo^R-cassette and deletion of 147 codons (codons 10 to 156) from the WT gene in the deletion mutant.

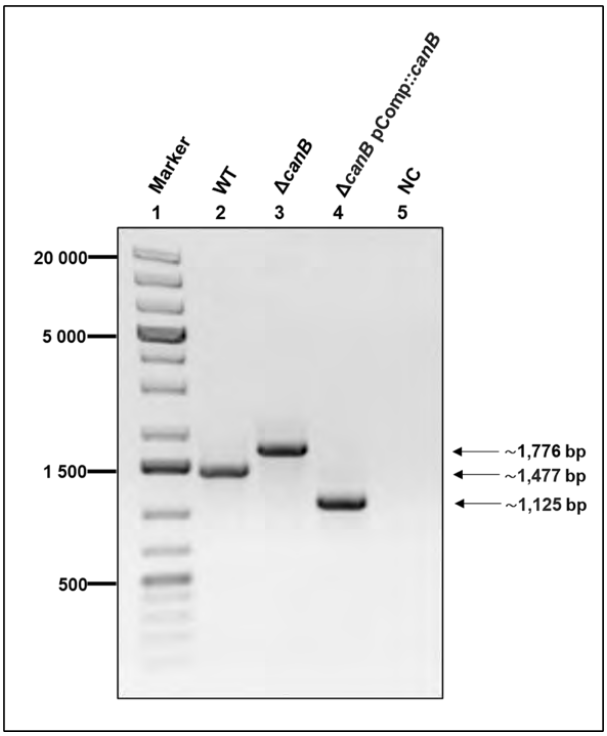

Figure 3.6.7. Agarose gel confirming the putative unmarked *Msm canB* mutant. PCR reactions were performed using genomic DNA isolated from the WT or putative marked (*canB*::Zeo^R) or unmarked (Δ*canB*) *Msm* mutant strains using primers canB-US-For and canB-DS-Rev. The PCR products were electrophoresed on 0.8% (w/v) agarose at 80 V for 50 min. The gDNA used as a template in the PCR reactions were as follows: **Lane 1:** Molecular Weight Marker; **Lane 2:** *Msm* WT gDNA; **Lane 3:** Δ*canB* gDNA; **Lane 4:** Δ*canB* pComp::*canA* gDNA; **Lane 5:** No DNA, negative control. Black arrows indicate the sizes of the predicted PCR amplicons.

For use in growth experiments, pMV306kan::*canB*, which expresses the *Msm canB* from its native promoter was introduced into the phage L5 integration site to generate the genetically complemented *Msm* Δ*canB* L5::pMV306kan::*canB* or Δ*canB* pComp::*canB* strain. RT-PCR analysis confirmed that while *canB* was expressed in WT *Msm*, its expression was eliminated in the *ΔcanB* deletion mutant (**Figure 3.6.8 Lanes 2 and 3, respectively**). Expression of the gene was, however, restored following genetic complementation in the *Msm* Δ*canB* L5::pMV306kan::*canB* strain (**Figure 3.6.8, Lane 4**). Expression of *canA* in the *Msm* WT and Δ*canA* L5::pMV306kan::*canA* strains was likewise observed (**Figure 3.6.9**), although analysis of Δ*canA* deletion mutant was precluded due to the essential nature of the gene.

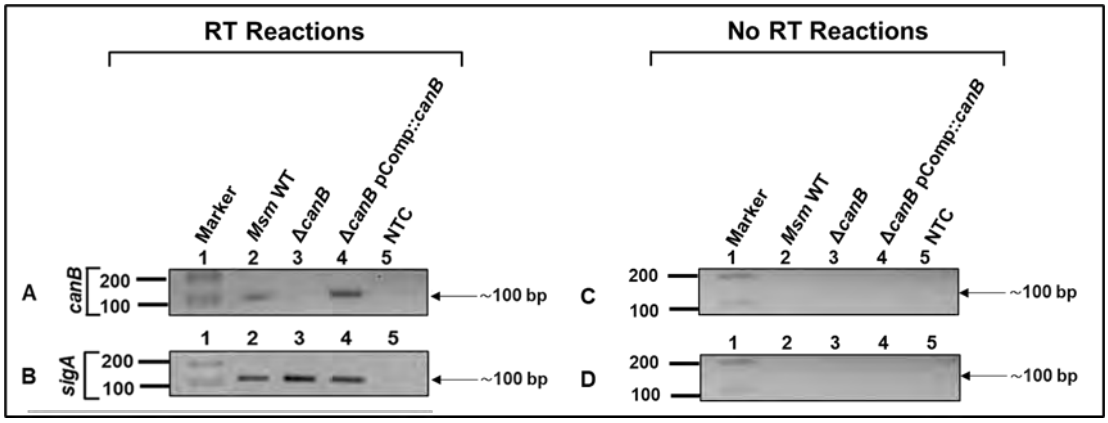

Figure 3.6.8. Semi-quantitative RT-PCR analysis of *canB* and *sigA* expression in the *Msm* WT, Δ*canB* KO mutant and Δ*canB* complemented strain. RNA obtained from each sample were reverse transcribed (RT) into cDNA and PCR amplified using either *canA* **(A)** or *sigA* **(B)**- specific primers. 'No RT reactions' were included to confirm the absence of gDNA contamination. The PCR products were electrophoresed on 2% (w/v) agarose at 80 V for 70 min. Figures (**A and B**) contain the RT reactions and panels (**C and D**) contain the No RT reactions. The cDNA used as a template in each reaction for **Figures A-D** was as follows: **Lanes 1:** Molecular Weight Marker; **Lanes 2:** *Msm* WT; **Lanes 3:** Δ*canB*; **Lanes 4:** Δ*canB* pComp::*canB*; **Lanes 5:** No Template Control (NTC). Black arrows indicate the DNA fragments.

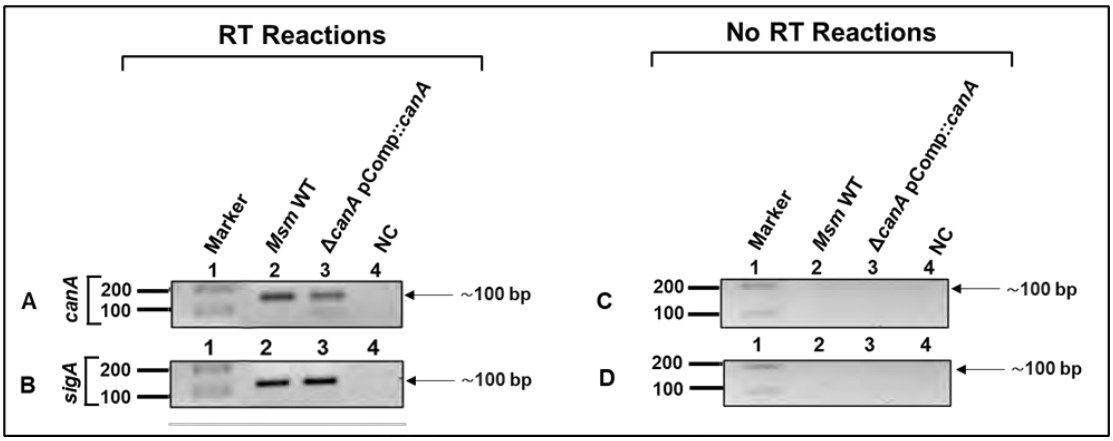

Figure 3.6.9. Semi-quantitative RT-PCR analysis of *canA* and *sigA* expression in the *Msm* WT and Δ*canA* complemented strain. RNA obtained from each sample were reverse transcribed (RT) into cDNA and PCR amplified using either *canA* **(A)** or *sigA* **(B)**- specific primers. 'No RT reactions' were included to confirm the absence of gDNA contamination. The PCR products were electrophoresed on 2% (w/v) agarose at 80 V for 70 min. Figures (**A and B**) contain the RT reactions and panels (**C and D**) contain the No RT reactions. The cDNA used as a template in each reaction for **Figures A-D** was as follows: **Lanes 1:** Molecular Weight Marker; **Lanes 2:** *Msm* WT; **Lanes 3:** Δ*canA* pComp*::canA*; **Lanes 4:** No Template Control (NTC). Black arrows indicate the DNA fragments.

The lack of *canB* expression in the deletion mutant was subsequently confirmed by qRT-PCR, where the expression of the gene was observed to be undetectable relative to that present in the WT strain (**Figure 3.6.10 A**). For *canA*, the expression of the gene was detectable in both *Msm* WT and the genetically complemented Δ*canA* L5::pMV306kan::*canA* strain, although expression was observed to be slightly significantly in the latter strain (**Figure 3.6.10 B**).

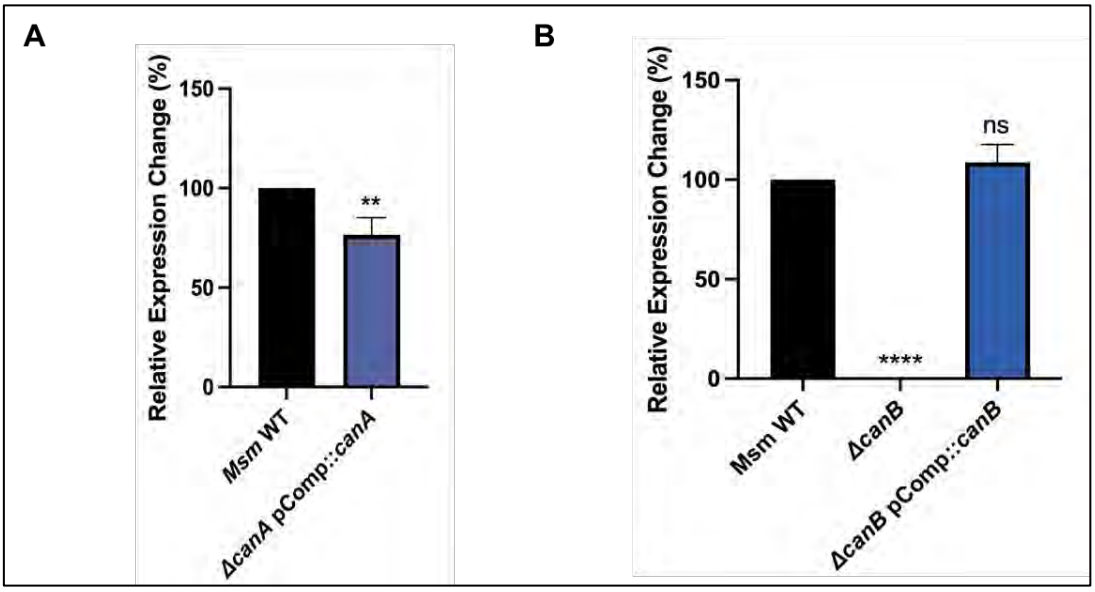

Figure 3.6.10. Relative expression levels of *canA* and *canB* in the *Msm* WT, KO and genetically complemented strains. *Msm* cultures were diluted to an OD_{600} of 0.1 and grown to the mid-exponential phase (OD_{600} ~0.8) before the isolation of total RNA. Equivalent amounts of RNA were converted to cDNA and the relative expression levels of **(A)** Δ*canA* pComp::*canA* and **(B)** Δ*canB and* Δ*canB* pComp::*canB* were determined using the 2-ΔΔCt method. Expression levels were normalised to *sigA* and the values depicted represent the percentage of *canA* transcripts. Statistical analysis was calculated using an ordinary on-way ANOVA test; ** and **** denotes $p < 0.05$ and 0.0001, respectively.

3.7 Phenotypic Analysis of the Δ*canB* Deletion Mutant

Our previous findings with the *Msm canB* KD strain suggested that CanB activity is not required for bacterial growth under standard laboratory conditions. To verify these findings, the growth kinetics of the *Msm* WT, Δ*canB* and Δ*canB* L5::pMV306kan::*canB* strain was compared in either liquid or on solid medium. Consistent with our previous observations with the *canB* KD mutants, no differences in the growth of the three strains were observed solid media when cells were grown under standard atmospheric conditions (**Figure 3.7.1 B** and **Supplementary Material, Figure E1**). In addition to supplying HCO_3^- for cellular metabolism, microbes often employ CA-enzymes to modulate their cytoplasmic pH by promoting the consumption or production of protons (H^+). To examine whether CanB,

possesses a specialised role in maintaining pH homeostasis, the growth of were also compared on solid media at several different pH's (**Figure 3.7.1 A** and **C)**. While the overall growth was generally observed to be reduced for all *Msm* strains at lower pH values (pH 6.0, **Figure 3.7.1 A**), no differences in the growth of the Δ*canB* mutant relative to either the WT or Δ*canB* L5::pMV306K::*canB* strains were observed. No decrease in the growth of the *canB* KD, relative to WT pLJR962 control, was furthermore observed following ATc mediated gene silencing at pH 5, 6, 6.8, 7 or 8 (data not shown). This suggests that CanB does not provide *Msm* cells with a growth advantage during growth at reduced or elevated pH, as has been observed for the enzymes from some organisms (Pal *et al*., 2017).

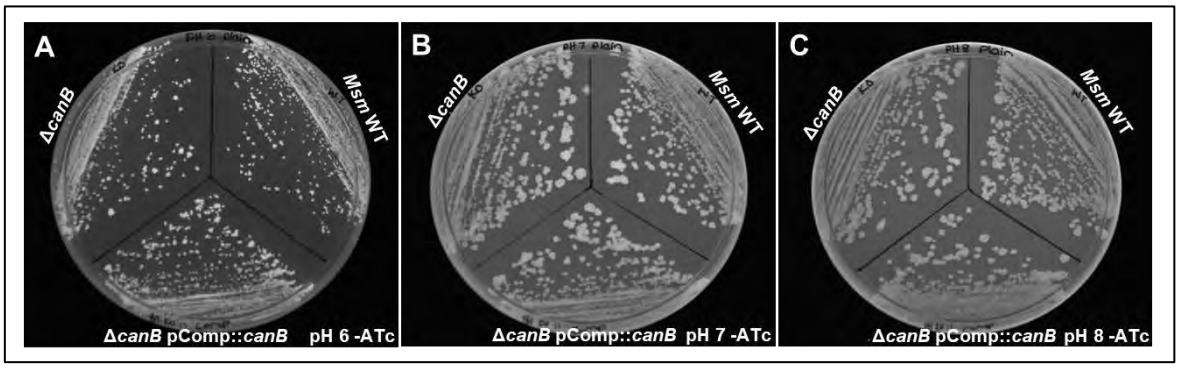

Figure 3.7.1. Comparison of the growth of the WT *Msm*, Δ*canB* mutant and Δ*canB* L5::pMV306kan::*canB* strains at different pH's. *Msm* strains were cultured to mid-log phase and diluted to a final OD_{600} of 0.01 in 7H9. 10 ml of the diluted cells was streaked onto the surface of 7H10 medium with pH values as follows: **A)** pH 6.0, **B**) pH 7.0 or **C)** pH 8.0. The plates were incubated at 37 °C and images taken after 3 days.

The growth of the *Msm* WT, Δ*canB* and Δ*canB* L5::pMV306kan::*canB* strain also observed to be highly similar in liquid medium (**Figure 3.7.2**). While the Δ*canB* mutant reached a slightly higher OD_{600} than the WT and complemented *Msm* strains following 24 hr growth in liquid medium (**Figure 3.7.2**), the difference did not reach the level of statistical significance. Overall, our findings in both solid and liquid media support the claim that CanB activity is largely dispensable for the growth of *Msm* under standard laboratory conditions used for the growth of this organism.

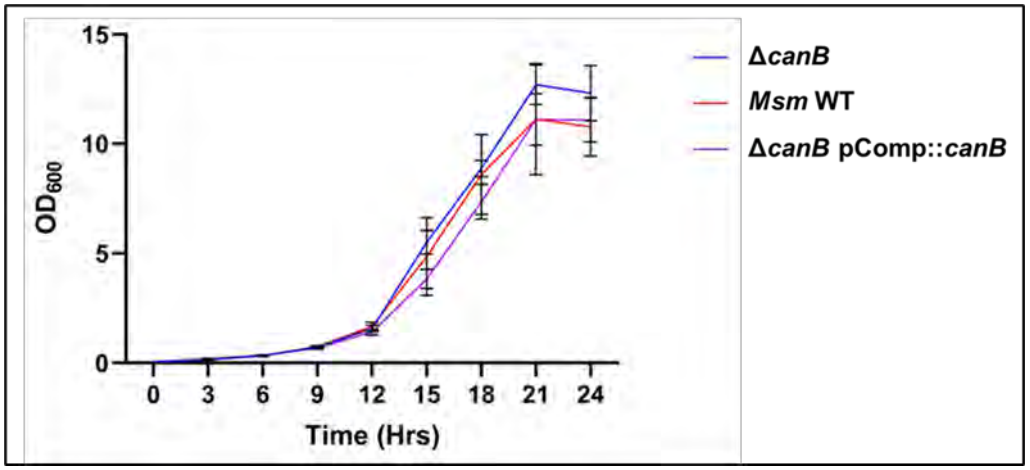

Figure 3.7.2. Growth kinetics of the *Msm* WT, *Msm canB* deletion mutant and the *canB* complemented strain. Each culture was diluted to an OD_{600} of 0.05 and incubated at 37 °C. Their growth was measured over a period of 24 hrs with OD_{600} measurements taken at 3 hr intervals. After time point 12, the samples were left incubating at 37 °C overnight and the OD_{600} was measured after 24 hrs. The average of three biological replicates is indicated with ± SD.

We also examined the effects of inactivating both CanA and CanB activity in *Msm*. For this the pLJR962::*canA1*, 2 and 3 CRISPRi plasmids were introduced into the Δ*canB* KO mutant and the effect of ATc-mediated silencing of *canA* expression in the WT and Δ*canB* genetic backgrounds compared. As shown in **Figure 3.7.3**, the growth of all of the *Msm* strains was highly similar in plates lacking (**A, C**) and supplemented (**B, D**) with ATc, irrespective of whether a functional copy of *canB* was present (**A, B**) or absent (**C, D**). The similar growth phenotypes observed for the "single" Δ*canB* KO and "double" Δ*canB* KO *canA1* KD mutants confirms that CanB does not contribute to the growth or survival of *Msm* under the environmental conditions employed in this study.

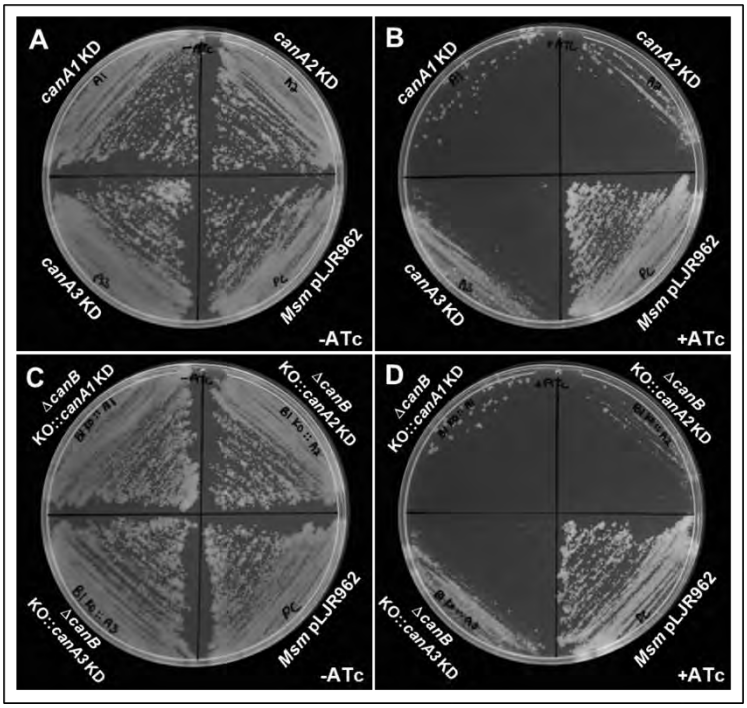

Figure 3.7.3. Examination of the effects of CRISPR-mediated silencing of *canA* expression in *Msm* Δ*canB* mutant. *Msm* strains were cultured to mid-log phase and diluted to a final OD_{600} of 0.01 in 7H9. A 5 µL aliquot of the diluted cells was streaked onto the surface of 7H10 medium with **(B and D)** or without ATc **(A and C)**. The plates were incubated at 37 °C and images taken after 3 days.

CA activity has recently been associated with the ability of some mycobacterial species to form biofilms (Belardinelli *et al*., 2021; Rose & Bermudez, 2016). We therefore examined whether the loss of CA gene expression influenced the ability of *Msm* strains to form biofilms. Analysis of biofilm formation by the *canA* and *canB* KD mutants (**Supplementary Material, Figure F1)**, did not reveal any significant differences between the strains ability to form biofilms in either the presence of absence of ATc. The efficiency by which ATc included in the growth media permeates into the biofilms growing at the air-liquid interface to effect gene silencing is, however, not known. Due to the essential nature of the *canA* gene, we were unable to test the ability of a *Msm* Δ*canA* deletion mutant to form biofilms. A role for CanB in biofilm formation was, nevertheless, assessed by comparing the ability of the *Msm* Δ*canB* mutant and complemented Δ*canB* mutant L5::pMV306kan::*canB* strain to form biofilms, relative to the WT strain. As shown below, the WT (**Figure 3.7.4 A**) and genetically complemented strains (**Figure 3.7.4 C**) both formed biofilms at the air-liquid interface under the standard assay conditions. While the *Msm* Δ*canB* KO strain was still capable of forming biofilms (**Figure 3.7.4 B**), its ability to do so was reduced in a small, but reproducible manner. This observation suggests that CanB may play a role in mediating HCO_3^- formation during biofilm growth, where CO_2 diffusion into cells is often impeded by extracellular polymeric substances, as has

recently been described for other microbial species (Fan *et al.*, 2019, 2021). Further work to verify such a role for CanB in *Msm,* as well as any other mycobacterial species, is, however, required.

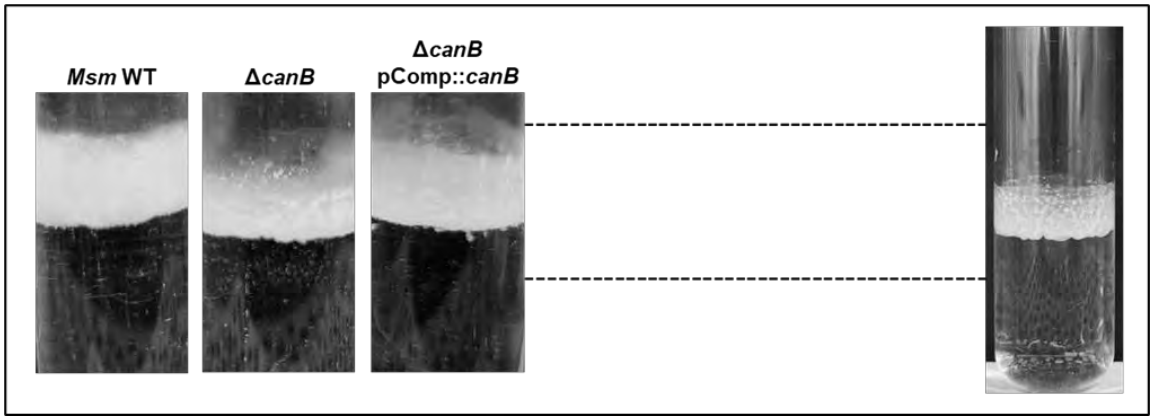

Figure 3.7.4. Representative photograph of biofilm formation by the WT, Δ*canB,* and Δ*canB* pComp::*canB* *Msm* strains. *Msm* strains were cultured to mid-log phase in biofilm medium as described in Chapter 2.10.3 and diluted to a final OD_{600} of 0.01 in 3 ml of the same medium in 16 mm glass test tubes. Cultures were incubated at 30 °C as static cultures for 5 days before biofilm formation at the air-liquid interface was examined and images taken. Data shown is representative of three independent replicates.

Chapter 4: Discussion

During the course of infection, *Mtb* can cause both pulmonary and extrapulmonary forms of TB (Khadka *et al*., 2018). The bacterium can inhabit a variety of anatomical and cellular niches during either of these disease manifestations, where it is exposed to a variety of physical and chemical stresses. These stresses include, amongst others, differences in temperature, pH, O_2, CO_2, or nutrient availability, as well as exposure to host immune defence mechanisms and antibiotics (Ehrt *et al*., 2015; Gutierrez & Enninga, 2022). These stresses are often detrimental to the growth and survival of *Mtb*, which has evolved a variety of mechanisms to mitigate their negative effects (Martin *et al*., 2015). A greater understanding of the mechanisms used by *Mtb* to promote its survival during infection may provide insights into the organism's vulnerabilities, which can be exploited to develop new therapeutics. One family of enzymes that is thought to increase the fitness of *Mtb* during infection is the CA family of enzymes. These enzymes have been shown to play an important role in heterotrophic bacteria such as *Mtb*, primarily through their ability to generate HCO_3^- required for the biosynthesis of essential TCA intermediates, amino acids, nucleotides, and fatty acids (Aspatwar *et al*., 2019). *Mtb* produces three β-class CAs (*Mt*CanA, *Mt*CanB and *Mt*CanC), whose activities have been shown to be essential for the growth of the organism both *in vitro* (Rock *et al*., 2022; Dechow, 2022; Degiacomi *et al*., 2023) and *in vivo* (Sassetti *et al*., 2003; DeJesus, 2017). The precise physiological role(s) of the *Mtb* CAs and the reason(s) underlying their reported essentiality have, however, not been established. While CanC appears to be limited to slow-growing, pathogenic mycobacteria, orthologues of CanA and CanB can be found in both SGM and FGM with either saprophytic or pathogenic lifestyles. We, therefore, used the fast-growing, environmental saprophyte, *Msm,* to examine the potential physiological role of the CanA and CanB enzymes in mycobacterial species. Based on the results of our study, we propose that CanA, encoded by the MSMEG_6082 gene and Rv3588c, serves as the primary CA enzyme in *Msm* and *Mtb,* respectively. Our results also suggest that the indispensability of the CanA enzymes is attributable to their ability to generate HCO_3^- in quantities sufficient to support the activity of several essential carboxylase enzymes. These theories are based on several lines of evidence presented in **Chapter 3**. Firstly, silencing gene expression of the *canA*, but not the *canB*, resulted in the reduced growth and survival of *Msm* when grown under both atmospheric (~0.035%) and physiological (5%) CO_2 conditions. Similarly, while the *canB* gene could be genetically inactivated without any apparent effect on the growth phenotypes of *Msm*, this could only be achieved for *canA* when a second functional copy of the gene was provided *in*

trans (**Figure 3.6.4**). Taken together, these findings indicate that CanA is essential for the growth of *Msm* and cannot be replaced by CanB, at least not under the growth conditions used during this study. The results of several recent studies, published while this work was underway, substantiate our findings. Using a CRISPRi-based approach, Bosch *et al.* (2021) demonstrated that silencing of *canA* (MSMEG_6082) but not *canB* (MSMEG_4985) inhibited the growth of *Msm.* In a separate study employing CRISPRi, Degiacomi *et al*., (2023) demonstrated that CanA (Rv3588c) was essential for the growth of *Mtb in vitro*. Dechow *et al.,* (2022) likewise demonstrated that the silencing of *canA* (Rv3588c), but not *canB* (Rv1284) or *canC* (Rv3273), imposed a growth defect on *Mtb* following infection of murine bone marrow-derived macrophages (BMDM). The authors also reported that they were unable to genetically inactivate the *Mtb canA* gene, even though this was possible for genes encoding other CAs used during the study (Dechow *et al.*, 2022). Taken together, these results suggest that CanA activity is essential for the growth of *Msm* and *Mtb in vitro* and/or *ex vivo*. Neither *canA*, *canB,* nor *canC* were, however, classified as essential in the aforementioned study of Brosch *et al.,* (2021), following CRISPRi-mediated gene silencing in *Mtb* H37Rv or HN878. Examination of the growth conditions employed in this study revealed that while *Msm* strains were routinely cultured under standard atmospheric conditions, *Mtb* strains were cultured in an environment supplemented with 5%. Since supplementation with CO_2 is known to mitigate the growth defects imposed by loss of CA-activity (see below), any growth phenotypes arising from the silencing of the *canA* (or *canB* and *canC*) gene may have been masked, resulting in the genes being classified as non-essential. Standard atmospheric conditions were, by contrast, used in the study of Degiacomi *et al*., (2023), which may explain the greater growth defects observed upon *canA* gene silencing in that study. Due to the growth-promoting properties of CO_2 on *Mtb* growth, many researchers routinely incubate *Mtb* cultures in environments supplemented with 5% CO_2. We were, however, unable to determine if the variable designation of the *Mtb canA* gene as either "essential" (Sassetti & Rubin, 2003; Griffin *et al.,* 2011) or "non-essential" (e.g., Sassetti *et al.,* 2003; Lamichane *et al*., 2003; DeJesus *et al.,* 2017; Minato *et al.,* 2019) in previously published genome-wide essentiality screens was due to the absence or presence of CO_2 supplementation, since the growth environment used in each study was not stipulated. In future, it would be of interest to determine if the essentiality of the *canA* gene in *Mtb* is conditional, with the presence or absence of growth dependent on the CO_2 concentration of the growth environment. The attenuation displayed by *Mtb canA* mutants during murine models of infection (Sassetti & Rubin, 2003; Dechow *et al.,* 2022*)*, nevertheless, suggests that

CanA is essential for growth *in vivo* and may therefore serve as a good target for pharmacological intervention.

In addition to supplementation with CO_2, the loss of CA activity can be reversed by supplementation with exogenous HCO_3^- or metabolites derived from HCO_3^- (Smith & Ferry, 2000; Merlin *et al*., 2003). As for CO_2, the growth defect of the ATc treated *canA* KD mutants could be partially rescued by supplementation with 10 mM HCO_3^- (**Figure 3.5.1 and 3.5.2**). While the ability of CO_2 and HCO_3^- to rescue the strains growth was not complete, our findings are consistent with the idea that CanA activity is required to maintain the intracellular balance of CO_2/HCO_3^- in *Msm.* In the majority of microbes studied to date, the growth rate of CA null mutants can be restored to WT levels by supplementation with physiological concentrations of CO_2 (Merlin *et al*., 2003; Udea *et al*., 2012), although concentrations below this (e.g. 1 - 5%) is often sufficient (Burghout *et al*., 2013; Kusian *et al*., 2002; Langereis *et al*., 2013; Ueda *et al*., 2012). At these elevated concentrations of CO_2, sufficient quantities of HCO_3^- are generated spontaneously to maintain the metabolic activity of the cell, making CA activity dispensable. In this study, CO_2 at a concentration of 5% was found to only partially restore the growth of the ATc-treated *canA2* and *canA3* KD mutants and had minimal effect on the *canA1* KD mutant (**Figure 3.5.1**). Similarly, our ability to isolate a *canA* KO mutant was not facilitated by growth at high CO_2 concentrations, as is often observed in other microbes (Kusian *et al.,* 2002). Similar findings were also obtained when using HCO_3^-, as opposed to CO_2 supplementation (**Figure 3.5.2**). These findings suggest that physiologically relevant concentrations of CO_2 (and HCO_3^-) are unable to compensate for the complete loss of CanA activity in *Msm,* making the *canA* gene essential at both atmospheric and physiological concentrations of CO_2. While it is possible that higher concentrations of CO_2 are capable of rescuing the growth of *Msm*, this was not examined in this study. While we did examine the effect of supplementation with higher HCO_3^- concentrations, this resulted in excessive alkalisation of (unbuffered) Middlebrook media, which in itself was growth inhibitory. As discussed in **Chapter 1**, HCO_3^- is negatively charged at physiological pHs and, therefore, unable to cross biological membranes. As far as we know, no dedicated, high-affinity transport system for importing HCO_3^- has been identified in *Msm* to date. The bacterium's ability to acquire exogenous HCO_3^- may, therefore, be limited, reducing the ability of this Ci compound to rescue the growth defects of the ATC-treated *canA* KD mutants. Until recently, CO_2, like other gases, has also been thought to be capable of freely diffusing across the lipid membranes found in biological systems (Chen *et al*., 2023; Michenkova *et al*., 2021). Some biological

membranes, particularly those with "exotic lipid compositions", have been shown to be CO_2 impermeable, however, and require protein channels to facilitate CO_2 transport (Michenkova *et al*.,2021; Chen *et al*., 2023). Whether the lipid-rich mycobacterial cell envelope impedes CO_2 diffusion into cells in a similar manner is currently unknown. In future studies, it would be of interest to examine whether the inability of physiological CO_2 concentrations to rescue the growth of the *Msm canA* mutants is attributable to the relatively poor diffusion of CO_2 across the mycobacterial cell envelope. Such a phenomenon would be expected to limit the amount of HCO_3^- that can be formed in the intracellular environment in a spontaneous, CanA-independent manner, thereby reducing bacterial growth not only at low but high CO_2 concentrations as well. The ability of biotin to decrease the CO_2 requirement of the *Mtb* CA mutants could also be investigated since supplementation with this vitamin, which serves as an essential cofactor of several HCO_3^--dependent carboxylases, has been shown to mitigate the stimulatory properties of high CO_2 concentrations on *Mtb* growth (Middlebrook & Cohn, 1958).

In heterotrophic organisms such as *Mtb*, CO_2/HCO_3^- is primarily consumed in reactions catalysed by cytosolic HCO_3^--dependent carboxylases such as PC, PEPC, AIRC and ACC, which are required for the replenishment of the TCA intermediate, OAA, as well as biosynthesis of certain amino acids, nucleotides, and FAs (see **Chapter 1.5.4**). To gain further insights into the requirement for CanA activity in *Msm*, we examined the ability of the CanA-deficient strains to grow in the presence of metabolites that bypass the need for their *de novo* biosynthesis by HCO_3^--dependent carboxylases (**Chapter 3.5**). The growth of ATc-treated *canA* KD mutants was shown to be improved when supplemented with adenine or combination of saturated and unsaturated Fas in the form of oleic and palmitic acid, respectively. Similar to the results observed for CO_2/ HCO_3^-, the improvement in growth was only partial. Individual supplementation with OAA, metabolic precursors of OAA (e.g., pyruvate, succinate, malate, or aspartate), uracil, casamino acids, or FAs had no effect on the growth of *Msm* following silencing of *canA* gene expression. A significant improvement in growth was, however, observed when media was supplemented with a combination of the metabolites listed above, or when the chemically defined 7H10 minimal media was replaced with LB media [LB, 0.5% glycerol (v/v), 0.2% glucose (w/v)], which is known to contain a combination of free sugars, sugar phosphates, oligosaccharides, amino acids, vitamins and nucleotides (Sezonov *et al*., 2007). These observations support the notion that the physiological role of CanA in *Msm* is to maintain sufficient concentrations of intracellular HCO_3^- to support the function of cytosolic,

HCO_3^--dependent carboxylase enzymes. A decrease or loss of CanA activity in *Msm* would, consequently, be expected to cause a drop in the intracellular concentrations of HCO_3^-, as well as any metabolites derived therefrom. This is likely to create a nutritional demand for the end-products of multiple HCO_3^--dependent carboxylases that, as discussed above, can be partially reversed by supplementation with physiological concentrations of CO_2/HCO_3^- (as discussed above) or metabolic end-products of individual carboxylase enzymes. Similar to the findings observed in other CA-deficient microbes, including *Streptococcus pneumoniae* (Burghout *et al.,* 2010) *Campylobacter jejunii* (Al-Haideri *et al.*, 2016), *S. cerevisiae* (Aguilera *et al*., 2005) and *Cryptococcus neoformans* (Bahn *et al*., 2005), the growth defect of the *Msm canA* mutants could be alleviated when in the presence of metabolites formed downstream of HCO_3^-. Taken together, these observations suggest that CanA is essential for *Msm* growth at both atmospheric and physiological CO_2 concentrations, with the cellular demand for CA activity being greatest in nutrient-poor conditions where metabolites cannot be scavenged from the environment. CA activity may, by contrast, become dispensable in certain nutrient-rich environments inhabited by *Msm*. As discussed above, *Mtb* CanA mutants are attenuated during infection, despite the elevated CO_2 (and HCO_3^-) concentrations present in mammalian hosts (Sassetti & Rubin, 2003; Dechow *et al.,* 2022). The observations suggest that pharmacological inhibition of CanA might also reduce *Mtb* growth and/or survival fitness during infection. Following its phagocytic uptake by macrophages, *Mtb's* access to nutrients in the phagosomal environment is severely restricted (Podinovskaia *et al.*, 2013; Gutierrez & Enninga, 2022). *Mtb* may, however, have greater access to nutrients following its escape into the cytosol of infected host cells (Simeone *et al*., 2021), or its release into the extracellular environment within necrotic tissue or cavities (Sarathy & Dartois, 2020). Our findings described here for the *Msm* CanA suggest that the essentiality of the *Mtb* CanA be examined in the presence of different concentrations of CO_2, HCO_3^- and/or various metabolites derived from HCO_3^- for this enzyme to be validated as a potential drug target in *Mtb* (Day *et al*., 2023).

As for the CanA enzyme, the requirement of CanB for the *in vitro* or *in vivo* growth of *Mtb* using genome-wide essentiality screens have been equivocal. While Sassetti and co-authors suggested that the gene was required for *Mtb* growth *in vitro* (Sassetti *et al*., 2003), this finding was contradicted using by later studies using similar approaches (Griffin *et al.,* 2011; DeJesus *et al.,* 2017; Bosch *et al.,* 2021). The reasons for these differences are not currently known but could be attributable to differences in the experimental approaches employed, including the use of different types of media (e.g., 7H10 vs. 7H11 agar) or incubation conditions (low vs.

high-CO_2 conditions), which could impact the ability to recover mutant strains. The *canB* gene was also found to be dispensable for the growth of *Mtb* in murine BMDMs (Dechow *et al*., 2022), but was required for survival following infection of C57BL/6J mice (Sassetti & Rubin, 2003). All three *Mtb* CA enzymes have been shown to possess CO_2 hydration activity *in vitro* (Minakuchi *et al.,* 2009). Consistent with its role as the primary CA in *Mtb*, CanA was found to possess the highest CA activity in *Mtb*, which is 2.3 and 2.5 × that of CanC and CanB, respectively (kcat's of 9.8×10^5 s^{-1}, 4.3×10^5 s^{-1} and 3.9×10^5 s^{-1}) (Carta *et al.,* 2009; Minakuchi *et al*., 2009; Nishimoria *et al*., 2010). Similar findings have also been obtained for the recombinant *Msm* CanA and CanB enzymes in our laboratory (T. Mdiniswa, personal communication). In this study, the *canB* gene (MSMEG_4985) was found to be dispensable for the growth of *Msm* under both low and high CO_2 concentrations following gene silencing or inactivation (**Chapter 3.5**). Despite its apparent dispensability, both the *Msm canA* and *canB* genes were constitutively expressed, with similar levels of transcripts detected at both low and high CO_2 concentrations (**Chapter 3.4**). The *Mtb* CanB enzyme has been shown to possess a redox-sensitive Cys residue (Cys^{61}), which can form a disulphide bond with the enzyme's active site Cys^{35} under oxidising conditions (Nienaber *et al*., 2015). This results in the loss of the active site Zn^{2+} cofactor, causing inactivation of the enzyme. This inactivation is reversible and can be restored under reducing conditions. The authors, therefore, proposed that the *Mtb* CanB might be regulated at the post-translational level in response to redox conditions (Nienaber *et al*., 2015). This mode or regulation may enable *Mtb* to modulate CanB activity in response to rapidly changing conditions, such as when switching from aerobic (oxidising) to anaerobic (reducing) conditions, or vice versa. In the *Msm* CanB, the Cys^{61} is replaced by Gly^{61}, making it unlikely that the activity of the enzyme is subject to regulation via the same mechanism observed for the *Mtb* enzyme. Since constitutive expression of *canB* when not required involves the expenditure of cellular resources it is possible that *Msm*, as hypothesised for *Mtb*, maintains the CanB enzyme in an inactive state until its enzymatic activity is required. This would allow CanB to be rapidly activated in response to a yet-to-be-identified environmental condition, where CanA may be unable to function efficiently. As stated above, redox conditions and oxygen tension are two conditions known to frequently change in the environmental niches that both *Mtb* and *Msm* inhabit. In future, it would be of interest to examine the effects of the loss of CanB activity on the fitness of *Msm* (and *Mtb*) during growth under different redox conditions or levels or aerobiosis, as well as their effects on the biochemical activity of the enzymes. CAs have also been shown to be important for maintaining pH homeostasis in a variety of microbes (Marcus *et al.,* 2005; Pal *et al*., 2017;

Supuran & Capasso, 2017). In *Mtb* and other bacterial species, the PhoPR two component regulatory system is a well-known sensor of acidic pH. The PhoPR regulon of *Mtb* has, consequently, been shown to be highly induced by acidic pH's *in vitro* as well as within the phagosome of macrophages. Dechow *et al*., (2022) recently demonstrated that in *Mtb*, PhoPR also serves as a CO_2 sensor, albeit in a manner that is independent of the intracellular or extracellular pH. Using mutational analyses, the authors showed that the ability of PhoPR to detect CO_2 was independent of CanA, CanB and CanC activity, despite the ability of these enzymes to produce or consume protons (H^+) during the interconversion of CO_2 and HCO_3^-. The three *Mtb* CAs may, therefore, play little role in buffering the cytoplasmic pH in response to changing CO_2 concentrations, as has been observed in organisms such as *Helicobacter pylori* (Marcus *et al.,* 2005) or *Leishmania major* (Pal *et al.,* 2017). In this study, we found that inactivation of *canB* did not decrease the fitness of *Msm,* relative to the WT, when bacteria were cultured at pHs ranging between 6, 7, or 8 (**Figure 3.7.1**). These findings argue against a specialised role for CanB in modulating the cellular pH in *Msm*.

A slight, but reproducible, growth defect was observed for strains lacking CanB when *Msm* was grown as biofilms, as opposed to planktonic cultures (**Figure 3.7.4**). This growth defect could be reversed by genetic complementation, confirming that the phenotype was due to lack of CanB expression. As discussed in the preceding section, the membranes composition of certain types of cells can limit the ability of CO_2 to diffuse into cells. In some bacterial species, the ability of CO_2 to diffuse into cells is further hampered during biofilm formation due to the production of extracellular polymeric substances, such as capsules, mucus and/or slime layers (Fan *et al*., 2019, 2021). To overcome this limitation, several bacterial species including *Staphylococcus aureus, Staphylococcus epidermidis, Bacillus anthracis, Legionella pneumophila,* and *Vibrio cholera,* employ membrane-localised HCO_3^- transporters, as opposed to cytosolic CAs to supply intracellular HCO_3^- for carboxylation reactions (Fan *et al*., 2019, 2021). In this regard, it is noteworthy that both the *Mtb* CanB and CanC enzymes have been shown to localise to the membrane fraction of *Mtb* cells (de Souza *et al*., 2011). While the physiological role of *Mtb* CanC remains to be established, it possesses an N-terminal transmembrane that displays homology to the SulP/SLC26 family of sodium-dependent anion transporters, which are known to mediate HCO_3^- transport in various bacterial species (Felce & Saier, 2004; Price *et al*., 2004). CanC may, therefore, facilitate the conversion of CO_2 into HCO_3^- using the enzymes CA domain, followed by the transport of HCO_3^- into the cytoplasm using its transmembrane domain. *Msm* lacks an orthologue of CanC enzyme, however. Since

CanB is also targeted to the cell membrane fraction in *Mtb*, it may potentially play a role in facilitating the formation and/or import of CO_2/HCO_3^- during growth in certain environments, such as biofilms, where CO_2 diffusion into cells may be limited. The expression of CAs and formation of HCO_3^- has recently been shown to be important for biofilm formation in mycobacterial species such as *M .abscessus*, *M. chelonae* and *M. avium* (Belardinelli *et al*., 2021; Rose & Bermudez, 2016). The ability to form biofilms has been shown to be important for the ability of *Msm* to survive adverse environmental conditions, as well as for *Mtb* to establish infections *in vivo* (Chakraborty *et al*., 2021). A role for CanB in promoting biofilm formation in either one of these mycobacterial species will, however, have to be established in future studies.

Summary and Future Work

The primary objective of the study was to establish the roles of the CanA and CanB enzymes in the physiology and metabolism of *Msm*. Our findings suggest the CanA serves as the primary CA in *Msm,* where its major function appears to be to supply carboxylase enzymes of central metabolism with sufficient HCO_3^- for biosynthetic reactions. Recent studies suggest that CanA is the only CA essential for the growth of *Mtb in vitro* (Degiacomi *et al*., 2023) and *ex vivo* (Dechow *et al*., 2022). The enzyme may, therefore, fulfil a similar metabolic role in *Mtb* as in *Msm*. This hypothesis would, however, have to be confirmed experimentally in future studies. The idea of targeting CanA is appealing since its inhibition is likely to affect the activity of enzymes involved in multiple biosynthetic pathways downstream of HCO_3^-. Numerous inhibitors of CanA's biochemical activity have also been identified to date (Aspatwar *et al*., 2019; Diagiacomi *et al*., 2023), which could serve as a starting point for the development of CanA inhibitors with activity against whole cells. Sulfonamides and their bioisosteres are examples of CA inhibitors, which are the main class of inhibitors and have been in clinical use for over 50 years (Nishimori *et al*., 2010). To validate the *Mtb* CanA enzyme as a drug target, it will be important to establish whether the environmental or nutritional conditions encountered by *Mtb* during infection (e.g., high CO_2/HCO_3^- or nutrient-rich conditions) would allow it to bypass the loss of CanA activity. While the CanB was unable to compensate for the loss of CanA activity in *Msm*, it will be important to demonstrate that the dual presence of CanB and CanC are unable to do the same for *Mtb.* This will be expedited by additional studies designed to elucidate the role(s) of the latter two enzymes in the biology of *Msm* and *Mtb*. The work presented here can serve as a foundation for further studies on this topic and will

hopefully provide greater insight into the overall role of CAs in the physiology of *Msm* and *Mtb* and their potential as drug targets.

Supplementary Material

Section A: Chemicals and Reagents

Table A1. Bacterial strains, plasmids, chemicals and reagents used in this study

PRODUCT NAME	SOURCE	REFERENCE
Bacterial Strains		
***Escherichia coli* Mach1**	ThermoFisher Scientific	C862003
***Escherichia coli* Top10**	ThermoFisher Scientific	C4040
Mycobacterium smegmatis mc²155	Laboratory Stock	Snapper *et al*., 1990
Plasmids		
pJV53	Addgene	#26904
pLJR962	Addgene	#115162
pML1342	Addgene	#32376
pML2714	Addgene	#117498
pMSG360Zeo	Addgene	#27154
pMV306hsp	Addgene	26155
Chemicals		
Ammonium Sulfate $(NH_4)_2SO_4$	Merck	101217
Calcium Chloride Dihydrate ($CaCl_2 \cdot 2H_2O$)	Saarchem Univar	SAAR1524920EM
Dimethyl Sulfoxide (DMSO)	Sigma-Aldrich	D8418
Ethanol	Merck	108543
Hydrochloric Acid (HCl)	Merck	SAAR3063020LP
Iron Sulfate Heptahydrate ($FeSO_4 \cdot 7H_2O$)	Merck	7782-63-0
Magnesium Sulfate ($MgSO_4$)	Merck	SAAR4124000EM
Manganese Chloride Tetrahydrate ($MnCl_2 \cdot 4H_2O$)	Sigma-Aldrich	203734
Monopotassium Phosphate (KH_2PO_4)	Acros Organics	205925000
(1,4-Piperazinediethanesulfonic acid) PIPES	Boehringer Mannheim	83676220-56
Potassium Chloride (KCl)	Merck	SAAR5043600EM
Sodium Chloride (NaCl)	Merck	SAAR5822320FL
Sodium Hydroxide (NaOH)	Merck	SAAR5823180EM
Ultra-Pure Distilled Water	ThermoFisher Scientific	10977-035
Growth Media & Supplements		
Acetamide	Sigma-Aldrich	00160

Adenine	Sigma-Aldrich	A8626
Agar Bacteriological	Merck	HG000BX1.500
Bovine Serum Albumin	Biowest	PAO20K7055
Casamino Acids	ThermoFisher Scientific	223120
Cholesterol	Sigma-Aldrich	57885
D-(+)-Glucose	Sigma-Aldrich	G7021
Glycerol	Merck	SAAR2676520LC
L-Aspartic Acid	Sigma-Aldrich	11189
L-Histidine	Sigma-Aldrich	H800
Malic Acid Disodium Salt	Sigma-Aldrich	M9138
Middlebrook 7H9 Agar	BD Difco	271310
Middlebrook 7H10 Agar	BD Difco	262710
Oxaloacetic Acid	Sigma-Aldrich	O7753
Palmitic Acid Methyl Ester	Sigma-Aldrich	P5177
Sodium Chloride	Sigma-Aldrich	S7653
Sodium Oleate	Sigma-Aldrich	143191
Sodium Pyruvate	ThermoFisher Scientific	11360070
Sodium Succinate Dibasic Hexahydrate	Sigma-Alrich	S2378
Tryptone Powder (Pancreatic Digest of Casein)	Merck	HG000BX4.250
Tween 80	Sigma-Aldrich	P8074
Uracil	Sigma-Aldrich	U0750
Yeast Extract Powder	Merck	HG000BX6.500
Antibiotics		
Ampicillin Sodium Salt	VWR Life Science	0339
Anhydrotetracycline Hydrochloride	Sigma-Aldrich	37919
Hygromycin B	ThermoFisher Scientific	10687010
Kanamycin Sulphate	VWR Life Science	0408
Zeocin	ThermoFisher Scientific	R25001
Kits		
DirectZol™ RNA MiniPrep Plus	Zymo Research	R2071

E.Z.N.A Plasmid DNA Mini Kit	Omega Bio-Tek	D6942
GeneJET Genomic DNA Purification Kit	ThermoFisher Scientific	K0721
GeneJET PCR Purification Kit	ThermoFisher Scientific	K0701
GeneJET Plasmid MiniPrep Kit	ThermoFisher Scientific	K0502
RapidOut DNA Removal Kit	ThermoFisher Scientific	K2981
Silica Bead Gel Purification Kit	ThermoFisher Scientific	K0513
Apparatus & Equipment		
BeadBug 3 Microtube Homogenizer	Benchmark Scientific	D1030
Blue Light Transilluminator	IORodeo	IMG-04-03
CFX Opus 96 Real-Time PCR System	Bio-Rad	12011319
ChemiDoc XRS+	Bio-Rad	1708265SP
Eutech pH 700	ThermoFisher Scientific	ECPH70040
Gene Pulser XCell	Bio-Rad	1652660
Jenway 6200 Spectrophotometer	Jenway	6200 Vis
Megafuge 1.0R	Heraeus	05718
Mini Gel Tank	ThermoFisher Scientific	A25977
MiniSpin Microfuge	Sigma-Aldrich	Z606235
Mini Sub Cell GT Horizontal Electrophoresis Chamber	Bio-Rad	1704487
MultiGene Mini PCR Thermal Cycler	Labnet International	Z739928
Nanodrop ND-1000 Spectrophotometer	ThermoFisher Scientific	ND-1000
SimpliAmp Thermal Cycler	Applied Biosystems	A24811
RNA Extraction, cDNA Synthesis, qPCR		
DNase I	Zymo Research	E1011-A
LunaScript RT SuperMix Kit	New England Biolabs	E3010
Luna Universal qPCR Master Mix	New England Biolabs	M3003
SuperScript IV VILO	ThermoFisher Scientific	11766050
TRIzol™ Reagent	ThermoFisher Scientific, Invitrogen	15596026
TRI Reagent™ Solution	ThermoFisher Scientific	AM9738
TRI Reagent	Zymo Research	R2050-1-50
Restriction Enzymes & Buffers		

10 × Anza Buffer	ThermoFisher Scientific	IVGM2008
10 × Buffer B	ThermoFisher Scientific	BB5
10 × Tango Buffer	ThermoFisher Scientific	BY5
Anza 1 NotI	ThermoFisher Scientific	IVGN0016
Anza 6 NheI	ThermoFisher Scientific	IVGN0066
Anza 10 DpnI	ThermoFisher Scientific	IVGN0106
Anza 11 EcoRI	ThermoFisher Scientific	IVGN0116
Anza 12 XbaI	ThermoFisher Scientific	IVGN0126
Anza 14 SalI	ThermoFisher Scientific	IVGN0148
Anza 16 HindIII	ThermoFisher Scientific	IVGN0166
Anza 20 SacI	ThermoFisher Scientific	IVGN0208
Anza 22 SmaI	ThermoFisher Scientific	IVGN0226
Anza 24 MssI	ThermoFisher Scientific	IVGN0244
BcuI	ThermoFisher Scientific	ER1251
BsmBI V2	New England Biolabs	R0739S
KspAI	ThermoFisher Scientific	ER1031
Agarose Gels		
50 × TAE Electrophoresis Buffer	ThermoFisher Scientific	B49
Ethidium Bromide, 10 mg/mL	VWR Life Science	X328
GeneRuler 50 bp DNA Ladder	ThermoFisher Scientific	SM0371
GeneRuler 1 kb Plus DNA Ladder	ThermoFisher Scientific	SM1332
TopVision Agarose Tablets	ThermoFisher Scientific	R2801
TriTrack Loading Dye (6 ×)	ThermoFisher Scientific	R1161
PCR Reagents		
Dimethyl Sulfoxide (100 %)	ThermoFisher Scientific	F-515
dNTP Solution Mix	New England Biolabs	N0447S
KAPA Taq Ready Mix PCR Kit	Sigma-Aldrich	KK1006
Phusion High-Fidelity DNA Polymerase	ThermoFisher Scientific	F-530S
Phusion™ Plus DNA Polymerase	ThermoFisher Scientific	F630XL
Platinum™ SuperFi II DNA Polymerase	ThermoFisher Scientific	12361010

Resin Chelex 100 Molecular Grade 200-400 Mesh	Bio-Rad	1421253
Taq 2 × Master Mix	New England Biolabs	M0270L
Modification Enzymes		
Anza DNA End Repair Kit	ThermoFisher Scientific	IVGN2504
Anza T4 DNA Ligase (5 U/µL)	ThermoFisher Scientific	EL0012
Anza T4 DNA Master Mix	ThermoFisher Scientific	IVGN2104
Anza T4 PNK 5' Phosphorylation	ThermoFisher Scientific	IVGN230-4
Instant Sticky-end Ligase Master Mix	New England Biolabs	M0370
RNase A	ThermoFisher Scientific	8003088
T4 DNA Ligase	Promega	M180A
Miscellaneous		
0.2 cm Gap Electroporation Cuvettes	ThermoFisher Scientific	P45050
1 cm Semi-Micro Cuvettes	Lasec	PGRE613101

Section B: Molecular Weight Markers

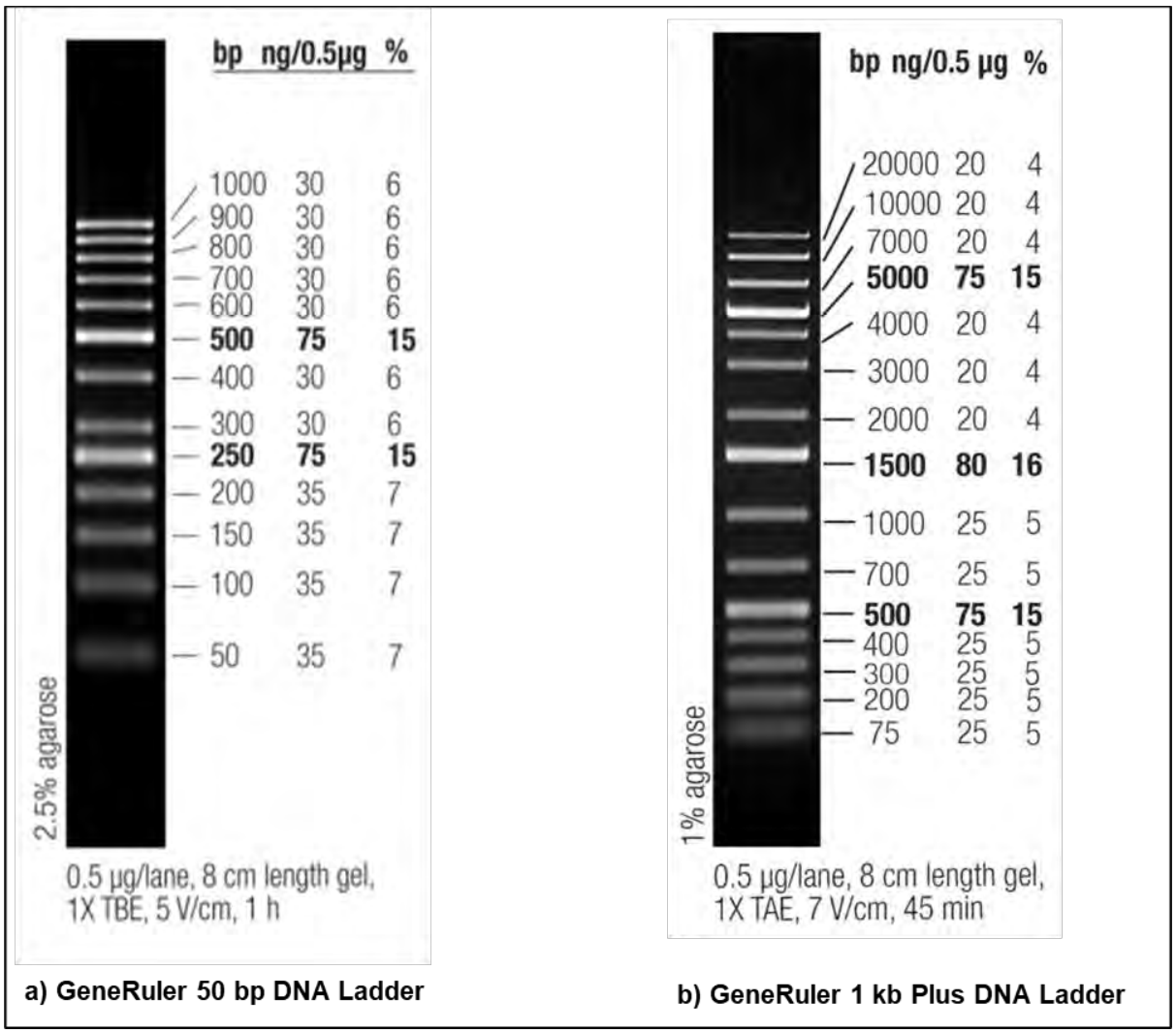

Figure B1. Molecular weight markers for DNA analysis used in this study.

Section C. Generation of Plasmid Vectors

C1: Generation of CRISPRi Plasmids and Knockdown Strains

Plasmids capable of silencing the expression of the *Msm canA* (MSMEG_6082) or *canB* (MSMEG_4985) genes were constructed by cloning short, dsDNA sequences (18-22 bp) that target the coding sequence of each gene into the CRISPRi-plasmid, pLJR962 (**Figure C1.1;** Rock *et al.* 2017). To this end, we first identified protospacer adjacent motifs (PAMs) with a predicted score of >5 (Rock *et al.* 2017) on the template strand of each gene (**Figure C1.2 A and B,** overleaf). Nucleotide sequences located immediately upstream (i.e. on the 5'-end) of the selected PAMs were used to design gene-specific 'forward' oligonucleotides, while their complementary sequences were used to design 'reverse' oligonucleotides. The 5'-ends of the selected forward and reverse oligonucleotides were modified by the addition of overhangs for the restriction enzyme BsmBI (GGGA and AAAC, respectively; see **Table 2.1** for primer sequences). Following synthesis, the complementary oligonucleotides were annealed and ligated into pLJR962 using Golden Gate Cloning, as described in **Chapter 2.9.1**.

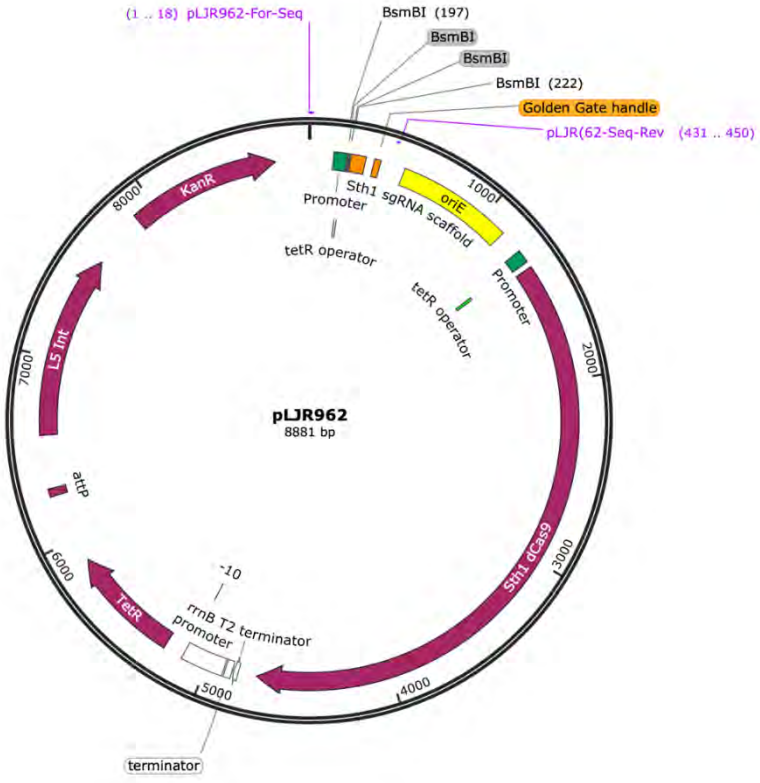

Figure C1.1 Plasmid map of pLJR962

(A)

```
ATGCCGAACTCAAATCCTGTGGCAGCGTGGAAAGCACTCAAGGACGGTAATGCCCGTTTCGTGGCGGGCC
TACGGCTTGAGTTTAGGACACCGTCGCACCTTTCGTGAGTTCCTGCCATTACGGGCAAAGCACCGCCCGG

AACCGCTGCACCCCAGCCAGGGGATCGAGCGCCGCGCGAGCCTCACCCAGGCGCAGCGTCCCACCGCGGT
TTGGCGACGTGGGGTCGGTCCCCTAGCTCGCGGCGCGCTCGGAGTGGGTCCGCGTCGCAGGGTGGCGCCA

GGTGTTCGGCTGCGGCGACAGCCGCGTCGCCGCAGAGATCCTGTTCGACCAGGGCCTCGGCGACATGTTC
CCACAAGCCGACGCCGCTGTCGGCGCAGCGGCGTCTCTAGGACAAGCTGGTCCCGGAGCCGCTGTACAAG

GTGGTGCGCACCGCGGGCCACGTCATCGACAACGCGGTGCTCGGGTCGATCGAATACGCCGTGACAGTGC
CACCACGCGTGGCGCCCGGTGCAGTAGCTGTTGCGCCACGAGCCCAGCTAGCTTATGCGGCACTGTCACG

TCAAGGTGCCGCTGATCGTGGTGCTCGGCCATGACAGCTGCGGTGCGGTCAAGGCGACGCTTTCCGCGCT
AGTTCCACGGCGACTAGCACCACGAGCCGGTACTGTCGACGCCACGCCAGTTCCGCTGCGAAAGGCGCGA

CGACGAGGGCGAGGTGCCCAGCGGGTTCGTCCGCGACATCGTCGAGCGTGTGACGCCCTCGATCCTGCTG
GCTGCTCCCGCTCCACGGGTCGCCCAAGCAGGCGCTGTAGCAGCTCGCACACTGCGGGAGCTAGGACGAC
   canA_sgRNA1
GGACGCAAGGCCGGGTTGAGCCGTGTCGACGAATTCGAGGCGCAGCACGTCAACGAGACCGTCGCGCAGT
CCTGCGTTCCGGCCCAACTCGGCACAGCTGCTTAAGCTCCGCGTCGTGCAGTTGCTCTGGCAGCGCGTCA
    canA_sgRNA2
      canA_sgRNA3
TGCAGATGCGCTCGACCGCGATTGCCCAGGGGCTCGCGGCAGGCACGCAGGCCATCGTCGGCACCACCTA
ACGTCTACGCGAGCTGGCGCTAACGGGTCCCCGAGCGCCGTCCGTGCGTCCGGTAGCAGCCGTGGTGGAT

CCACCTCGCGGACGGGCGCGTGGAGTTGCGCAGCCACCTGGGCGATATCGGCGAAGTCTGA
GGTGGAGCGCCTGCCCGCGCACCTCAACGCGTCGGTGGACCCGCTATAGCCGCTTCAGACT
```

(B)

```
ATGTCTGTCACTGATCAGTACCTGGCGAACAACGAGGAATACGCGAAGACGTTCAGCGGGCCACTTCCGC
TACAGACAGTGACTAGTCATGGACCGCTTGTTGCTCCTTATGCGCTTCTGCAAGTCGCCCGGTGAAGGCG

TGCCGCCCAGCAAGCACGTGGCGGTGGTGGCCTGCATGGACGCCCGGCTCGACGTCTACCGCATCCTGGG
ACGGCGGGTCGTTCGTGCACCGCCACCACCGGACGTACCTGCGGGCCGAGCTGCAGATGGCGTAGGACCC
      canB_sgRNA1
CCTCGGCGACGGTGAGGCCCACGTGATCCGCAACGCCGGCGGCGTGATCACCGACGACGAGATCCGGTCC
GGAGCCGCTGCCACTCCGGGTGCACTAGGCGTTGCGGCCGCCGCACTAGTGGCTGCTGCTCTAGGCCAGG
   canB_sgRNA4
CTGGCCATCAGCCAGCGCCTGCTGGGCACCAAGGAGATCATCCTCATCCACCACACCGACTGCGGCATGC
GACCGGTAGTCGGTCGCGGACGACCCGTGGTTCCTCTAGTAGGAGTAGGTGGTGTGGCTGACGCCGTACG
                          canB_sgRNA5          canB_sgRNA3
TGACGTTCACCGACGACGAGTTCAAGCGTGCCATCCAGGGCGAGACCGGCATCAAACCCGAATGGGCCGC
ACTGCAAGTGGCTGCTGCTCAAGTTCGCACGGTAGGTCCCGCTCTGGCCGTAGTTTGGGCTTACCCGGCG
       canB_sgRNA2
CGAGTCGTTCACCGACCTCGAAGAGGATGTCCGGCAGTCGCTGCGCCGCATCGAGGCCAGCCCGTTCGTC
GCTCAGCAAGTGGCTGGAGCTTCTCCTACAGGCCGTCAGCGACGCGGCGTAGCTCCGGTCGGGCAAGCAG

ACCAAGCACGAATCCCTGCGCGGCTTCATCTTCGACGTCGCGACGGGCAAGCTCGCCGAGGTCACGCTCT
TGGTTCGTGCTTAGGGACGCGCCGAAGTAGAAGCTGCAGCGCTGCCCGTTCGAGCGGCTCCAGTGCGAGA

GA
CT
```

Figure C1.2, Sequence and location of the Sth1 dCas9 protospacer adjacent motifs (PAMs) and sgRNA targeting sequences of *Msm canA* and *canB* genes. The double-stranded DNA sequence of the **(A)** *canA* and **(B)** *canB* genes are shown. The start and stop codons of the genes are highlighted in green and red, respectively. The PAM sequences recognised by dCas9 on the non-coding strand are indicated in blue. The *canA*- or *canB*-targeting sequences on the 5'-end of the PAM sequences are underlined and labelled. The PAM sequences for canA_sgRNA2 and canA_sgRNA3 overlap by three nucleotides; the three nucleotides highlighted in orange are present in the canA_sgRNA2, but not canA_sgRNA3 targeting sequence.

The Golden Gate cloning reactions were introduced into competent *E. coli* cells and the ligation of the annealed, dsDNA oligonucleotides into pLJR962 confirmed by colony PCR using the relevant, PAM-specific 'forward' oligonucleotide primer in conjunction with a plasmid-specific, reverse primer, pLJR-Seq-Rev (**Table 2.2**).

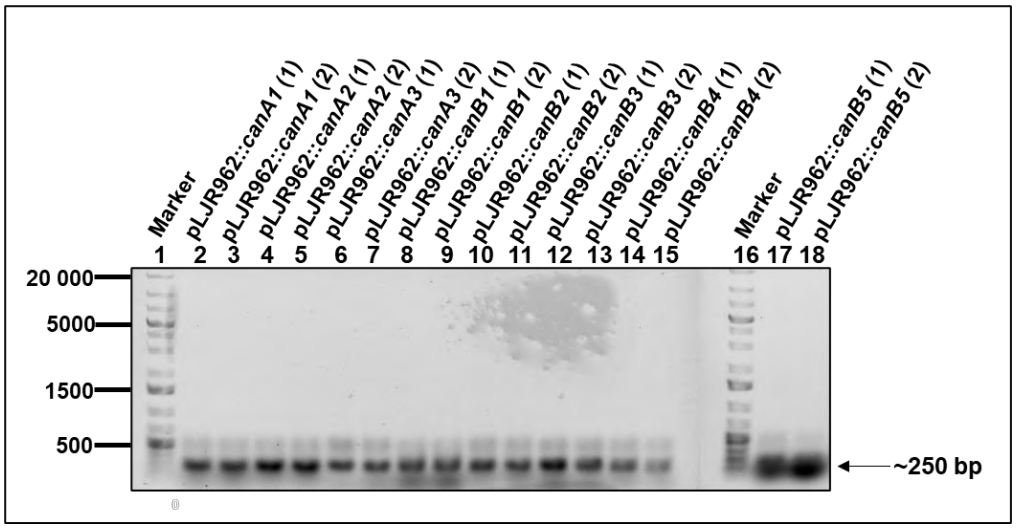

Figure C1.3. Agarose gel confirming the presence of sgRNA targeting sequences into pLJR962. The introduction of sgRNA targeting sequences into pLJR962 was confirmed by colony PCR of cell lysates obtained from two randomly selected Kan^R transformants. PCR reactions were electrophoresed on 0.8% (w/v) agarose at 80 V for 45 min prior to visualisation under UV light. **Lane 1:** Molecular Weight Marker; **Lane 2 and 3**: pLJR962::*canA*1(1) and (2); **Lane 4 and 5:** pLJR962::*canA2(*1) and (2); **Lane 6 and 7:** pLJR962::*canA3*(1) and (2); **Lane 8 and 9: pLJR962**::*canB1*(1) and (2); **Lane 10 and 11**: pLJR962::c*anB2*(1) and (2); **Lane 12 and Lane 13**: pLJR962::*canB3*(1) and (2); **Lane 14 and Lane 15**: pLJR962::*canB4*(1) and (2); **Lane 16 and 17**: pLJR962::*canB5*(1) and (2). Black arrows indicate the sizes of the predicted PCR amplicons.

Following purification of the recombinant CRISPRi-plasmids from the colony-PCR positive clones, the presence of the sgRNA targeting sequences in the BsmBI sites of the pLJR962-derivatives was confirmed by DNA sequencing (**Chapter 2.9.1**) using the vector-specific primers, pLJR962-Seq-For and pLJR962-Seq-Rev (**Table 2.2**). Once confirmed, the three *canA* (pLJR962::*canA1*, 2 and 3) and five *canB* (pLJR962::*canB1*, 2, 3, 4 and 5) plasmids were introduced into *Msm* by electroporation, followed by plating and selection of transformants on 7H10/Kan media. Analysis of genomic DNA isolated from selected Kan^R transformants by PCR and agarose gel electrophoresis revealed the presence of single amplicons of ~450 bp when using the pLJR962-Seq-For/pLJR962-Seq-Rev primer pair (**Figure C1.4)**.

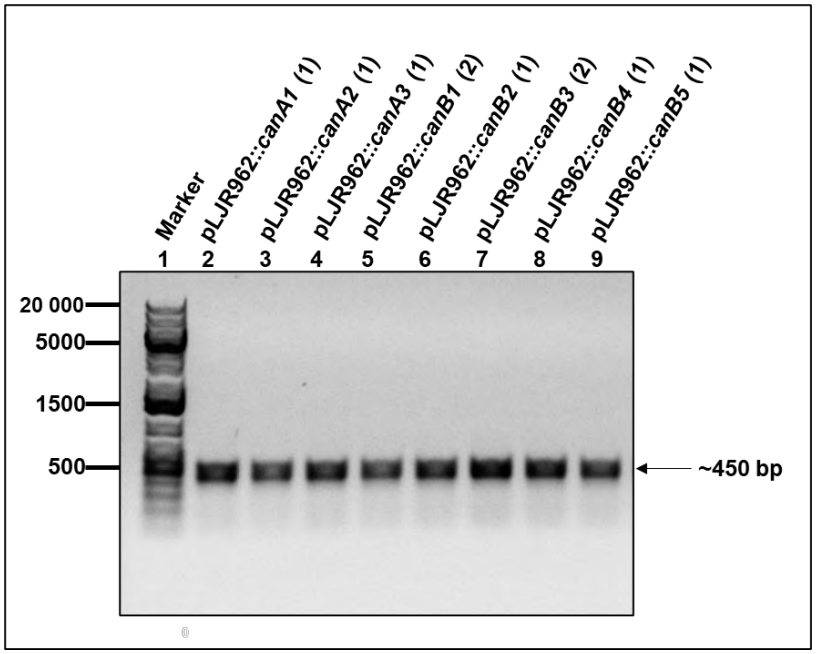

Figure C1.4. Agarose gel confirming the presence of pLJR962 in representative kanamycin-resistant *Msm* strains following electroporation. PCR amplification of the DNA inserts was performed using genomic DNA obtained from Kan^R transformants and primers pLJR962-Seq-For and pLJR962-Seq-Rev. Each PCR reaction was electrophoresed on a 0.8% (w/v) agarose gel at 80 V for 45 min prior to visualisation under UV light. **Lane 1**: Molecular Weight Marker; **Lane 2**: pLJR962::canA1 (1); **Lane 3**: pLJR962::canA2 (1); **Lane 4**: pLJR962::canA3 (1); **Lane 5**: pLJR962::canB1(2); **Lane 6**: pLJR962::canB2(1); **Lane 7**: pLJR962::canB3 (2); **Lane 8**: pLJR962::canB4 (1); **Lane 9**: pLJR962::canB5 (1). Numbers in parentheses indicate the recombinant clone number for each knockdown strain.

The PCR products were subsequently purified and the identity of the *Msm* KD strains confirmed by verifying the presence of the anticipated *canA* or *canB* sgRNA targeting sequences within each strain by DNA sequencing. Once the identity of the strains were confirmed, they were subjected to genetic and physiological analysis as described in the Results (**Chapter 3).**

C2. Generation of Vectors for L5 Gene Switching Experiments

To generate Hyg^R complementation vectors for use in L5 gene switching experiments (Pashley and Parrish, 2003), the *Msm canA* and *canB* genes, together with their upstream and downstream regulatory regions, were PCR amplified and cloned into the integrating vector, pML1342 as described in **Chapter 2.9.4**. As shown below, PCR amplification of *canA* and *canB* with the canA-Comp-For/canA-Comp-Rev or canB-Comp-For/canB-Comp-Rev primer pairs (**Table 2.2**) produced amplicons of ~1,346 bp and 1,251 bp, respectively (**Figure C2.1**, **Lanes 2 and 4**), which is consistent with their predicted sizes (**Table 2.3**)

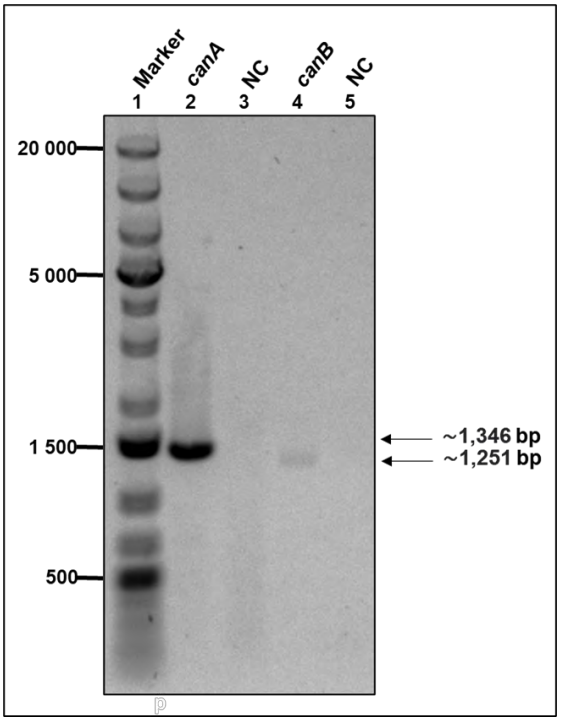

Figure C2.1. Agarose gel electrophoresis of the successful amplification of the *canA* and *canB* gene by PCR. To amplify *canA* and *canB*, PCR reactions were performed using genomic DNA isolated from WT *Msm* and the canA-Comp-For/canA-Comp-Rev or canB-Comp-For/canB-Comp-Rev primer pairs, respectively. The PCR products were electrophoresed on a 0.8% (w/v) agarose gel at 80 V for 45 min prior to visualization under UV light. **Lane 1**: Molecular Weight Marker; **Lane 2**: *canA*; **Lane 3**: Negative control (NC); **Lane 4**: *canB*; **Lane 5**: Negative control (NC).

The blunt-ended PCR products produced by Phusion DNA polymerase were purified and ligated into pML1342, which had been linearised with MssI. Following the introduction of the ligation reaction into *E. coli* chemical competent cells and selection on LB/Kan media, plasmid DNA was isolated from representative Kan^R transformants and analysed by RE digestion with either EcoRI alone (for pML1324::*canA*), or both EcoRI and SalI (for pML1342::*canB*), respectively. As expected, restriction of the parental vector, pML1342 with EcoRI and SalI

produced four bands with sizes of ~2,874 bp, ~1,768, 648 and 114 bp (**Figure C2.2, Lane 4**). For the recombinant pML1342::*canA* plasmid, RE digestion with EcoRI produced two bands with sizes of ~5,328 and 1,422 bp (**Figure C2.2, Lane 2)**, which is consistent with insertion of the DNA fragment harbouring *canA* in the same direction as the *xylE* reporter on pML1342 (**Figure C2.3)**. Likewise, for pML1342::*canB*, RE digestion with EcoRI and SalI produced five bands of ~2,988, 2,512, 648, 496 and 114 bp (**Figure C2.2, Lane 3)**, consistent with insertion of the DNA fragment harbouring *canB* occurring in the same direction as the *xylE* reporter on pML1342. (**Figure C2.3**). The DNA sequence and orientation of the PCR amplified inserts was subsequently confirmed by DNA sequencing before being used in the experiments described in **Section 3.3.1**.

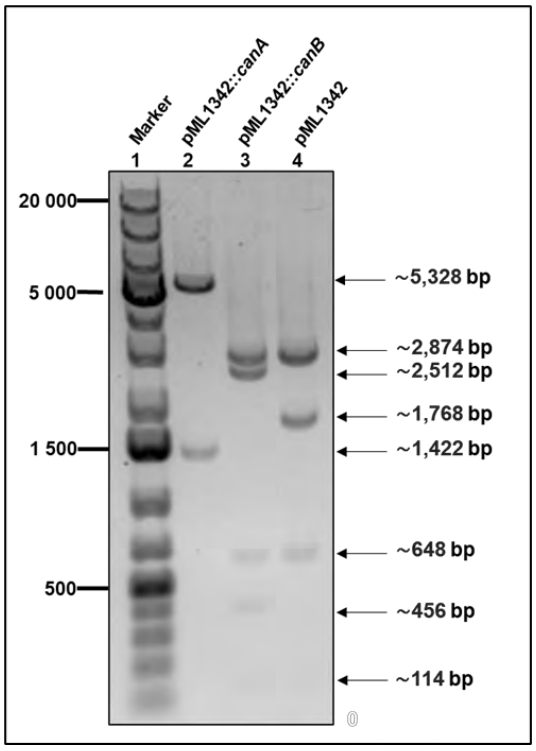

Figure C2.2. Agarose gel electrophoresis of restriction enzyme digests to verify the identity of recombinant plasmids pML1342::*canA* and pML1342::*canB*. pML1342::canA and pML1342::canB were restricted with EcoRI, or EcoRI and SalI, respectively. The parental pML1342 vector was restricted with EcoRI and SalI. The products of the restriction enzyme digest were electrophoresed on a 0.8% (w/v) agarose gel at 80 V for 45 min prior to visualization under UV light. **Lane 1**: Molecular Weight Marker; **Lane 2**: pML1342::*canA*; **Lane 3**: pML1342::*canB*; **Lane 4**: Parental pML1342 vector (control).

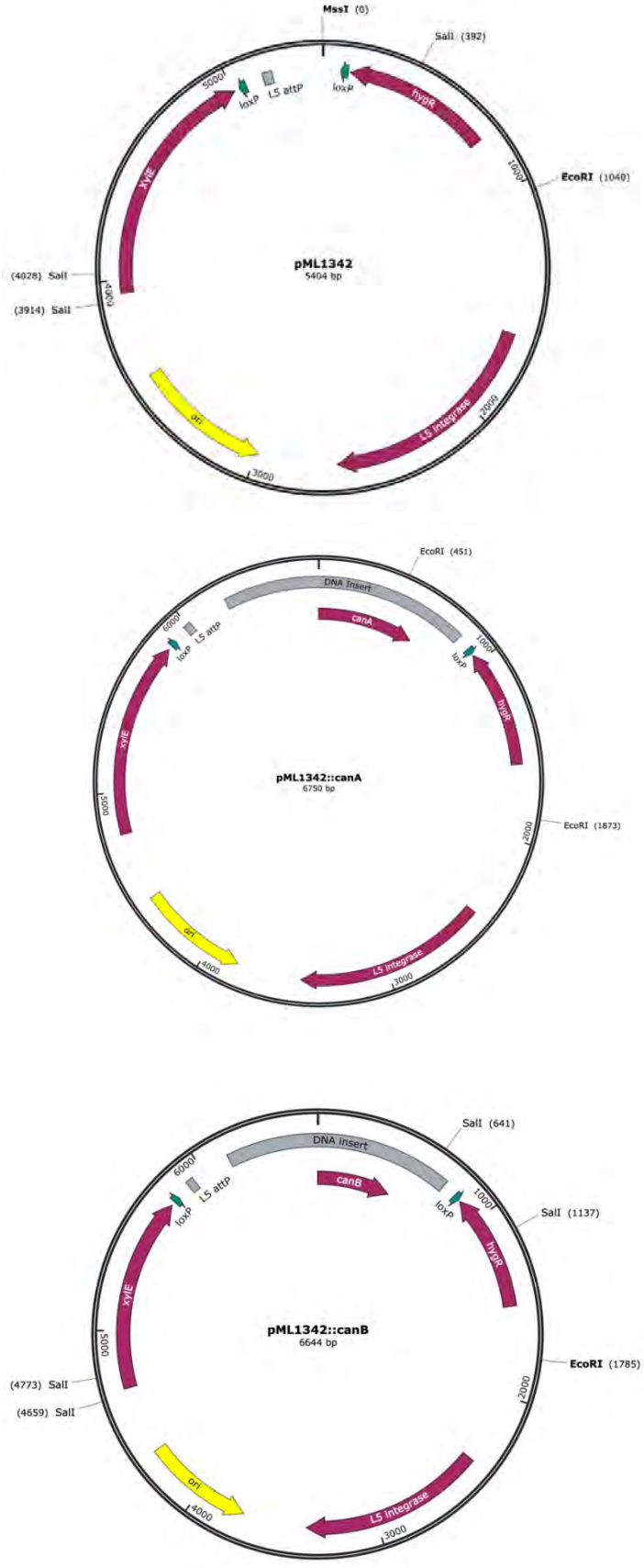

Figure C.2.3 Plasmid maps of pML1342, pML1342::*canA* and pML1342::*canB*

Section D: Comparison of Growth of *canA1* and *canB1* KD Mutants at Different ATc Concentrations

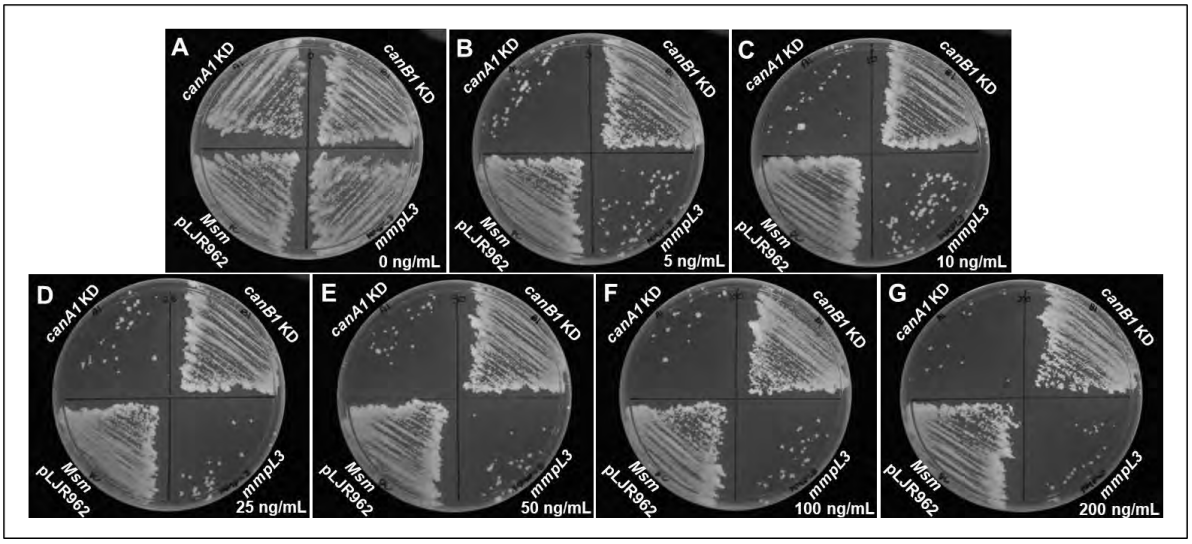

Figure D1. Relative growth of the WT *Msm* (pLJR962) control strain and knockdown mutants at varying concentrations of ATc. WT *Msm* harbouring the parental control vector, pLJR962 or the CRISPRi *can*A (A1), *canB* (B1) and *mmpL3* knockdown mutant strains were cultured and grown to mid-exponential phase and diluted to a final OD_{600} of 0.01. 10 ml of the cultures were streaked onto the surface of 7H10 agar medium supplemented with the indicated concentrations of ATc. The plates were grown at 37°C for 72 hrs before imaging.

Section E: Comparison of the Growth of *Msm* WT, Δ*canB* and *canB1* KD Strains at Low and High CO2 Concentrations

The *Msm* WT, Δ*canB* and *canB1* KD strains were streaked on 7H10 plates as described in the figure legend and incubated at low and high CO_2 concentrations. As seen in **Figure E1**, no significant differences in the growth of *Msm* WT and either the *Msm* Δ*canB* KO (**A, B**) or *Msm canB1* KD (**C, D, E, F**) mutant strains were observed at either low (**A, C, D**) or high CO_2 **(B, E, F**) concentrations, or presence **(D, F**) and absence (**C, E**) of ATc. This suggests that *canB* is dispensable for the growth and survival of *Msm* under these conditions.

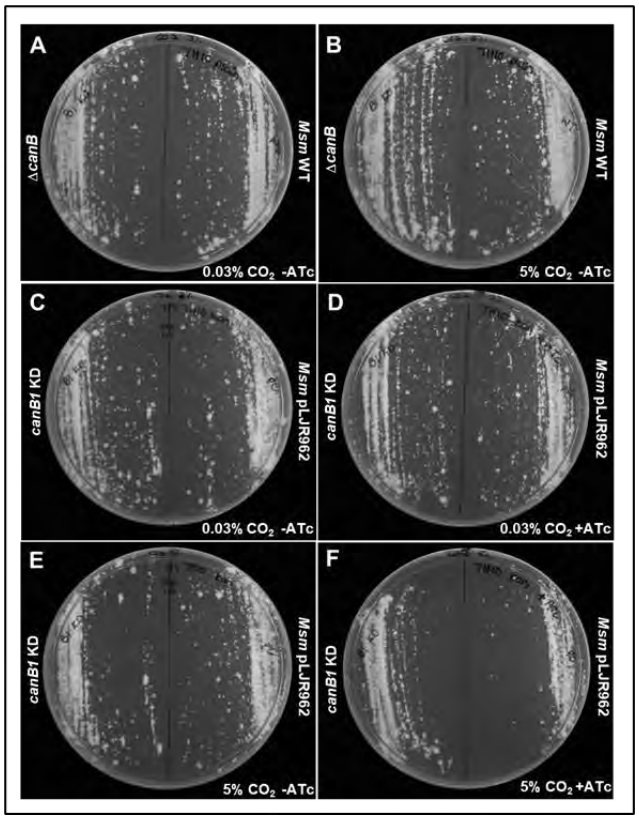

Figure E1. Comparison of the growth of the *Msm* WT, *canB1* KD mutant, *Msm* pLJR962 and *canB1* KO strains at low (0.03%) and high (5%) CO_2 concentrations. Plates **A, C and D** were incubated at atmospheric (0.03%) CO_2, while plates **B, E and F** were incubated in the presence of physiological (5%) CO_2 concentrations. Plates **C and E** were grown in the absence of ATc and plates **D and F** were grown in the presence of ATc, as described in **Chapter 2, Section 2.8.4**. The plates were incubated at 37 °C and images were taken after 3 days.

Section F: Comparison of Biofilm Formation by the *canA1* and *canB1* KD Mutants

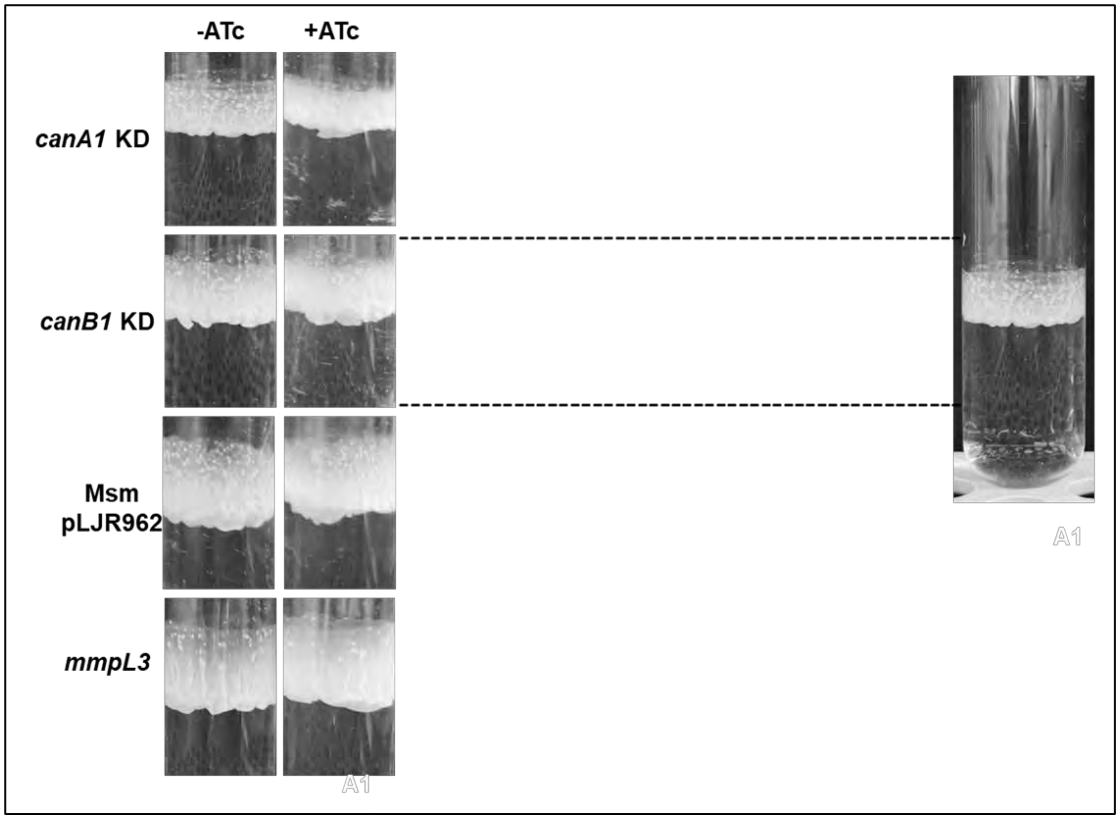

Figure F1. Biofilm formation in the *Msm canA* and *canB* KD1 mutants in the presence and absence of ATc. *Msm* WT containing the parental control vector, pLJR962 (PC), or the *Msm canA1* (A1) and *canB* (B1) knockdown mutants were cultured to an OD_{600} of ~1.0 in M63 biofilm medium and diluted to a final OD_{600} of 0.001 in 3 ml of the same medium in 16 mm test tubes in the presence and absence of ATc, as described in **Chapter 2, Section 2.8.3**. Cultures were incubated as static cultures at 30 °C for 5 days before biofilm formation was examined and images taken.

References

Aguilera, J., VanDijken, J. P., Winde, J. H., & Pronk, J. T. (2005). "Carbonic anhydrase (Nce103p): an essential biosynthetic enzyme for growth of *Saccharomyces cerevisiae* at atmospheric carbon dioxide pressure." *Biochemical Journal* 391 (Pt 2), 311-316. doi: 10.1042/BJ20050556

Al-Haideri, H., White, M. A., & Kelly, D. J. (2016). "Major contribution of the type II beta carbonic anhydrase CanB (Cj0237) to the capnophilic growth phenotype of *Campylobacter jejuni*." *Environmental Microbiology*, 18(2), 721-735. doi: 10.1111/1462-2920.13092

Andreu, N., Zelmer, A., Fletcher, T., Elkington, P. T., Ward, T. H., Ripoll, J., Parish, T., Bancroft, G. J., Schaible, U., Robertson, B. D., Wiles, Siouxsie. (2010). "Optimisation of Bioluminescent Reporters for Use with Mycobacteria." *PLUS ONE*, 10.1371/journal.pone.0010777

Aspatwar, A., Kairys, V., Rala, S., Parikka, M., Bozdag, M., Carta, F., Supuran, C. T., & Parkkila, S. (2019). "*Mycobacterium tuberculosis* β-Carbonic Anhydrases: Novel Targets for Developing Antituberculosis Drugs." *International Journal of Molecular Sciences*, 20(20). 10.3390/ijms20205153

Aspatwar, A., Tolvanen, M. E. E., Barker, H., Syrjänen, L., Valanne, S., Purmonen, S., Waheed, A., Sly, W. S., & Parkkila, S. (2022). "Carbonic anhydrases in metazoan model organisms: molecules, mechanisms, and physiology." *Physiological Reviews*, 102(3), 1327–1383. doi: 10.1152/physrev.0018.2021

Badger, M. (2003). "The roles of carbonic anhydrases in photosynthetic $CO(_2)$ concentrating mechanisms." *Photosynthesis Research*, 77(2–3), 83–94. doi: 10.1023/A:1025821717773

Baker, J. J., Dechow, S. J. and Abramovitch, R. B. (2019). "Acid fasting: Modulation of *Mycobacterium tuberculosis* metabolism at acidic pH." *Trends in Microbiology*, 27(11), pp. 942–953. doi: 10.1016/j.tim.2019.06.005

Baker, J. J., Johnson, B. K. & Abramovitch, R. B. (2014). "Slow growth of Mycobacterium tuberculosis at acidic pH is regulated by phoPR and host-associated carbon sources." *Molecular Microbiology*, 94(1), 56–69. doi: 10.1111/mmi.12688

Barkan, D., Rao, V., Sukenick, G.D., & Glickman, M.S., (2010). "Redundant Function of cmaA2 and mmaA2 in *Mycobacterium tuberculosis* cis Cyclopropanation of Oxygenated Mycolates." *J Bacteriol* 192, 3661–3668. doi: 10.1128/JB.00312-10

Barry, C. E., Boshoff, H. I., Dartois, V., Dick, T., Ehrt, S., Flynn, J., Schnappinger, D., Wilkinson, R. J., & Young, D. (2009). "The spectrum of Latent tuberculosis: Rethinking

the biology and intervention strategies." *Nature Reviews Microbiology*, 7(12), 845-855. doi: 10.1038/nrmicro2236

Barry, C. E., Lee, R. E., Mdluli, K., Sampson, A. E., Schroeder, B. G., Slayden, R. A., & Yuan, Y. (1998). "Mycolic acids: Structure, biosynthesis and physiological functions." *Progress in Lipid Research*, 37(2–3), 143–179. doi: 10.1016/s0163-7827(98)00008-3

Batt, S. M., Minnikin, D. E., & Besra, G. S. (2020). "The thick waxy coat of mycobacteria, a protective layer against antibiotics and the host's immune system." *Biochemical Journal*, *477*(10), 1983–2006. doi: 10.1042/BCJ20200194

Behr, M. A., Kaufmann, E., Duffin, J., Edelstein, P. H., & Ramakrishnan, L. (2021). "Latent Tuberculosis: Two Centuries of Confusion." *American Journal of Respiratory and Critical Care Medicine*, *204*(2), 142–148. doi: 10.1164/rccm.202011-4239PP

Belardinelli, J. M., Li, W., Avanzi, C., Angala, S. K., Lian, E., Wiersma, C. J., Palcekova, Z., Martin, K. H., Angala, B., de Moura, V. C. N., Kerns, C., Jones, V., Gonzalez-Juarrero, M., Davidson, R. M., Nick, J. A., Borlee, B. R., Jackson, M. (2021). "Unique Features of *Mycobacterium abscessus* Biofilms Formed in Synthetic cystic Fibrosis Medium." *Frontiers in Microbiology*, 12. doi: 10.3389/fmicb.2021.743126

Berney, M. & Berney-Meyer, L. (2017). "*Mycobacterium tuberculosis* in the Face of Host-Imposed Nutrient Limitation." *Microbiology Spectrum*, 5(3). doi: 10.1128/microbiolspec.tbtb2-0030-2016

Blomgran, R., Desvignes, L., Briken, V., & Ernst, J. D. (2012). "*Mycobacterium tuberculosis* inhibits neutrophil apoptosis, leading to delayed activation of naive CD4 T-cells," *Cell Host & Microbe*, 11(1), 81–90. doi:10.1016/j.chom.2011.11.012

Bogdan, C. (2015). "Nitric oxide synthase in innate and adaptive immunity: An update." *Trends in Immunology*, 36(3), 161–178. doi: 10.1016/j.it.2015.01.003

Briancesco, R., Semproni, M., Paradiso, R., & Bonadonna, L. (2014). "Nontuberculous mycobacteria: an emerging risk in engineered environmental habitats." *Annals of Microbiology*, *64*(2), 735–740. doi: 10.1007/s13213-013-0708-8

Burghout, P., Quintero, B., Bos, L., Beilharz, K., Veening, J. W., de Jonge, M. I., van der Linden, M., van der Ende, A., & Hermans, P. W. M. (2013). "A single amino acid substitution in the MurF UDP-MurNAc-Pentapeptide synthetase renders *Streptococcus pneumoniae* dependent on CO_2 and temperature." *Molecular Microbiology*, 89(3), 494-506. 10.1111/mmi.12292

Bussi, C. & Gutierrez, M. G. (2019). "*Mycobacterium tuberculosis* infection of host cells in space and Time." *FEMS Microbiology Reviews*, 43(4), 341–361. doi:10.1093/femsre/fuz006

Capasso, C. (2023). "Carbonic Anhydrases: A Superfamily of Ubiquitous Enzymes." *International Journal of Molecular Sciences*, *24*(8). doi: 10.3390/ijms24087014

Capasso, C., & Supuran, C. T. (2015). "Bacterial, fungal and protozoan carbonic anhydrases as drug targets." *Expert Opinion on Therapeutic Targets*, *19*(12), 1689–1704. doi: 10.1517/14728222.2015.1067685

Carta, F., Maresca, A., Covvarubias, A. S., Mowbray, S. L., Jones, T. A., & Supuran, C. T. (2009). "Carbonic anhydrase inhibitors. Characterization and inhibition studies of the most active beta-carbonic anhydrase from *Mycobacterium tuberculosis*, Rv3588c." *Bioorganic & Medicinal Chemistry Letter*, 19(23), 6649-6654. doi: 10.1016/j.bmcl.2009.10.009

Casey, J. R. (2006). "Why bicarbonate?" *Biochemistry and Cell Biology*, *84*(6), 930–939. doi: 10.1139/o06-184

Centers for Disease Control and Prevention. (2022). *Drug-Resitant TB*. https://www.cdc.gov/tb/topic/drtb/default.htm

Chackerian, A. A., Alt, J. M., Perera, T. V., Dascher, C. C., & Behar, S. M. (2002). "Dissemination of *Mycobacterium tuberculosis* influenced by host factors and precedes the initiation of T-cell immunity." *Infection and Immunity*, 70(8), 4501–4509. doi: 10.1128/iai.70.8.4501-4509.2002

Chandra, P., Grigsby, S.J. & Philips, J.A. (2022). "Immune evasion and provocation by *Mycobacterium tuberculosis*.", *Nature Reviews Microbiology*, 20(12), 750–766. doi: 10.1038/s41579-022-00763-4

Chang, D. P. & Guan, X. L. (2021). "Metabolic versatility of mycobacterium tuberculosis during infection and dormancy." *Metabolites*, 11(2), 88. doi:10.3390/metabol11020088

Chegwidden, W. R., Dodgson, S. J., & Spencer, I. M. (2000). "The roles of carbonic anhydrase in metabolism, cell growth and cancer in animals". In W. R. Chegwidden, N. D. Carter, & Y. H. Edwards (Eds.), *The Carbonic Anhydrases: New Horizons*, 343–363. doi: 10.1007/978-3-0348-8446-4_16

Chen, J., Yue, K., Shen, L., Zheng, C., Zhu, Y., Han, K., & Kai, L. (2023). "Aquaporins and CO_2 diffusion across biological membrane." *Frontiers in Physiology*, 14. doi: 10.3389/fphys.2023.1205290

Choi, I., Son, H. & Baek, J.-H. (2021). "Tricarboxylic acid (TCA) cycle intermediates: Regulators of immune responses." *Life*, 11(1), 69. doi: 10.3390/life11010069

Cirillo, D. M., Ghodousi, A., & Tortoli, E. (2021). "*Mycobacterium tuberculosis*: The Organism's Genomics and Evolution." *Essential Tuberculosis*, 11–17. doi: 10.1007/978-3-030-66703-0_2

Cochrane, G. M., C. G. Newstead, R. V. Nowell, P. Openshaw, and C. B. Wolff. 1982. "The Rate of Rise of Alveolar Carbon Dioxide Pressure during Expiration in Man." *The Journal of Physiology* 333 (December): 17–27. doi: 10.0.0.113/jphysiol.1982.sp014435

Cohen, S. B., Gern, H. B., Delahaye, J. L., Adams, K. N., Plumlee, C. R., Winkler, J. K., Sherman, D. R., Gerner, M. Y., & Urdahl, K. B. (2018). "Alveolar macrophages provide an early *Mycobacterium tuberculosis* niche and initiate dissemination." *Cell Host & Microbe*, 24(3). 10.1016/j.chom.2018.08.001

Cohn, Maurice L., William F. Russell, and Gardner Middlebrook. 1960. "Effects of Carbon Dioxide and Daylight in Culturing Tubercle Bacilli." *The American Review of Respiratory Disease* 82 (4): 579–80. doi: 10.1128/jcm.36.9.2565-2570.1998

Conradie, F., Diacon, A. H., Ngubane, N., Howell, P., Everitt, D., Crook, A. M., Mendel, C. M., Egizi, E., Moreira, J., Timm, J., McHugh, T. D., Wills, G. H., Bateson, A., Hunt, R., Van Niekerk, C., Li, M., Olugbosi, M., Spigelman, M., & Nix-TB Trial Team. (2020). "Treatment of Highly Drug-Resistant Pulmonary Tuberculosis." *The New England Journal of Medicine*, *382*(10), 893–902. doi: 10.1056/NEJMoa1901814

Cook, G. M., Berney, M., Gebhard, S., Heinemann, M., Cox, R. A., Danilchanka, O., & Niederweis, M. (2009). "Physiology of mycobacteria." *Advances in Microbial Physiology*, 81–319. doi: 10.1016/s0065-2911(09)05502-7

Covarrubias, A., Larsson, A., Högbom, M., Lindberg, J., Bergfors, T., Björkelid, C., Mowbray, S., Unge, T. & Jones, T. (2005). "Structure and Function of Carbonic Anhydrases from

Cronan, M. R. (2022). "In the thick of it: Formation of the tuberculous granuloma and its effects on host and therapeutic responses." *Frontiers in Immunology*, 13. doi: 10.3389/fimmu.2022.820134

Cummins, Eoin P., Moritz J. Strowitzki, and Cormac T. Taylor. 2020. "Mechanisms and Consequences of Oxygen and Carbon Dioxide Sensing in Mammals." *Physiological Reviews* 100 (1): 463–88. doi: 10.1152/physrev.00003.2019

Cvetnić, Ž., Tuk, M. Z., Duvnjak, S., Reil, I., Mikulić, M., Pavlinec, Ž., Cvetnić, M., & Špičić, S. (2018). "Tuberculosis and Nontuberculosis Mycobacteria In Human and Animal Infection." 18(2). doi: 10.7251/VETJEN1802342C

Daffé, M., & Marrakchi, H. (2019). "Unraveling the Structure of the Mycobacterial Envelope." *Microbiology Spectrum*, 7(4). doi: 10.1128/microbiolspec.GPP3-0027-2018

Daniel, J., Maamar, H., Deb, C., Sirakova, T. D., & Kolattukudy, P. E. (2011). "Mycobacterium tuberculosis uses host triacylglycerol to accumulate lipid droplets and acquires a dormancy-like phenotype in lipid-loaded macrophages." *PLoS Pathogens*, 7(6). doi: 10.1371/journal.ppat.1002093

Dartois, V. A., & Rubin, E. J. (2022). "Anti-tuberculosis treatment strategies and drug development: Challenges and priorities." *Nature Reviews Microbiology*, 20(11), 685-701. doi: 10.1038/s41579-022-00731-y

Davis, J.M. and Ramakrishnan, L. (2009). "The role of the granuloma in expansion and dissemination of early tuberculous infection." *Cell*, 136(1), 37–49. doi:10.1016/j.cell.2008.11.014

Day, N. J., Santucci, P., & Gutierrez, M. G. (2023). "Host cell environments and antibiotics efficacy in tuberculosis." *Trends in Microbiology*. doi: 10.1016/j.tim.2023.08.009

De Souza, G.A., Leversen, N. A., Malen, H., & Wiker, H. G. (2011). "Bacterial proteins with cleaved or uncleaved signal peptides of the general secretory pathway." *Journal of Proteomics*, 75(2), 502-510. doi: 10.1016/j.jprot.2011.08.016

Dechow, S. J., Goyal, R., Johnson, B. K., & Abramovitch, R. B. (2022). "Carbon dioxide regulates *Mycobacterium tuberculosis* PhoPR signaling and virulence." In *bioRxiv* (p. 2022.04.12.488064). doi: 10.1101/2022.04.12.488064

Degiacomi, G., Gianibbi, B., Recchia, D., Stelitano, G., Truglio, G. I., Marra, P., Stamilla, A., Makarov, V., Chiarelli, L. R., Manetti, F., Pasca, M. R. (2023). "CanB, a Druggable Cellular Target in *Mycobacterium tuberculosis*." *ACS Omega* 8(28), 25209-25220. doi: 10.1021/ascomega.3c02311

DeJesus, M. A., Gerrick, E. R., Xu, W., Park, S. W., Long, J. E., Boutte, C. C., Rubin, E. J., Schnappinger, D., Ehrt, S., Fortune, S. M., Sassetti, C. M., & L, T. R. (2017). "Comprehensive Essentiality Analysis of the *Mycobacterium tuberculosis* Genome via Saturating Transposon Mutagensis." *mBio*, 8(1). doi: 10.1128/mBio.02133-16

Del Prete, S., Nocentini, A., Supuran, C. T., & Capasso, C. (2020). "Bacterial ι-carbonic anhydrase: a new active class of carbonic anhydrase identified in the genome of the Gram-negative bacterium *Burkholderia territorii*." *Journal of Enzyme Inhibition and Medicinal Chemistry*, 35(1), 1060–1068. doi: 10.1080/14756366.2020.1755852

Dheda, K., Gumbo, T., Gandhi, N. R., Murray, M., Theron, G., Udwadia, Z., Migliori, G. B., & Warren, R. (2014). "Global control of tuberculosis: From extensively drug-resistant to untreatable tuberculosis." *The Lancet Respiratory Medicine*, 2(4), 321–338. doi: 10.1016/s2213-2600(14)70031-1

DiMario, R. J., Machingura, M. C., Waldrop, G. L., & Moroney, J. V. (2018). "The many types of carbonic anhydrases in photosynthetic organisms." *Plant Science: An International Journal of Experimental Plant Biology*, 268, 11–17. doi: 10.1016/j.plantsci.2017.12.002

Dowdy, D.W., Basu, S. & Andrews, J.R. (2013). "Is passive diagnosis enough?." *American Journal of Respiratory and Critical Care Medicine*, 187(5), 543–551. doi: 10.1164/rccm.2001207-1217oc

Drain, P. K., Bajema, K. L., Dowdy, D., Dheda, K., Naidoo, K., Schumacher, S. G., Ma, S., Meermeier, E., Lweinsohn, D. M., & Sherman, D. R. (2018). "Incipient and subclinical tuberculosis: A clinical review of early stages and progression of infection." *Clinical Microbiology Reviews*, 31(4). doi: 10.1128/cmr.00021-18

Dulberger, C. L., Rubin, E. J., & Boutte, C. C. (2020). "The mycobacterial cell envelope - a moving target." *Nature Reviews. Microbiology*, 18(1), 47–59. doi: 10.1038/s41579-019-0273-7

Ehrt, S., & Schnappinger, D. (2009). "Mycobacterial survival strategies in the phagosome: defence against host stresses." *Cellular Microbiology*, 11(8), 1170-1778. doi: 10.1111/j.1462-5822.2009.01335.x

Ernst, J. D. (2012). "The immunological life cycle of tuberculosis." *Nature Reviews Immunology*, 12(8), 581–591. doi: 10.1038/nri3259

Esmail, H., Dodd, P.J. and Houben, R.M. (2018). "Tuberculosis transmission during the subclinical period: Could unrelated cough play a part?" *The Lancet Respiratory Medicine*, 6(4), 244–246. doi: 10.1016/s2213-2600(18)30105-x

Fan, Sook-Ha, Miki Matsuo, Li Huang, Paula M. Tribelli, and Friedrich Götz. (2021). "The MpsAB Bicarbonate Transporter Is Superior to Carbonic Anhydrase in Biofilm-Forming Bacteria with Limited CO_2 Diffusion." *Microbiology Spectrum* 9 (1): e0030521. doi: 10.1128/spectrum.00305-21

Fan, Sook-Ha, Patrick Ebner, Sebastian Reichert, Tobias Hertlein, Susanne Zabel, Aditya Kumar Lankapalli, Kay Nieselt, Knut Ohlsen, and Friedrich Götz. (2019). "MpsAB Is Important for *Staphylococcus aureus* Virulence and Growth at Atmospheric CO2 Levels." *Nature Communications* 10 (1): 3627. doi: 10.1038/s41467-019-11547-5

Fatima, S., Kumari, A., Das, G., & Dwivedi, V. P. (2020). "Tuberculosis vaccine: A journey from BCG to present." *Life Sciences*, 252, 117594. doi: 10.1016/j.lfs.2020.117594

Felce, J., Saier, M. H., Jr. (2004). "Carbonic anhydrases fused to anion transporters of the SulP family: evidence for a novel type of bicarbonate transporter." *Journal of Molecular Microbiology and Biotechnology*, 8(3), 169-176. doi: 10.1159/000085789

Felce, Jeremy, and Milton H. Saier Jr. 2004. "Carbonic Anhydrases Fused to Anion Transporters of the SulP Family: Evidence for a Novel Type of Bicarbonate Transporter." *Journal of Molecular Microbiology and Biotechnology* 8 (3): 169–76. doi: 10.1159/000085789

Gagneux, S. (2018). "Ecology and evolution of *Mycobacterium tuberculosis*." *Nature Reviews. Microbiology*, 16(4), 202–213. doi: 10.1038/nrmicro.2018.8

Geers, C., & Gros, G. (2000). "Carbon dioxide transport and carbonic anhydrase in blood and muscle." *Physiological Reviews*, 80(2), 681-715. doi: 10.1152/physrev.2000.80.2.681

Goude, R., Roberts, D. M., Parish, T. (2015). "Electroporation of Mycobacteria", in: Parish, T., Roberts, D.M. (Eds.), Mycobacteria Protocols, *Methods in Molecular Biology*, 117–130. doi: 10.1007/978-1-4939-2450-9_7

Griffin, J. E., Gawronski, J. D., Dejesus, M. A., Loerger, T. R., Akerley, B. J., & Sassetti, C. M. (2011). "High-resolution phenotypic profiling defines genes essential for mycobacterial growth and cholesterol catabolism." *PLOS Pathog,* 7(9), e1002251. doi: 10.1371/journal.ppat.1002251

Guinn, K. M., & Rubin, E. J. (2017). "Tuberculosis: JUST THE FAQS." *mBio*, 8(6). doi: 10.1128/mBio.01910-17

Guitierrez, M. G., & Enninga, J. (2022). "Intracellular niche switching as host subversion strategy of bacterial pathogens." *Current Opinion in Cell Biology*, 76. doi: 10.1016/j.ceb.2022.102081

Hirakawa, Y., Senda, M., Fukuda, K., Yu, H. Y., Ishida, M., Taira, M., Kinbara, K., & Senda, T. (2021). "Characterization of a novel type of carbonic anhydrase that acts without metal cofactors." *BMC Biology*, 19(1), 105. doi: 10.1186/s12915-021-01039-8

Houben, R. M. G. J., & Dodd, P. J. (2016). "The Global Burden of Latent Tuberculosis Infection: A Re-estimation Using Mathematical Modelling." *PLoS Medicine*, 13(10), e1002152. doi: 10.1371/journal.pmed.1002152

Huff, J., Czyz, A., Landick, R., & Niederweis, M. (2010). "Taking phage integration to the next level as a genetic tool for mycobacteria." *Gene*, 468(1-2), 8-19. doi: 10.1016/j.gene.2010.07.012

Inoue, H., Nojima, H., Okayama, H. (1990). High efficiency transformation of *Escherichia coli* with plasmids. *Gene*, 96, 23–28. doi: 10.1016/0378-1119(90)90336-p

Jackson, M. (2014). "The mycobacterial cell envelope-lipids." *Cold Spring Harbor Perspectives in Medicine*, 4(10). doi: 10.1101/cshperspect.a021105

Jankute, M., Cox, J. A. G., Harrison, J., & Besra, G. (2015). "Assembly of the Mycobacterial Cell Wall." *Annual Review of Microbiology*, 69(1), 405–423. doi:10.1146/annurev-micro-091014-104121

Jilani, T. N., Avula, A., Gondal, Z., Siddiqui, A. H. (2022). "Active Tuberculosis."

Kalscheuer, R., Palacios, A., Anso, I., Cifuente, J., Anguita, J., Jacobs, W. R., Guerin, M. E., & Prados-Rosales, R. (2019). "The *Mycobacterium tuberculosis* capsule: A cell structure with key implications in pathogenesis." *Biochemical Journal*, 476(14), 1995–2016. doi: 10.1042/bcj20190324

Kang, D. D., Lin, Y., Moreno, J-R., Randall, T. D., & Khader, S. A. (2011). "Profiling early lung immune responses in the mouse model of tuberculosis." *PLoS ONE*, 6(1). doi: 10.1371/journal.pone.0016161

Ke, J., Behal, R. H., Back, S. L., Nikolau, B. J., Wurtele, E. S., & Oliver, D. J. (2000). "The role of pyruvate dehydrogenase and acetyl-coenzyme A synthetase in fatty acid synthesis in developing Arabidopsis seeds." *Plant Physiology*, 123(2), 497–508. doi: 10.1104/pp.123.2.497

Kempker, R. R., Heinrichs, M. T., Nikolaishvili, K., Sabulua, I., Bablishvili, N., Gogishvili, S., Avaliani, Z., Tukvadze, N., Little, B., Bernheim, A., Read, T. D., Guarner, J., Derendorf, H., Peloquin, C. A., Blumberg, H. M., & Vashakidze, S. (2017). "Lung tissue concentrationsof pyrazinamide among patients with drug-resistant pulmonary tuberculosis."*Antimicrobial Agents and Chemotherapy*. 61(6). doi: 10.1128/aac.00226-17

Kim, C.-J., Kim, N.-H., Song, K.-H., Choe, P. G., Kim, E. S., Park, S. W., Kim, H.-B., Kim, N.-J., Kim, E.-C., Park, W. B., & Oh, M.-D. (2013). "Differentiating rapid- and slow-growing mycobacteria by difference in time to growth detection in liquid media." *Diagnostic Microbiology and Infectious Disease*, 75(1), 73–76. doi: 10.1016/j.diagmicrobio.2012.09.019

Kloprogge, F., Cancseco, J. O., Phee, L., Saouki, Z., Kipper, K., Witney, A. A., Stoker, N., & McHugh, T. D. (2022). "Emergence of phenotypic and genotypic antimicrobial resistance in *Mycobacterium Tuberculosis*." *Scientific Reports*, 12(1). doi: 10.1038/s41598-022-25827-6

Kostiuk, B., Becker, M. E., Churaman, C. N., Black, J. J., Payne, S. M., Pukatzki, S., & Koestler, B. J. (2023). "*Vibrio cholerae* Alkalizes Its Environment via Citrate Metabolism to Inhibit Enteric Growth In Vitro." *Microbiology Spectrum*, 11(2), e0491722. doi: 10.1128/spectrum.04917-22

Kostiuk, B., Becker, M. E., Churaman, C. N., Black, J. J., Payne, S. M., Pukatzki, S., & Koestler, B. J. (2023). "*Vibrio cholerae* Alkalizes Its Environment via Citrate Metabolism to Inhibit Enteric Growth *In Vitro*." *Microbiol Spectr*, 11(2), e0491722. doi: 10.1128/spectrum.049117-22

Kumar, A., Farhana, A., Guidry, L., Saini, V., Hondalus, M., & Steyn, A. J. C. (2011). "Redox homeostasis in mycobacteria: The key to tuberculosis control?" *Expert Reviews in Molecular Medicine*, 13. doi: 10.1017/s1462399411002079

Kusian, B., Sultemeyer, D., Bowein, B (2002). "Carbonic anhydrase is essential for growth of *Ralstonia eutropha* at ambient CO_2 concentrations." *Journal of Bacteriology,* 184(18), 5018-5026. doi: 10.1128/JB.184.18.5018-5026.2002

Lamichhane, G., Zignol, M., Blades, N. J., Geiman, D. E., Dougherty, A., Grosett, J., Broman, K. W., & Bishai, W. R. (2003). "A postgenomic method for predicting essential genes at subsaturation levels of mutagenesis: Application to *Mycobacterium tuberculosis*."

Proceedings of the National Academy of Sciences, 100(12), 7213-7218. doi: 10.1073/pnas.1231432100

Langereis, J. D., Zomer, A., Stunnenberg, H. G., Burghout, P., & Hermans, P. W. M. (2013). "Nontypeable *Haemophilus influenza* carbonic anhydrase is important for environmental and intracellular survival." *Journal of Bacteriology*, 195(12), 2737-2746. doi: 10.1128/JB.01870-12

Lenaerts, A., Barry, C. E,. & Dartois, V. (2015). "Heterogeneity in tuberculosis pathology, microenvironments and therapeutic responses." *Immunological Reviews*, 264(1), 288–307. doi: 10.1111/imr.12252

Lerner, T. R., Borel, S. & Gutierrez, M. G. (2015). "The innate immune response in human tuberculosis." *Cellular Microbiology*, 17(9), 1277–1285. doi: 10.1111/cmi.12480

Lerner, T. R., Queval, C. J., Lai, R. P., Russell, M. R. G., Fearns, A., Greenwood, D. J., Collinson, L., Wilkinson, R. J., & Gutierrez, M. G. (2020). *Mycobacterium tuberculosis* cords within lymphatic endothelial cells to evade host immunity. *JCI Insight*, 5, 136937. doi: 10.1172/jci.insight.136937

Lin P. L., Rodgers M., Smith L., Bigbee M., Myers A., Bigbee C., Chiose, I., Capuano, S. V., Fuhrman, C., Klein, E., & Flynn, J. L. (2009). "Quantitative comparison of active and latent tuberculosis in the cynomolgus macaque model." *Infect. Immun.* 77, 4631–4642. doi: 10.1128/IAI.00457-09

Livak, K. J., Schmittgen, T. D. (2001). "Analysis of Relative Gene Expression Data Using Real-Time Quantitative PCR and the 2−ΔΔCT Method." *Methods* 25, 402–408. doi: 10.1006/meth.2001.1262

Lory, S. (2014). "The Family Mycobacteriaceae." In E. Rosenberg, E. F. DeLong, S. Lory, E. Stackebrandt, & F. Thompson (Eds.), *The Prokaryotes: Actinobacteria*, 571–575. doi: 10.1007/978-3-642-30138-4_339

Lovewell, R. R., Baer, C. E., Mishra, B. B., Smith, C. M., & Sassetti, C. M. (2021). "Granulocytes act as a niche for *Mycobacterium tuberculosis* growth." *Mucosal Immunology*, 14(1), 229–241. doi:10.1038/s1385-020-0300-z

Lu, Z., Jiang, W., Zhang, J., Lynn, H. S., Chen, Y., Zhang, S., Ma, Z., Geng, P., Guo, X., Zhang, H., & Zhang, Z. (2019). "Drug resistance and epidemiology characteristics of multidrug-resistant tuberculosis patients in 17 provinces of China." *PLUS ONE*, 14(11). doi: 10.1371/journal.pone.0225361

MacMicking, J. D., North, R. J., LaCourse, R., Mudgett, J. S., Shah, S. K., & Nathan, C. F. (1997). "Identification of nitric oxide synthase as a protective locus against tuberculosis." *Proceedings of the National Academy of Sciences*, 94(10), 5243–5248. doi: 10.1073/pnas.94.10.5243

MacPherson, P., Lebina, L., Bosch, Z., Milovanovic, M., Ratsela, A., Lala, S., Variava, E., Golub, J. E., Webb, E. L., & Martinson, N. A. (2020). "Prevalence and risk factors for latent tuberculosis infection among household contacts of index cases in two South African provinces: Analysis of Baseline Data from a cluster-randomised trial." *PLOS ONE*, 15(3). doi: 10.1371/journal.pone.0230376

Mangtani, P., Abubakar, I., Ariti, C., Beynon, R., Pimpin, L., Fine, P. E. M., Rodrigues, L. C., Smith, P. G., Lipman, M., Whiting, P. F., & Sterne, J. A. (2014). "Protection by BCG vaccine against tuberculosis: a systematic review of randomized controlled trials." *Clinical Infectious Diseases: An Official Publication of the Infectious Diseases Society of America*, 58(4), 470–480. doi: 10.1093/cid/cit790

Marcus, E. A., Moshfegh, A. P., Sachs, G., & Scott, D. R. (2005). "The Periplasmic α-Carbonic Anhydrase Activity of *Helicobacter pylori* Is Essential for Acid Accimilation." *Journal of Bacteriology*, 187(2), 729-738. doi: 10.1128/jb/187.2.729-738.2005

Martin, C., Carey, A., & Fortune, S. (2015). "A Bug's Life in the Granuloma." *Seminars in Immunopathology*, 38(2), 213-220. doi: 10.1007/s00281-015-0533-1

Martinez, L., Cords, O., Liu, Q., Acuna-Villaorduna, C., Bonnet, M., Fox, G. J., Carvalho, A. C. C., Chan, P.-C., Croda, J., Hill, P. C., Lopez-Varela, E., Donkor, S., Fielding, K., Graham, S. M., Espinal, M. A., Kampmann, B., Reingold, A., Huerga, H., Villalba, J. A., Andrews, J. R. (2022). "Infant BCG vaccination and risk of pulmonary and extrapulmonary tuberculosis throughout the life course: a systematic review and individual participant data meta-analysis." *The Lancet. Global Health*, *10*(9), e1307–e1316. doi: 10.1016/S2214-109X(22)00283-2

Mattila, J. T., Ojo, O. O., Kepka-Lenhart, D., Marino, S., Kim, J. H., Eum, S. Y., Via, L. E., Clifton E Barry 3rd, Edwin Klein, Denise E. Kirschner, Sideny M. Morris Jr., Philana Ling Lin., & Joanne L Flynn. (2013). "Microenvironments in tuberculous granulomas are delineated by distinct populations of macrophage subsets and expression of nitric oxide synthase and arginase isoforms." *The Journal of Immunology*, 191(2), 773–784. doi:10.4049/jimmunol.1300113

Mattow, Jens, Frank Siejak, Kristine Hagens, Frank Schmidt, Christian Koehler, Achim Treumann, Ulrich E. Schaible, and Stefan H. E. Kaufmann. 2007. "An Improved Strategy for Selective and Efficient Enrichment of Integral Plasma Membrane Proteins of Mycobacteria." *Proteomics* 7 (10): 1687–1701. doi: 10.1002/pmic.200600928

McNeil, M. & Cook, G., (2019). "Utilization of CRISPR Interference to Validate MmpL3 as a Drug Target in *Mycobacterium tuberculosis*." *Antimicrobial Agents and Chemotherapy*, 63(8). doi: 10.1128/AAC.00629-19

Merlin, C., Masters, M., McAteer, S., & Coulson, A. (2003). "Why is carbonic anhydrase essential to *Escherichia coli*?" *Journal of Bacteriology*, 185(21), 6415-6424. doi: 10.1128/JB.185.21.6415-6424.2003

Michenkova, M., Taki, S., Blosser, M. C., Hwang, H. J., Kowatz, T., Moss, F. J., Occhipinti, R., Qin, X., Sen, S., Shinn, E., Wang, D., Zeise, B. S., Zhao, P., Malmstadt, N., Vahedi-Faridi, A., Tajkhorshid, E., & Boron, W. F. (2021). "Carbon dioxide transport across membranes. *Interface Focus*, 11(2), 20200090." doi: 10.10098/rsfs.2020.0090

Middlebrook, G., and M. L. Cohn. 1958. "Bacteriology of Tuberculosis: Laboratory Methods." *American Journal of Public Health and the Nation's Health* 48 (7): 844–53. doi: 10.2105/aiph.48.7.844

Minakuchi, T., Nishimori, I., Vullo, D., Scozzafava, A., & Supuran, C. T. (2009). "Molecular coloning. characterization and inhibition studies of the Rv1284 beta-carbonic anhydrase from *Mycobacterium tuberculosis* with sulfonamides and a sulfamate." *Journal of Medicinal Chemistry*, 52(8), 2226-2232. doi: 10.1021/jm9000488

Minakuchi, Tomoko, Isao Nishimori, Daniela Vullo, Andrea Scozzafava, and Claudiu T. Supuran. 2009. "Molecular Cloning, Characterization, and Inhibition Studies of the Rv1284 Beta-Carbonic Anhydrase from *Mycobacterium tuberculosis* with Sulfonamides and a Sulfamate." *Journal of Medicinal Chemistry* 52 (8): 2226–32. doi: 10.1021/jm9000488

Munoz-Elias, E. J. & McKinney, J. D. (2006). "Carbon metabolism of intracellular bacteria." *Cellular Microbiology*, 8(1), 10–22. doi:10.1111/j.1462-5822.2005.00648.x

Mycobacterium tuberculosis." *Journal of Biological Chemistry*, 280(19), 18782-18789. doi: 10.1074/jbc.M414348200

Nguyen, G. T., Green, E. R., & Mecsas, J. (2017). "Neutrophils to the roscue: Mechanisms of NADPH oxidase activation and bacterial resistance." *Frontiers in Cellular and Infection Microbiology*, 7. doi: 10.3389/fcimb.2017.00373

Nienaber, Lisa, Elysia Cave-Freeman, Megan Cross, Lyndel Mason, Ulla-Maja Bailey, Parisa Amani, Rohan A Davis, Paul Taylor, and Andreas Hofmann. 2015. "Chemical Probing Suggests Redox-Regulation of the Carbonic Anhydrase Activity of Mycobacterial Rv1284." *The FEBS Journal* 282 (14): 2708–21. doi: 10.1111/febs.13313

Nishimoria, I., Minakuchia, T., Marescab, A., Cartab, F., Supuran, A. S. A. C. T. (2010). "The β-Carbonic Anhydrases from *Mycobacterium tuberculosis* as Drug Targets." *Current Pharmaceutical Design*, 16(29), 3300-3309. doi: 10.2174/138161210793429814

Nocentini, A., Capasso, C., & Supuran, C. T. (2023). "Carbonic Anhydrase Inhibitors as Novel Antibacterials in the Era of Antibiotic Resistance: Where Are We Now?" *Antibiotics (Basel, Switzerland)*, 12(1). doi: 10.3390/antibiotics12010142

Ofer, N., Wishkautzan, M., Meijler, M., Wang, Y., Speer, A., Niederweis, M., & Gur, E. (2012). "Ectoine Biosynthesis in *Mycobacterium smegmatis*." *Appl. Environ. Microbiol*, 78, 7483–7486. doi: 10.1128/AEM.01318-12

Pai, M., Behr, M. A., Dowdy, D., Dheda, K., Divangahi, M., Boehme, C. C., Ginsberg, A., Swaminathan, S., Spigelman, M., Getahun, H., Menzies, D., & Raviglione, M. (2016). "Tuberculosis." *Nature Reviews Disease Primers*, 2(1). doi: 10.1038/nrdp.2016.76

Pal, D. S., Abbasi, M., Mondal, D. K., Varghese, B. A., Paul, R., Singh, S., & Datta, R. (2017). "Interplay between a cytosolic and a cell surface carbonic anhydrase in pH homeostasis and acid tolerance of Leishmania." *Journal of Cell Science,* 130(4), 754-766. doi: 10.1242/jcs.199422

Pandey, A. K. & Sassetti, C. M. (2008). "Mycobacterial persistence requires the utilization of host cholesterol." *Proceedings of the National Academy of Sciences*, 105(11), 4376–4380. doi: 10.1073/pnas.0711159105

Pashley, C. A., & Parish, T. (2003). "Efficient switching of mycobacteriophage L5-based integrating plasmids in *Mycobacterium tuberculosis*." *FEMS Microbiol Letters*, 229(2), 211-215. doi: 10.1016/S0378-1097(03)00823-1

Patterson, B., & Wood, R. (2019). "Is cough really necessary for TB transmission?" *Tuberculosis*, 117, 31-35. doi: 10.1016/j.tube.2019.05.003

Pavlik, I., Ulmann, V., Hubelova, D., & Weston, R. T. (2022). "Nontuberculous Mycobacteria as Sapronoses: A Review." *Microorganisms*, 10(7). doi: 10.3390/microorganisms10071345

Pereira, A. C., Ramos, B., Reis, A. C., & Cunha, M. V. (2020). "Non-Tuberculous Mycobacteria: Molecular and Physiological Bases of Virulence and Adaptation to Ecological Niches." *Microorganisms*, 8(9). doi:10.3390/microorganisms8091380

Pisu, D., Huang, L., Narang, V., Theriault, M., Le-Bury, G., Lee, B., Lakudzala, A. E., Mzinza, D. T., Mhango, D. V., Mitini-Nkhoma, S., Jambo, K. C., Singhal., A., Mwandumba, H. C., & Russell, D. G. (2021). "Single cell analysis of *M. tuberculosis* phenotype and macrophage lineages in the infected lung." *Journal of Experimental Medicine*, 218(9). doi: 10.1084/jem.20210615

Price, G. D. (2011). "Inorganic carbon transporters of the cyanobacterial CO_2 concentrating mechanism." *Photosynthesis Research*, 109(1–3), 47–57. doi: 10.1007/s11120-010-9608-y

Price, G. D., Woodger, F. J., Badger, M. R., Howitt, S. M., & Tucker, L. (2004). "Identification of a SulP-type bicarbonate transporter in marine cyanobacteria." *Proceedings of the National Academy of Sciences of the United States of America*, 101(52), 18228-18233. doi: 10.1073/pnas.0405211101

Qualls, J. E., & Murray, P. J. (2015). "Immunometabolism within the tuberculosis granuloma: Amino acids, hypoxia, and cellular respiration." *Seminars in Immunopathology*, 38(2), 139–152. doi:10.1007/s00281-015-0534-0

Rahlwes, K.C., Dias, B. R. S., Campos, P. C., Alvarez-Arguedas, S., & Shiloh, M. U. (2023). "Pathogenicity and virulence of *Mycobacterium tuberculosis*." *Virulence*, 14(1). doi: 10.1080//21505594.2022.2150449

Ravesloot-Chávez, M. M., Van Dis, E. & Stanley, S. A. (2021). "The innate immune response to *Mycobacterium tuberculosis* infection." *Annual Review of Immunology*, 39(1), 611–637. doi: 10.1146/annurev-immunol-093019-010426

Richards, A. S., Sossen, B., Emery, J. C., Horton, K. C., Heinsohn, T., Frascella, B., Balzarini, F., Oradini-Alacreu, A., Hacker, B., Odone, A., McCreesh, N., Grant, A. D., Kranzer, K., Cobelens, F., Esmail, H., & Houben, R. M. G. J. (2023). "Quantifying progression and regression across the spectrum of pulmonary tuberculosis: A data synthesis study." *The Lancet Global Health*, 11(5). doi:10.1016/S2214-109X(23)00082-7

Rock, J., Hopkins, F., Chavez, A., Diallo, M., Chase, M., Gerrick, E., Pritchard, J., Church, G., Rubin, E., Sassetti, C., Schnappinger, D. & Fortune, S., 2017. "Programmable transcriptional repression in Mycobacteria using an orthogonal CRISPR interference platform." *Nature Microbiology*, 2(4). doi: 10.1038/nmicrobiol.2016.274

Rose, S. J. & Bermudez, L. E. (2016). "Identification of bicarbonate as a trigger and genes involved with extracellular DNA export in mycobacterial biofilms." *mBio*, 7(6). doi: 10.1128/mbio.01597-16

Ruhl, C. R., Pasko, B. L., Khan, H. S., Kindt, L. M., Stamm, C. E., Franco, L. H., Hsia, C. C. Zhou, M., Davis, C, R., Qin, T., Gautron, L., Burton, M. D., Mejia, G. L., naik, D. K., Dussor, G., Price, T. J., & Shiloh, M. U. (2020). "*Mycobacterium tuberculosis* Sulfolipid-1 Activates Nociceptive Neurons and Induces Cough." *Cell*, 181(2), 293-305. doi: 10.1016/j.cell.2020.02.026

Russell, D. W., & Sambrook, J. (2001). "Molecular Cloning: A laboratory Manual" (Vol. 1). Cold Spring Harbor Laboratory.

Sarathy, J. P., & Dartois, V. (2020). "Caseum: A Niche for *Mycobacterium tuberculosis* Drug-Tolerant Persisters." *Clinical Microbiology Reviews*, 33(3). doi: 10.1128/CMR.00159-19

Sassetti, C., Boyd, D. & Rubin, E. (2003). "Genes Required for Mycobacterial Growth Defined by High Density Mutagenesis." *Molecular Microbiology*, 48(1), 77-84. doi: 10.1046/j.1365-2958.2003.03425.x

Saunders, B. M., & Cooper, A. M. (2000). "Restraining mycobacteria: Role of granulomas in mycobacterial infections." *Immunology & Cell Biology*, 78(4), 334-341. doi: 10.1046/j.1440-1711.2000.00933.x

Schaefer, W. B., M. L. Cohn, and G. Middlebrook. 1955. "The Role of Biotin and Carbon Dioxide in the Cultivation of *Mycobacterium Tuberculosis*." *Journal of Bacteriology* 69 (6): 706–12. doi: 10.1128/jb.69.6.706-712.1955

Schairer, D. O., Chouake, J. S., Nosanchuk, J. D., & Friedman, A. J. (2012). "The potential of nitric oxide releasing therapies as antimicrobial agents." *Virulence*, 3(3), 271-279. doi: 10.4161/viru.20328

Schmittgen, T. D., Livak, K. J., 2008. "Analyzing real-time PCR data by the comparative CT method." *Nat Protoc* 3, 1101–1108. doi: 10.1038/nprot.2008.73

Sezonov, G., Joseleau-Petit, D., & D'Ari, R. (2007). "*Escherichia coli* physiology in Luria-Bertani broth." *Journal of Bacteriology*, 189(23), 8746-8749. doi: 10.1128/jb.01368-07

Simeone, R., Sayes, F., Lawaree, E., & Brosch, R. (2021). "Breaching the phagosome, the case of the tuberculosis agent." *Cellular Microbiology*, 23(7), e13344. doi: 10.1111/cmi.13344

Singer-Sam, J., Tanguay, R. L., Riggs, A. O. (1989). "Use of Chelex to improve the PCR signal from a small number of cells." *Nucleic Acid Res*, 18(3), 687. doi: 10.1093/nar/18.3.687

Smith, K. S., & Ferry, J. G. (2000). "Prokaryotic carbonic anhydrases." *FEMS Microbiology Reviews*, 24(4), 335–366. doi: 10.1111/j.1574-6976.2000.tb00546.x

Smith, K. S., Jakubzick, C., Whittam, T. S., & Ferry, J. G. (1999). "Carbonic anhydrase is an ancient enzyme widespread in prokaryotes." *Proceedings of the National Academy of Sciences of the United States of America*, 96(26), 15184–15189. doi: 10.1073/pnas.96.26.15184

Snapper, S. B., Melton, R. E., Mustafa, S., Kieser, T., & Jr', W. R. J. (1990). "Isolation and characterization of efficient plasmid transformation mutants of Mycobacterium smegmatis 10." *Molecular Microbiology*, 4(11), 1911. doi: 10.1111/j.1365-2958.1990.tb02040.x

Sparks, I. L., Derbyshire, K. M., Jacobs, W. R., Jr., & Morita, Y. S. (2023). "*Mycobacterium smegmatis*: The Vanguard of Mycobacterial Research." *Journal of Bacteriology*, 205(1), e0033722. doi: 10.1128/jb.00337-22

Srivastava, S., Dey, S., & Mukhopadhyay, S. (2023). "Vaccines against Tuberculosis: Where Are We Now?" *Vaccines*, 11(5). doi: 10.3390/vaccines11051013

Stuck, L., van Haaster, A. M., Kapata-Chanda, P., Klinkenberg, E., Kapata, N., & Cobelens, F. (2022). "How "subclinical" is subclinical tuberculosis? an analysis of national prevalence survey data from Zambia." *Clinical Infectious Diseases*, 75(5), 842–848. doi: 10.1093/cid/ciab1050

Sundarsingh, T. J. A., Ranjitha, J., Rajan, A., & Shankar, V. (2020). "Features of the biochemistry of *Mycobacterium smegmatis*, as a possible model for Mycobacterium tuberculosis." *Journal of Infection and Public Health*, 13(9), 1255–1264. doi: 10.1016/j.jiph.2020.06.023

Supuran, C. T. (2016). “Structure and function of carbonic anhydrases.” *Biochemical Journal*, 473(14), 2023–2032. doi: 10.1016/s0163-7258(96)00198-2

Supuran, C. T. (2016). “Structure and function of carbonic anhydrases.” *Biochemical Journal*, 473(14), 2023-2032. doi: 10.1042/BCJ20160115

Supuran, C. T. (2018). “Carbonic Anhydrases and Metabolism.” *Metabolites*, 8(2), 25. doi: 10.3390/metabo8020025

Supuran, C. T. (2024). Chapter 3.1 - Carbonic anhydrases. In C. T. Supuran & W. A. Donald (Eds.), *Metalloenzymes*, 139–156. doi: 10.1016/B978-0-12-823974-2.00014-0

Supuran, C. T., & Capasso, C. (2017). “An Overview of the Bacterial Carbonic Anhydrases.” *Metabolites* 7(4). doi: 10.3390/metabo7040056

Thornell, Ian M., Xiaopeng Li, Xiao Xiao Tang, Christian M. Brommel, Philip H. Karp, Michael J. Welsh, and Joseph Zabner. 2018. “Nominal Carbonic Anhydrase Activity Minimizes Airway-Surface Liquid PH Changes during Breathing.” *Physiological Reports* 6 (2). doi: 10.14814/phy2.13569

Tiberi, S., Utjesanovic, N., Galvin, J., Centis, R., D’Ambrosio, L., van den Boom, M., Zumla, A., & Migliori, G. B. (2022). “Drug resistant TB - latest developments in epidemiology, diagnostics and management.” *International Journal of Infectious Diseases: IJID: Official Publication of the International Society for Infectious Diseases*, *124 Suppl 1*, S20–S25. doi: 10.1016/j.ijid.2022.03.026

Tiemersma, E. W., van der Werf, M. J., Borgdorff, M. W., Williams, B. G., & Nagelkerke, N. J. D. (2011). “Natural history of tuberculosis: duration and fatality of untreated pulmonary tuberculosis in HIV negative patients: a systematic review.” *PloS One*, 6(4), e17601. doi: 10.1371/journal.pone.0017601

Tortoli, E. (2019). Chapter 1 – “The Taxonomy of the Genus Mycobacterium.” In A. Velayati & P. Farnia (Eds.), *Nontuberculous Mycobacteria (NTM),* 1–10. doi: 10.1016/B978-0-12-814692-7.00001-2

Tresguerres, M., Buck, J., & Levin, L. R. (2010). “Physiological carbon dioxide, bicarbonate, and pH sensing.” *Pflugers Archiv: European Journal of Physiology*, 460(6), 953–964. doi: 10.1007/s00424-010-0865-6

Turenne, C. Y. (2019). “Nontuberculous mycobacteria: Insights on taxonomy and evolution.” *Infection, Genetics and Evolution: Journal of Molecular Epidemiology and Evolutionary Genetics in Infectious Diseases*, 72, 159–168. doi: 10.1016/j.meegid.2019.01.017

Ueda, K., Nishida, H., & Beppu, T. (2012). "Dispensibilities of carbonic anhydrase in proteobacteria." *International Journal of Evolutionary Biology*, 2012, 324549. doi: 10.1155/2012/324549

van Kessel, J. C., & Hatfull, G. F. (2007). "Recombineering in *Mycobacterium tuberculosis*." *Nature Methods*, 4(2), 147-152. doi: 10.1038/nmeth996

Wayne, L. G. & Hayes, L. G. (1996). "An in vitro model for sequential study of Shiftdown of *Mycobacterium tuberculosis* through two stages of nonreplicating persistence." *Infection and Immunity*, 64(6), 2062–2069. doi:10.1128/iai.64.6.2062.1996

WHO. (2022). *Global Tuberculosis Report 2022*. https://www.who.int/teams/global-tuberculosis-programme/tb-reports/global-tuberculosis-report-2022

WHO. (2023). *Global Tuberculosis Report 2023*. https://www.who.int/teams/global-tuberculosis-programme/tb-reports/global-tuberculosis-report-2023

Wong, A. I., & Rock, J. M. (2021). "CRISPR Interference (CRISPRi) for Targeted Gene Silencing in Mycobacteria." *Methods Molecular Biology*, 343-364. doi: 10.1007/978-1-0716-1460-0_16

Woodman, M. E., Savage, C. R., Arnold, W. K., Stevenson, B. (2016). "Direct PCR of IntactBacteria (Colony PCR)." *Current Protocols in Microbiology*, 42. doi: 10.1002/cpmc.14

Wu, Y. Zeng, J., Roscoe, B. P., Liu, O., Yao, Q., Lazzarotto, C, R., Clement, K., Cole, M. A., Luk, K., Baricordi, C., Shen, A. H., Ren, C., Esrick, E. B., Manis, J. P., Dorfman, D. M., Williams, D. A., Biffi, A., Brugnara, C., Biasco, L., Brendel, C., Pinello, L., Tsai, S. Q., Wolfe, S. A., & Bauer, D. E., (2019). "Highly efficient therapeautic gene editing of human hematopoietic stem cells." *Nat Med*, 5, 776-783. doi: 10.1038/s41591-019-0401-y

Yang, C.-S., Lee, J-S., Rodgers, M., Min, C-K., Lee, J-Y., Kim, H. J., Lee, K-H., Kim, C-J., Oh, B., Zandi, E., Yue, Z., Kramnik, I., Liang, C., & Jung, J. U. (2012). "Autophagy protein rubicon mediates phagocytic NADPH oxidase activation in response to microbial infection or TLR stimulation." *Cell Host & Microbe*, 11(3), 264–276. doi:10.1016/j.chom.2012.01.018

Yates, R. M., Hermetter, A., & Russell, D. G. (2005). "The kinetics of phagosome maturation as a function of phagosome/lysosome fusion and acquisition of hydrolytic activity." *Traffic*, 6(5), 413–420. doi: 10.1111/j.1600-0854.2005.00284.x